

2016

# Metabolic Regulation of Gene Expression through Differential Histone Acylation: The Regulation and Function of Histone Crotonylation

Benjamin R. Sabari

Follow this and additional works at: [http://digitalcommons.rockefeller.edu/student\\_theses\\_and\\_dissertations](http://digitalcommons.rockefeller.edu/student_theses_and_dissertations)

 Part of the [Life Sciences Commons](#)

---

## Recommended Citation

Sabari, Benjamin R., "Metabolic Regulation of Gene Expression through Differential Histone Acylation: The Regulation and Function of Histone Crotonylation" (2016). *Student Theses and Dissertations*. 419.  
[http://digitalcommons.rockefeller.edu/student\\_theses\\_and\\_dissertations/419](http://digitalcommons.rockefeller.edu/student_theses_and_dissertations/419)



**METABOLIC REGULATION OF GENE EXPRESSION THROUGH  
DIFFERENTIAL HISTONE ACYLATION: THE REGULATION AND  
FUNCTION OF HISTONE CROTONYLATION**

A Thesis Presented to the Faculty of  
The Rockefeller University  
in Partial Fulfillment of the Requirements for  
the degree of Doctor of Philosophy

by  
Benjamin R. Sabari  
June 2016



# METABOLIC REGULATION OF GENE EXPRESSION THROUGH DIFFERENTIAL HISTONE ACYLATION: THE REGULATION AND FUNCTION OF HISTONE CROTONYLATION

Benjamin R. Sabari, Ph.D.

The Rockefeller University 2016

Histone lysine acetylation (Kac) plays a critical role in gene regulation by affecting the accessibility of the DNA wrapped around histones and by recruiting effector complexes. Three major classes of proteins are associated with Kac, namely “writers,” enzymes that covalently modify specific lysine residues, “readers,” protein domains that specifically bind modified residues, and “erasers,” enzymes that catalyze the removal of the modification. While histone acetylation is well characterized within this paradigm, little is known about the regulation and function of an expanding list of histone lysine acylations. Lysine propionylation, butyrylation, and crotonylation were all discovered by proteomics-based approaches as I started in the Allis Lab. With reports suggesting that lysine crotonylation (Kcr) was the most functionally distinct from Kac I embarked to purify and identify the writers, readers, and erasers and thereby characterize the regulation and function of histone Kcr.

To identify writers of Kcr I purified a histone crotonyltransferase (HCT) activity from nuclear extract by fractionation, which resulted in the purification of p300, a well-studied transcriptional co-activator and histone acetyltransferase (HAT). Together with colleagues in the Roeder lab, we established that p300's

HCT activity directly stimulates transcription to a greater degree than p300's HAT activity. This work is discussed in Chapter 2.

I developed several genetic and chemical approaches to manipulate the cellular concentrations of acetyl-CoA and crotonyl-CoA and established that acyl-CoA metabolism determines the state of differential histone acylation (Kac versus Kcr) thereby coupling the metabolic state to gene regulation. This work is discussed in Chapter 3.

With these methods, I next studied the impact of Kcr in the macrophage inflammatory response, a classic model of signal-dependent gene activation. Through bioinformatics analysis of RNA-seq and ChIP-seq of macrophages in various conditions, I established that increased histone Kcr leads to enhanced expression of p300-regulated genes. This work is discussed in Chapter 4.

These data suggested that there was a reader for Kcr with positive regulatory activity. In collaboration with colleagues in the Li lab, we identified the YEATS domain as a novel Kcr reader. Through a series of structural, biophysical, bioinformatic, and genetic studies we showed that AF9 and the YEATS-Kcr interaction is responsible for the enhanced expression of increased Kcr. This work is discussed in Chapter 5. As discussed in Chapter 6, I have also identified and characterized several decrotonylase (eraser) activities.

The regulation of histone crotonylation or the functional consequence of a histone being acetylated versus crotonylated (differential acylation) has remained unclear since the discovery of the modification was reported. In my thesis work, I have demonstrated that the differential acylation state of histones is an integration of environmental and metabolic information, which serves a functional role in the regulation of gene expression.

*For my first teachers, my parents*

## ACKNOWLEDGEMENTS

I would like to thank my advisor and mentor Dr. David Allis. His support and guidance have been instrumental for my thesis work and scientific development. It is difficult to not be motivated and inspired by Dave's enthusiasm for all things chromatin. I also thank Dr. Robert Roeder for his support throughout my graduate work. Bob has been engaged in my thesis work from the very early days and has been an exceptional mentor and advisor, always willing to meet to discuss new data or new ideas. I thank Dr. Robert Darnell for being the chair of my faculty advisory committee and for always asking the tough questions during committee meetings. I thank Dr. Katherine Wellen for acting as my external examiner.

I am indebted to my collaborators who through their complementary skill sets have helped me find new and exciting aspects of a topic I felt I had analyzed from every angle. I am indebted to Dr. Zhanyun Tang for his work on histone crotonylation in cell-free transcription systems and beyond. Drs. Justin Cross and Vladimir Yong-Gonzalez were instrumental in establishing the LC-MS protocol for measuring crotonyl-CoA. Drs. Haitao Li and Yuanyuan Li introduced a completely new wrinkle into my thesis work when they identified AF9 as a crotonyllysine reader and shared this data with us. I must thank Yingming Zhao and his colleagues for agreeing to collaborate with a young graduate student and for starting the investigation into histone lysine crotonylation.

I would like to thank the members of the Allis lab, current and past, who have made this an exceptional environment to do and learn science. Every member of the Allis lab has taught me important skills and helped me in ways

big and small; I am indebted to each of them. I am grateful to Drs. Peter Lewis, Fabio Casadio, and Ronen Sadeh for teaching me how to develop a critical eye for experimental detail, mostly by being such tough critics of my work as a young graduate student. I thank Peter Lewis for teaching me innumerable biochemical techniques. I thank Dr. Kyung-Min Noh for introducing me to the lab as my “rotation coach.” I thank Dr. Laura Banaszynski for discussions over ChIP-seq and RNA-seq. I thank Dr. Steve Josefowicz for introducing me to the macrophage inflammatory response as a model system and for inspiring a large swath of my research. I thank Drs. Bryce Carrey and Chao Lu for all their discussion on the metabolic regulation of chromatin. Marisa Cerio, Jamie Winshell, Dr. Carol McDonald, and Marylene Leboeuf all deserve special thanks for holding the Allis lab together.

I am thankful for the financial and administrative support I have received through the David Rockefeller Graduate Program. I am grateful to the NSF for financial support through the Graduate Research Fellowship Program. I thank all the staff in the Dean’s Office, and all those that make the Rockefeller Graduate Program run smoothly.

I cannot thank my family and friends enough for their love and support throughout this journey. I especially thank my parents, Joyce and Naftali, for always being there for me. And most of all, I thank Bridget for her constant support through all the ups and downs of this long journey, for being patient with me when “another thirty minutes” turns into three hours, and for being my unending source of joy and laughter.

## TABLE OF CONTENTS

ACKNOWLEDGEMENTS.....	iv
TABLE OF CONTENTS .....	vi
LIST OF FIGURES.....	x
CHAPTER 1: GENERAL INTRODUCTION.....	1
A Brief History of Histone Acetylation .....	7
The Transcriptional Co-Activator p300/CBP .....	14
Metabolic Regulation of Histone Acetylation .....	16
Histone Crotonylation .....	21
CHAPTER 2: PURIFICATION OF A HISTONE CROTONYL- TRANSFERASE ACTIVITY AND CHARACTERIZATION OF ITS ROLE IN TRANSCRIPTION .....	26
Introduction.....	26
Results .....	27
HAT and HCT Activities Co-Purify with p300 from HeLa S3 Nuclear Extract .....	27
p300 has HCT Activity In Vitro and In Cells .....	33
p300-Catalyzed Histone Crotonylation Stimulates Transcription in a Cell-Free System .....	38
Discussion .....	41

CHAPTER 3: THE RELATIVE CONCENTRATIONS OF CROTONYL-COA AND ACETYL-COA REGULATE GLOBAL HISTONE CROTONYLATION .....	46
Introduction.....	46
Results .....	47
Crotonyl-CoA and Acetyl-CoA Compete for p300's	
Acyltransferase Activity .....	47
LC-MS Measurements of Crotonyl-CoA and Acetyl-CoA .....	49
Sodium Crotonate Does Not Have HDAC Inhibitor Activity .....	52
ACSS2 is Responsible for Synthesizing Crotonyl-CoA from Crotonate .....	53
Impairing Acetyl-CoA Synthesis Leads to Higher Levels of Histone Crotonylation.....	55
Discussion.....	57

CHAPTER 4: EXPERIMENTAL MANIPULATION OF [CROTONYL-COA] AFFECTS ACTIVATION AND EXPRESSION OF P300 TRAGET GENES IN LPS- INDUCED INFLAMMATORY RESPONSE .....	61
Introduction.....	61
Results .....	63
H3K18Cr is Associated with Active Chromatin and Correlates with p300	
Localization .....	63
H3K18Cr and H3K18Ac are Induced at "De Novo-Activated" Regulatory Elements Upon LPS Stimulation .....	67

Increasing Crotonyl-CoA Concentrations by Crotonate Addition Increases H3K18Cr at “De Novo-Activated” Genes and Enhances Gene Expression .....	67
Increasing Cellular Concentrations of Crotonyl-CoA Prior to LPS Stimulation Enhances Cytokine and Chemokine Secretion Upon LPS Stimulation .....	75
Knockdown of Acss2 Reduces H3K18Cr at the Promoters of “De Novo- activated” Genes and Attenuates Gene Expression .....	77
Discussion .....	80

## CHAPTER 5: MOLECULAR COUPLING OF HISTONE CROTONYLATION

AND ACTIVE TRANSCRIPTION BY AF9 YEATS DOMAIN .....	83
Introduction .....	83
Results .....	88
The YEATS Domain Has Histone Crotonyl-lysine Binding Activity .....	88
Structural Basis for Crotonyl-Lysine Recognition by AF9 YEATS .....	91
Mutagenesis and Binding Studies .....	94
YEATS Domain Is a Crotonyl-Lysine Reader in the Cellular Context .....	95
Bromodomains Do Not Exhibit YEATS-Like Preference for Crotonyl-lysine .....	96
Structural Basis for Differential Recognition of H3K18 Acylation by BRD3 and AF9 .....	99
Kcr and AF9 YEATS Co-Localize Genome-Wide .....	102
The AF9-Kcr Interaction Positively Regulates Gene Expression in a YEATS-dependent Manner .....	107

Discussion.....	114
CHAPTER 6: IDENTIFICATION AND CHARACTERIZATION OF DECROTONYLASE ACTIVITIES .....	119
Introduction.....	119
Results .....	123
Nuclear Localized Sirtuins Exhibit Substrate Dependent Decrotonylase Activities .....	123
Overexpression of SIRT2, SIRT6, or SIRT7 Reduces Global Levels of H3K18Cr.....	128
HDAC1 Exhibits Decrotonylase Activity.....	130
Discussion.....	132
CHAPTER 7: GENERAL DISCUSSION .....	135
Histone Crotonyltransferase(s).....	135
Intracellular Concentrations of Crotonyl-CoA and other Acyl-CoAs .....	141
The Influence of Environmental Short Chain Fatty Acids.....	145
Conclusion .....	147
CHAPTER 8: METHODS.....	148
CHAPTER 9: REFERENCES.....	172

## LIST OF FIGURES

Figure 1.1: Structural and Functional Organization of the Eukaryotic Genome by Histones and Histone PTMs.....	2
Figure 1.2: The Current “Snapshot” of Histone Modifications .....	4
Figure 1.3: Reversible Histone Acetylation in Transcription.....	8
Figure 1.4: Cytosolic and Nuclear Metabolism of Acetyl-CoA .....	20
Figure 1.5: Diversity of Histone Lysine Acylation .....	23
Figure 2.1: Purification of an HCT Activity .....	28
Figure 2.2: Proteomics Analysis of Partially Purified HCT Activity .....	31
Figure 2.3: p300 Has Intrinsic HCT activity .....	34
Figure 2.4: p300 Catalyzes H3K18cr .....	36
Figure 2.5: Histone Cronylation Stimulates Transcription.....	39
Figure 3.1: The Relative Concentrations of Acetyl-CoA and Crotonyl-CoA Determine the Reaction Products .....	48
Figure 3.2: Manipulation of Intracellular Crotonyl-CoA Concentration by Treatment of Cells with Sodium Crotonate .....	51
Figure 3.3: Crotonate is Not an HDAC Inhibitor .....	52
Figure 3.4: Knockdown of ACSS2 Reduces Cellular Levels of H3K18cr .....	54
Figure 3.5: Reducing Acetyl-CoA Leads to an Increase in Histone Cronylation .....	56
Figure 3.6: Metabolic Regulation of Histone Cronylation.....	58

Figure 4.1: H3K18Cr, H3K18Ac, and p300 Co-Localize Genome-Wide .....	65
Figure 4.2: Two Classes of LPS-Stimulated Genes, as Defined by p300 Localization.....	68
Figure 4.3: LC-MS Measurements of Crotonyl-CoA and Acetyl-CoA in RAW264.7 Cells.....	69
Figure 4.4: Crotonate Treatment Correlates With Increased H3K18Cr, Decreased H3K18Ac and Increased Gene Expression.....	70
Figure 4.5: De Novo-Activated Genes Are Further Stimulated By Crotonate Pre- Treatment .....	73
Figure 4.6: RNA-seq Analysis of Crotonate Pre-Treatment.....	74
Figure 4.7: Increased Cellular Crotonyl-CoA Concentration Prior to LPS Stimulation Leads to Enhanced Cytokine and Chemokine secretion Upon LPS Stimulation.....	76
Figure 4.8: Knockdown of Acss2 Prior to LPS Stimulation Leads to a Decreased Induction of H3K18Cr at, and Decreased Stimulation of, “De Novo-Activated” Inflammatory Genes Upon LPS Stimulation .....	78
Figure 4.9: Metabolic Regulation of Transcription Through Differential Acylation .....	81
Figure 5.1: YEATS Domain Proteins are Associated with Transcriptional Regulation .....	85
Figure 5.2: Identification of AF9 YEATS Domain as a Histone Crotonyl-Lysine Reader .....	89

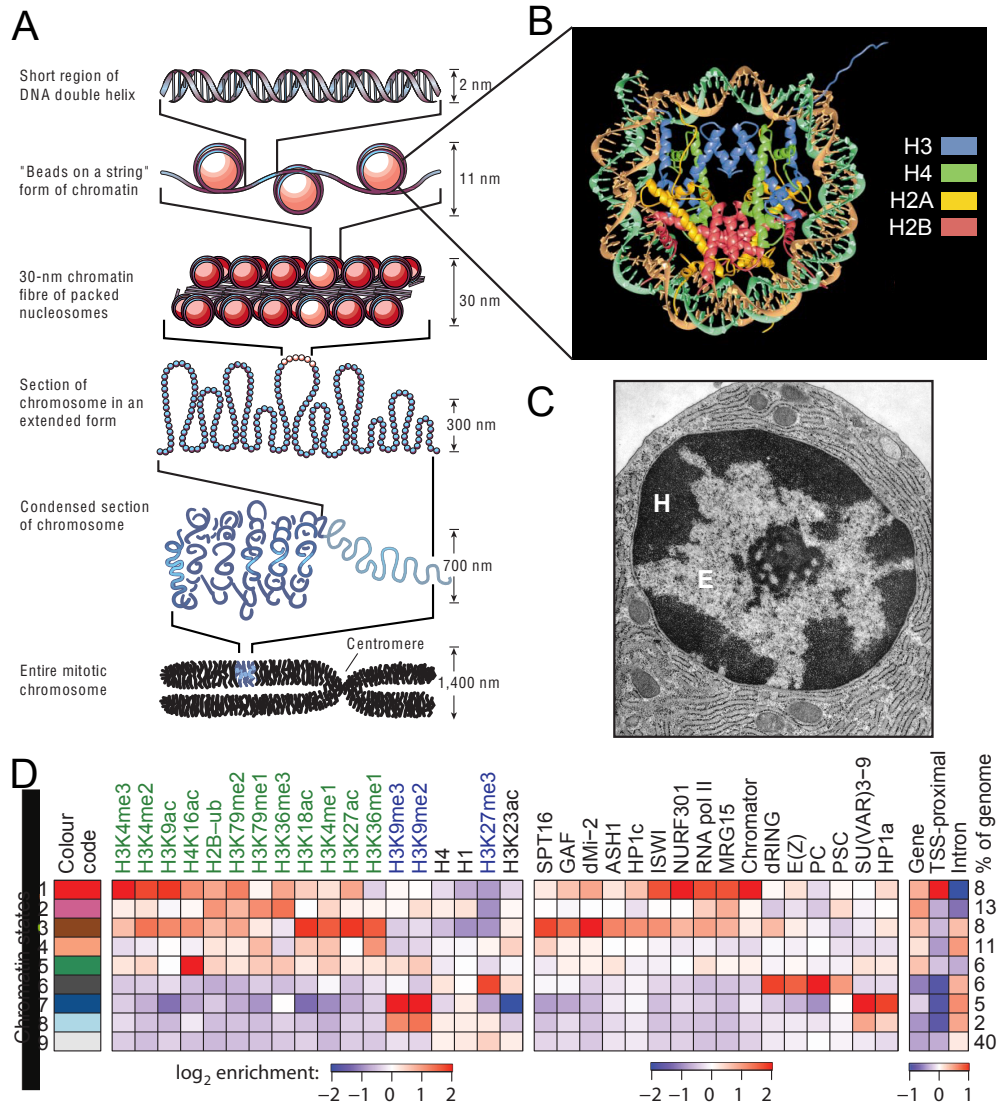
Figure 5.3: Molecular Basis for H3K9cr and H3K18cr Readout by AF9 YEATS Domain .....	92
Figure 5.4: The YEATS Domain Prefers Kcr to Kac Marked Nucleosomes.....	97
Figure 5.5: Bromodomains Do Not Exhibit Crotonyllysine Preference and the Underlying Molecular Basis .....	100
Figure 5.6: ChIP-Seq for AF9 and FLAG-AF9 .....	103
Figure 5.7: Genome-Wide Co-Localization of H3K18cr and AF9.....	105
Figure 5.8: FLAG-AF9 ChIP-Seq.....	108
Figure 5.9: The Increased Recruitment of AF9 Due to Crotonate Pre-Treatment is YEATS-Kcr Dependent .....	110
Figure 5.10: The Transcriptional Response to Increased Crotonyl-CoA is Dependent on AF9 and the YEATS-Kcr Interaction.....	112
Figure 6.1: Purification of Recombinant Sirtuins .....	122
Figure 6.2: Sirtuin Activity Assay with Acid Extracted Histones as Substrate....	124
Figure 6.3: Composition of Oligonucleosome and Octamer Substrates .....	126
Figure 6.4: Sirtuin Activity Assay with p300-catalyzed Octamers or Oligonucleosomes as Substrate.....	127
Figure 6.5: Overexpression of SIRT2, SIRT6, and SIRT7 in 293T cells Reduces Global Levels of H3K18Cr and H3K18Ac .....	129
Figure 6.6: HDAC1 has Decrotonylase Activity .....	131
Figure 7.1: The Regulation and Function of Histone Crotonylation .....	136

Figure 7.2: Unidentified Histone Crotonyltransferase(s).....	138
Figure 7.3: Ion-Exchange Chromatography of p300 Does Not Separate its HCT and HAT Activities .....	140
Figure 7.4: Metabolic Enzymes Involved in Acetyl-CoA or Crotonyl-CoA metabolism.....	144

## CHAPTER 1: GENERAL INTRODUCTION

The physiological form of eukaryotic nuclear DNA is chromatin, a nucleic acid-protein complex. In its simplest form, chromatin is composed of repeating nucleosomal units, each containing an octamer of histone proteins (two copies each of the core histones H3, H4, H2A, and H2B) and 147 base pairs (bp) of DNA (Kornberg, 1977). The nucleosome (Luger et al., 1997) is the first order of compaction mediated by histones required to fit the immense quantity of genomic DNA into the relatively small nuclear volume while maintaining appropriate access (**Figures 1.1A and 1.1B**). A wealth of discoveries over the past two decades has transformed the long-standing view of histones from being passive static scaffolds to dynamic modulators of virtually all DNA-templated events, such as replication, genomic maintenance, and transcription. Much of this progress in understanding the active role of histones has been due to the study of the regulation and function of histone post-translation modifications (PTMs).

Histone proteins are subject to a wide variety of PTMs of both chemical type and site that, alone or in combination, are characteristic of functional chromatin states. The combinatorial potential of histone PTMs is often referred to as the “histone code,” a language written on the histone proteins distinct from the genetic code written within the DNA double helix. The identification and characterization of histone-modifying enzymes as the products of genes previously associated with transcriptional and epigenetic regulators led to the proposal that the information encoded in the patterns of histone PTMs represents a form of epigenetic regulation of gene expression and cellular memory (Jenuwein and Allis, 2001; Strahl and Allis, 2000).



**Figure 1.1: Structural and Functional Organization of the Eukaryotic Genome by Histones and Histone PTMs.**

(A) Illustration of genomic compaction. Adapted from (Felsenfeld and Groudine, 2003). (B) Structure of the nucleosome. Adapted from (Luger et al., 1997). (C) Electron Micrograph of a guinea pig plasma cell. Electron dense heterochromatin is marked with an H and electron poor euchromatin is marked with an E. Adapted from Columbia University Histology Manual. (D) Designation of nine distinct chromatin states of the *Drosophila melanogaster* genome as defined by CHIP-seq for histone PTMs and other chromatin factors. Adapted from (Kharchenko et al., 2011).

Two distinct chromatin states can be defined visually as heterochromatin and euchromatin. Under electron microscopy heterochromatin appears condensed while euchromatin appears open (**Figure 1.1C**), these chromatin states are functionally distinct as heterochromatin is generally transcriptionally silent while euchromatin transcriptionally active. Particular histone PTMs associate with and determine these functional chromatin states (Felsenfeld and Groudine, 2003). With advances in high-throughput sequencing, genome-wide maps of histone PTMs and other transcriptional machinery have been generated by chromatin immunoprecipitation followed by sequencing (ChIP-seq) (Zhou et al., 2010). These data have allowed for a finer characterization of the functional organization of the eukaryotic genome (Figure 1.1D) (Kharchenko et al., 2011). From two states discernable by visual density with electron microscopy the field recently described nine or up to fifteen distinct chromatin states derived in large part from bioinformatics analysis of ChIP-Seq data of distinct subgroupings of histone PTMs genome-wide (Ernst et al., 2011).

With the application of high-sensitivity mass spectrometry to the identification of histone PTMs the current catalogue of observed histone PTMs is immense and growing (**Figure 1.2**) (Huang et al., 2014). Taking into account data on all four core histone proteins (H3, H4, H2A, and H2B) and the linker histone H1, roughly 500 unique histone modifications have been detected comprising 23 different types of chemical modification. The direct function or the regulatory mechanisms for a majority of these modifications remains unknown. Three major classes of proteins are involved in the regulation and function of histone PTMs and they are colloquially termed “writers,” enzymes that catalyze the covalent

**Figure 1.2: The Current “Snapshot” of Histone Modifications.**

Histone proteins are decorated by a variety of post-translational modifications (PTMs), which are critical to the dynamic modulation of chromatin structure and function, contributing to the cellular gene expression program. Histone PTMs can influence chromatin either directly, by changing the physical characteristic of the histone protein (e.g. lysine acetylation negates the residue's positive charge), or indirectly, by recruitment of modification- and site-specific effector proteins ("readers"). The function of a given histone PTMs is therefore mediated by both the physical properties of the modification (i.e. size and charge) and the location of the modified residue within the quaternary structure of the nucleosome. Recent studies, many powered by high-sensitivity mass spectrometry, have expanded our understanding of the extent to which histone proteins are modified. These studies have not only expanded the sites of well-studied modification, but have also revealed several new types of histone PTMs with a large diversity of structure, charge, and site of modification. Presented here is a compilation of data for histone PTMs observed from studies on human, mouse, or rat. Red boxes highlight the chemical structures of acetyl-lysine and crotonyl-lysine, the subject of this thesis. This figure is adapted from the *Cell SnapShot* (Huang, Sabari, et al. 2014).



modification of specific histone residues, “readers,” effector protein domains that bind histones in a modification specific manner, and “erasers,” enzymes that remove the modification. The combined activities of these three protein classes establish functional chromatin landscapes. Characterization and identification of the writers, readers, and erasers for any given modification is the first step to establishing the function of the modification. For example, the identification of a histone acetyltransferase (HAT) as a known transcriptional co-activator and a histone deacetylase (HDAC) as a transcriptional co-repressor prompted a breakthrough in the understanding of histone acetylation and its role in transcriptional regulation (Brownell et al., 1996; Taunton et al., 1996). This was followed soon thereafter by the identification of the bromodomain, a protein domain found in many transcriptional regulators with unknown function, as a reader of acetyl-lysine (Dhalluin et al., 1999). Together with a wave of subsequent research, these studies established a model for the function of histone acetylation in gene regulation, discussed in the next section (**Figure 1.3**).

My thesis work has focused on characterizing the regulation and function of one of these recently described and under-studied histone PTMs, histone lysine crotonylation (Kcr). To this end I have identified writers, readers, and erasers of histone crotonylation, demonstrated that acyl-CoA metabolism regulates the abundance of the modification, and characterized its role in gene expression. Lysine crotonylation is chemically similar to lysine acetylation in its linkage to the  $\epsilon$  amine of lysine, yet it is distinct in its extended and rigid hydrocarbon chain (**Figure 1.2**, see red boxes). The majority of my thesis work will be comparing the regulation and function of histone crotonylation to that of the more established histone acetylation. In this chapter, I will review the

literature on histone acetylation and its role in transcription, focus on the role of p300/CBP, provide background on the metabolic regulation of histone acetylation, and conclude with an introduction to histone crotonylation.

### **A Brief History of Histone Acetylation**

In 1871 Friedrich Miescher published his work on extracts derived from purified nuclei of white blood cells that contained both acid and basic substances, what we would today consider DNA and histones, respectively. Miescher went on to study the nuclein of salmon sperm and prepare high purity preparation of its acidic component making him the first to isolate DNA (van Holde, 1989). In 1884 Albrecht Kossel purified the basic component of nuclein from goose erythrocytes by extraction with hydrochloric acid and termed the acid-soluble protein *histon* (Doenecke and Karlson, 1984; Kossel, 1884). This simple purification of histones by acid extraction is still a commonly used lab practice and is used throughout this thesis.

Through the early 20<sup>th</sup> century, histones were considered a homogenous group of proteins until Stedman and Stedman identified multiple forms of histone proteins in their analysis of histones extracted from various tissues and species (Stedman, 1950). This heterogeneity of histone proteins led to the proposal that distinct phenotypes could result from the type of histone(s) associated with DNA (Stedman and Stedman, 1951). Although the Stedmans' claims were later dismissed, their hypothesis presented histones as more than mere scaffolds for DNA and inspired further research into the sequence and

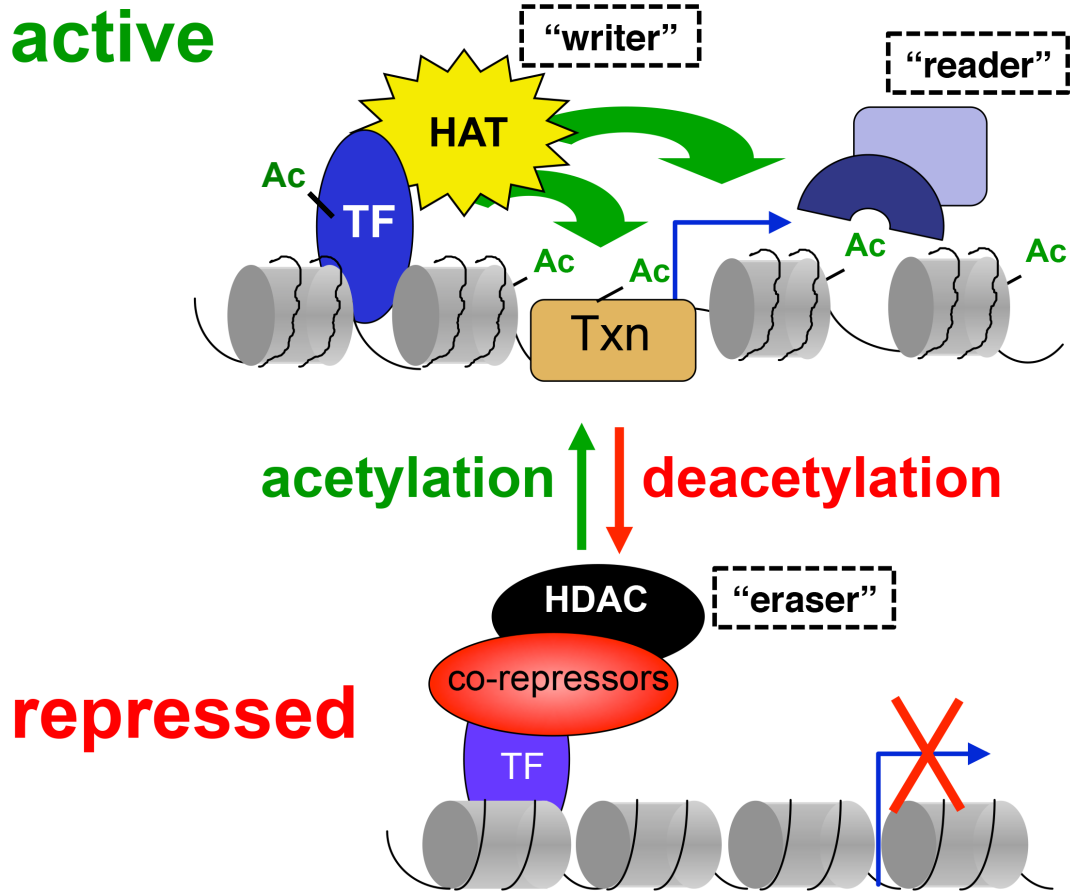


**Figure 1.3: Reversible Histone Acetylation in Transcription.**

Ordered recruitment of transcription factors (DNA-binding activators) recruit p300 and other co-activators allowing for histone modifications and remodeling, which facilitates the recruitment and stabilization of the transcription apparatus (Txn) through protein-DNA (activator-DNA), protein-protein (activator-co-activator), and protein-PTM (reader-histone) interactions allowing for the effective activation of transcription. This process is reversible by the recruitment of HDAC co-repressor complexes, which will deacetylate histones and non-histone substrates.

structure of the histone proteins (van Holde, 1989). In the 1960's nucleosomal histones were shown to be generally repressive to RNA synthesis (Huang and Bonner, 1962). Around the same time chemical analysis of the composition of histone proteins identified acetyl-lysine (Phillips, 1963) and methyl-lysine (Murray, 1964) as constituents of histones. At The Rockefeller Institute, Vincent Allfrey and colleagues performed a series of critical experiments that established a new paradigm for the active role of histones in gene regulation. They first demonstrated that intact nuclei readily took up and incorporated labeled acetate (acetate-2-C<sup>14</sup>) into histone proteins, even in the presence of translation inhibitors. These experiments established that histone acetylation was post-translational. Allfrey and colleagues next reproduced the studies showing that histones inhibited RNA synthesis, but demonstrated that chemically acetylated histones were inert (Allfrey et al., 1964). These observations led Allfrey to the following statement:

Specific (and presumably reversible) changes in histone structure ... may permit DNA to serve as a template in the RNA polymerase reaction. This raises the possibility that relatively minor modifications of histone structure, taking place on the intact protein molecule, offer a means of switching-on or -off RNA synthesis at different loci along the chromosome. (Allfrey et al., 1964)

Allfrey's prescient conclusions were not widely accepted for another thirty years, yet in that time many studies built upon this early hypothesis.

In the mid-1970's Riggs and colleagues showed that a previously reported butyrate-induced differentiation of Friend Leukemia cells into globin-secreting cells (Leder and Leder, 1975) was accompanied by an increase in histone acetylation (Riggs et al., 1977; 1978). Soon after, Davie and Allfrey demonstrated that butyrate was an inhibitor of histone deacetylase activity (Boffa et al., 1978;

Candido et al., 1978). These studies provided early evidence that the highly dynamic regulation of histone acetylation was involved in cellular differentiation. Furthermore, these studies illustrated the potential for small molecule intervention at the level of chromatin and provided an experimental tool to perturb histone acetylation by addition of butyrate to cells in culture. These observations also introduced the potential for histone modifications and their physiological output to be modulated by naturally occurring metabolites, in this case the short-chain fatty acid butyrate, a premise I raise in my thesis work.

The late 1980's to early 1990's provided a string of studies that further illustrated the importance of histone acetylation in regulation of gene expression. A number of groups utilizing the power of genetics in *S. cerevisiae* demonstrated that mutating the four highly conserved lysine residues on the histone H4 tail to either arginine or alanine resulted in growth defects, replication timing defects, abnormal silencing of telomeric chromatin, and defects in repression and activation of the mating type locus (Johnson et al., 1990; Megee et al., 1990; Park and Szostak, 1990). These four lysine residues were known to be acetylated to varying degrees *in vivo* yet, aside from substituting lysine for the acetyl-lysine mimic glutamine, these studies could not make direct claims on the role of histone acetylation per se.

Development of acetyl-histone-specific antibodies further established the connection between histone acetylation and gene activity. By immunofluorescence, the transcriptionally silent micronucleus of *Tetrahymena thermophila* was shown to be hypo-acetylated as compared to the transcriptionally active macronucleus (Lin et al., 1989), the hyper-active *Drosophila melanogaster* X-chromosome was shown to be hyper-acetylated (Turner

et al., 1992), and the mammalian inactive X-chromosome was shown to be hypoacetylated (Jeppesen and Turner, 1993). By chromatin immunoprecipitation (ChIP), actively transcribed regions of the genome were shown to be hyperacetylated (Hebbes et al., 1988), while silenced regions were shown to be hypoacetylated (Braunstein et al., 1993). Furthermore, histone acetylation was shown to be generally coincident with DNaseI hypersensitivity (Hebbes et al., 1994), a classic characteristic of actively transcribed chromatin (Weintraub and Groudine, 1976).

In 1996 two studies established a direct link between the regulation of histone acetylation and gene regulation by purification and characterization of a histone acetyltransferase (HAT) and histone deacetylase (HDAC). Many unsuccessful attempts had been made by various groups to purify HAT and HDAC activities from extract and the success of these groups relied on the utilization of unique and novel techniques. Allis and colleagues used extracts from the macronuclei of the protozoan *Tetrahymena thermophila*, a source known to have enriched HAT activity (Vavra et al., 1982). Utilizing an elegant in-gel assay, they identified a 55 kDa protein from *Tetrahymena* macronuclear extracts with HAT activity (Brownell and Allis, 1995). Once the protein was sequenced and its gene cloned it was identified as a homolog of the yeast transcriptional co-activator Gcn5 (Brownell et al., 1996). Soon after, Schreiber and colleagues utilized a potent HDAC inhibitor, trapoxin, as an affinity matrix for the purification of HDAC activity that they identified as a homolog of the yeast transcriptional co-repressor Rpd3 (Taunton et al., 1996). Taken together, these studies provided a direct link between gene regulation and the regulation of histone acetylation, prompting a new wave of research focused on the writers

and erasers of histone acetylation. With sequence homology searches to the mapped active sites of Gcn5 and Rpd3, dozens of new enzymes were identified and characterized, generally reinforcing the original discovery that HATs and HDACs are positive and negative transcriptional regulators, respectively. In a later section I will explore the HATs p300/CBP, as they are the most relevant to my thesis work. HDACs will be discussed later in Chapter 6.

The long-held mechanism for histone acetylation's positive role in transcription was considered to be due to the charge negation that occurs to the lysine residue upon acetylation, thus disrupting electrostatic interactions between the histone tails and the phosphate backbone of DNA leading to a looser configuration and increased accessibility to DNA-binding activators (cis-mechanisms). By observations with electron microscopy Woodcock and colleagues demonstrated that hyper-acetylated chromatin isolated from butyrate-treated cells did not form the compacted 30nm fiber observed in untreated cells (Annunziato et al., 1988). Wolffe and colleagues further demonstrated that histone acetylation facilitates transcription factor binding to nucleosomal DNA (Lee et al., 1993). These *in vitro* studies were corroborated by the previously mentioned ChIP studies by Crane-Robinson and colleagues showing that histone acetylation is found at sites of DNaseI hypersensitivity (Hebbes et al., 1994).

A distinct trans-mechanism for histone acetylation function was proposed by Zhou and colleagues when they demonstrated that the bromodomain of P/CAF, a human homolog of Gcn5, bound acetylated histone peptides (Dhalluin et al., 1999). Several of the newly discovered HATs contained a conserved protein domain called the bromodomain also present in a number of transcriptional regulators, such as Brm/Brg, Swi/Snf, and TAF1 (Haynes et al.,

1992; Jeanmougin et al., 1997). While its function remained unclear, the bromodomain was proposed to function as an interaction domain with chromatin, potentially facilitating recruitment and localization. Zhou and colleagues proposed that histone acetylation could generate docking platforms for effector proteins in a similar way previously observed for SH2-domains and tyrosine phosphorylation. Multiple reader domains have now been identified for the major classes of histone PTMs, including acetylation, methylation, and phosphorylation exhibiting exquisite site and modification type sensitivity and are now considered a major mechanism of histone PTM function (Patel and Wang, 2013). By 2000 a concise model for the regulation and function of histone acetylation was established (**Figure 1.3**).

In the early 2000's genome-wide profiles of histone acetylation were generated by ChIP followed by microarray analysis (ChIP-on-chip), which showed that acetylation marked active regions of the yeast and fly genome (Kurdistani et al., 2004; Schübeler et al., 2004). Higher resolution array data revealed that histone acetylation marked the promoters and distal regulatory elements of active genes (Pokholok et al., 2005; Roh et al., 2005). Following the increased output and efficiency of high-throughput sequencing ChIP-seq became the dominant technique for mapping histone modifications at high-resolution. ChIP-seq of histone acetylation has led to the high-confidence mapping of enhancers in a number of cell types (Creyghton et al., 2010; Heintzman et al., 2009; Rada-Iglesias et al., 2011) and has led to the discovery of novel classes of regulatory elements involved in the regulation of key developmental genes (Parker et al., 2013; Whyte et al., 2013) and aberrant activation of oncogenic transcription factors (Lovén et al., 2013; Mansour et al., 2014).

As foreshadowed by studies with butyrate and other synthetic HDAC inhibitors, the chemical inhibition of writers, readers and erasers of histone PTMs in the treatment of cancer is a topic of major interest and promise (Cai et al., 2015; Dawson and Kouzarides, 2012). The HDAC inhibitor, vorinostat, was clinically approved in 2006 for the treatment of T cell lymphoma. Since then, other HDAC inhibitors have been approved or are in clinical trial for the treatment of various malignancies (Falkenberg and Johnstone, 2014). Following impressive preclinical data (Delmore et al., 2011; Filippakopoulos et al., 2011) small molecule inhibitors of the bromodomain proteins, particularly inhibitors of the BET family, are currently in clinical trial for treatment of NUT midline carcinoma and various hematological malignancies (Filippakopoulos and Knapp, 2014). Furthermore, recurrent mutations in the writers, readers, and erasers of histone acetylation and other histone PTM have been found in a number of patient derived tumors (Plass et al., 2013), establishing chromatin regulators as a major class of drug targets in the treatment of cancer.

### **The Transcriptional Co-Activator p300/CBP**

Before being characterized as a HAT, p300 was identified as a binding partner of the adenovirus oncogene E1A and was shown to be required for the activity of certain enhancer elements (Eckner et al., 1994). Independently, CBP was identified as a cyclic-AMP and phosphorylation dependent binding partner of the transcription factor CREB with a role in transcriptional activity (Chrivia et al., 1993). Once both factors were cloned and sequenced it became clear that p300 and CBP were highly related proteins with shared sequence and function (Arany et al., 1994). Given their role as transcriptional co-activators and integrators of

signal-dependent transcriptional activity (Chakravarti et al., 1996; Kamei et al., 1996), knockout of either CBP or p300, even heterozygous null of either gene, led to embryonic lethality in mice (Yao et al., 1998). In 1996, stoked by the identification of GCN5 as a HAT, two independent groups reported that CBP/p300 have intrinsic HAT activities, further highlighting the direct link between histone acetylation and transcriptional activation (Bannister and Kouzarides, 1996; Ogryzko et al., 1996). p300/CBP were shown to interact with a wide range of transcriptional activators (Shikama et al., 1997) and their HAT activities were also shown to be involved in activation of enhancer elements. Notably, studies utilizing the beta-interferon enhancer demonstrated a critical role for the recruitment of p300/CBP via specific interactions with the p65 subunit of NF- $\kappa$ b and ordered histone acetylation followed by chromatin remodeling and promoter unmasking (Agalioti et al., 2000; Merika et al., 1998). These cell-based assays could not directly establish the role of p300's histone acetylation per se in the activation of transcription as most of the observations were based on correlative and associative observations. Furthermore, it was reported that p300 also acetylated non-histone factors, such as p53, with functional consequences, calling into question whether histone tails were the direct functional targets of acetylation (Gu and Roeder, 1997).

Direct testing came with the development of cell-free transcription assays utilizing a DNA template chromatinized with recombinant histones and purified factors, allowing for elegant and precise experimentation. In studies utilizing the synthetic activator Gal4-VP16, maximal RNA synthesis was shown to require the activator, p300, and acetyl-CoA (Kundu et al., 2000). Furthermore, by using recombinant histones with lysine to arginine mutations, the transcription

reaction was shown to be dependent on the acetylation of specific lysine residues on the histone tails (An et al., 2002), directly demonstrating that p300-catalyzed histone acetylation was critical for transcriptional activation.

The current model presents an ordered recruitment of transcription factors (DNA-binding activators) that in turn recruit p300 and other co-activators allowing for histone modifications and remodeling, which facilitate the recruitment and stabilization of the transcription apparatus through protein-DNA (activator-DNA), protein-protein (activator-co-activator), and protein-PTM (reader-histone) interactions (**Figure 1.3**). More recently, Gerschbach and colleagues demonstrated that targeting the minimal HAT domain of p300 to specific genomic loci activated the expression of target genes in a HAT-dependent manner (Hilton et al., 2015). Intriguingly, the activation mediated by p300 was more substantial than the activation induced by targeting a potent synthetic activator domain (VP64), suggesting that histone acetylation may be sufficient to nucleate the assembly of the transcriptional apparatus and activation of transcription.

### **Metabolic Regulation of Histone Acetylation**

Histone PTMs, including histone acetylation, are part of a complex regulatory process that establishes gene expression programs during development and disease. Strikingly, almost all histone-modifying enzymes require metabolites as essential co-factors, suggesting a link between these two pathways. The histone methyl-transferases require S-adenosyl-methionine (SAM), a product of one-carbon metabolism. The histone demethylases require either alpha-ketoglutarate, an intermediary product in the citric acid cycle, or flavin adenine dinucleotide

(FAD), a redox cofactor. The sirtuin class of deacetylases requires nicotinic adenine dinucleotide (NAD<sup>+</sup>), a redox cofactor. And most relevant to my studies, the histone acetyltransferases require acetyl-CoA, a central metabolite in the citric acid cycle, fatty acid metabolism, and cholesterol biosynthesis.

The regulation of enzymatic activity by the concentration of its cofactors requires that the  $K_m$  of the enzyme be in range of the natural fluctuations of the cofactor within the cell. For example, phosphorylation catalyzed by protein kinases is not thought to be regulated by the cellular concentration of ATP, as this concentration is tightly regulated and well above the typical  $K_m$  for a given kinase (Kaelin and McKnight, 2013). On the other hand, a series of landmark studies have established that levels of acetyl-CoA are within the range to influence histone acetylation (Fan et al., 2015; Su et al., 2016). The nuclear concentration of acetyl-CoA in cells grown in culture is estimated at 2-13 $\mu$ M (Lee et al., 2014) placing it below the  $K_m$  of several mammalian HATs, such as p300. These accurate measurements of subcellular acetyl-CoA are fairly new and most of the literature has used levels of histone acetylation as proxy measurement of acetyl-CoA concentrations.

Several studies in *S. cerevisiae* have illustrated the role of nuclear-localized synthesis of acetyl-CoA in the regulation of histone acetylation and thereby gene expression. Boeke and colleagues demonstrated that the acetyl-CoA used for histone acetylation was generated locally in the nucleus by Acetyl-CoA Synthetase (Acs2). This enzyme charges acetate to free CoA in an ATP-dependent reaction. They demonstrated that Acs2 was predominantly nuclear-localized and that knockout of Acs2 led to a reduction in global histone acetylation and a downregulation of ~70% of all genes assayed by microarray

(Takahashi et al., 2006). This work linked a metabolic enzyme to the regulation of gene expression, but it was unclear whether acetyl-CoA concentrations fluctuated in a regulated manner that could be exploited by gene regulatory networks.

Yeast grown in the nutrient-limiting environment of a chemostat spontaneously enter a synchronized cycle where they go through robust oscillations in metabolism and gene expression (Tu et al., 2005). Tu and colleagues showed that during these cycles the levels of acetyl-CoA fluctuate rhythmically, increasing and peaking as the cell enters the growth phase. These acetyl-CoA peaks were coincident with peaks in global histone acetylation and in the local acetylation at promoters of critical growth-related genes, which they found to be dependent on Gcn5 (Cai et al., 2011). They concluded that these 6-fold shifts in the concentration of acetyl-CoA and the concomitant histone acetylation represented a metabolic signal to the cell to induce cell growth and proliferation. These studies in yeast demonstrated that concentrations of acetyl-CoA can regulate histone acetylation and that the natural fluctuations of acetyl-CoA are sufficient to control this process.

While single cell eukaryotes rely on acetate as the major source of acetyl-CoA, metazoans use glucose as their main carbon source and have minimal exposure to extracellular acetate. While mammalian cells have a homolog of Acs2 (ACSS2) they have evolved a novel pathway for generation of cytosolic and nuclear acetyl-CoA by conversion of glucose-derived citrate to acetyl-CoA. This reaction is catalyzed by ATP-Citrate Lyase (ACL), an enzyme Wellen and colleagues established as the dominant source of acetyl-CoA used for histone acetylation (Wellen et al., 2009). Wellen and colleagues demonstrated that

glucose availability affected histone acetylation in an ACL-dependent manner and that knockdown of ACL reduced global histone acetylation. Furthermore, they established that ACL, and not ACSS2, is required for dynamic histone acetylation in response to growth factor signaling and adipocyte differentiation. These studies demonstrated that nutrient availability regulates histone acetylation and thereby regulates gene expression programs involved in differentiation and environment sensing (Wellen et al., 2009).

As demonstrated by Wellen and colleagues, for mammalian cells grown in culture, the concentration of acetyl-CoA in the nucleus and thereby histone acetylation is tied to the metabolic state of the cell through glucose (Everitts et al., 2013; Wellen et al., 2009) (**Figure 1.4**). Glucose is converted into pyruvate through the process of glycolysis. Pyruvate is transported into the mitochondria where it is converted to acetyl-CoA in an irreversible reaction by the pyruvate dehydrogenase (PDH) complex. The acetyl-CoA generated by PDH in the mitochondria has no active transport out of the mitochondria, is too large for passive diffusion across the mitochondrial double membrane, and is therefore effectively trapped and ready to fuel the tricarboxylic acid (TCA) cycle. The first step of the TCA cycle is the condensation of acetyl-CoA and oxaloacetate by citrate synthase to yield citrate and free CoA-SH. Citrate can be transported out of the mitochondria through the tricarboxylate transport system. ACL can then convert citrate into acetyl-CoA, in a reversal of the citrate synthase reaction. This ACL-derived acetyl-CoA can then be used for fatty acid synthesis (via Acetyl-CoA Carboxylase, ACC1), cholesterol synthesis (via acetyl-CoA acetyltransferase, ACAT), or as the high-energy donor of acetyl to histone lysine acetylation (via p300 and other HATs) (**Figure 1.4**). A recent study found that

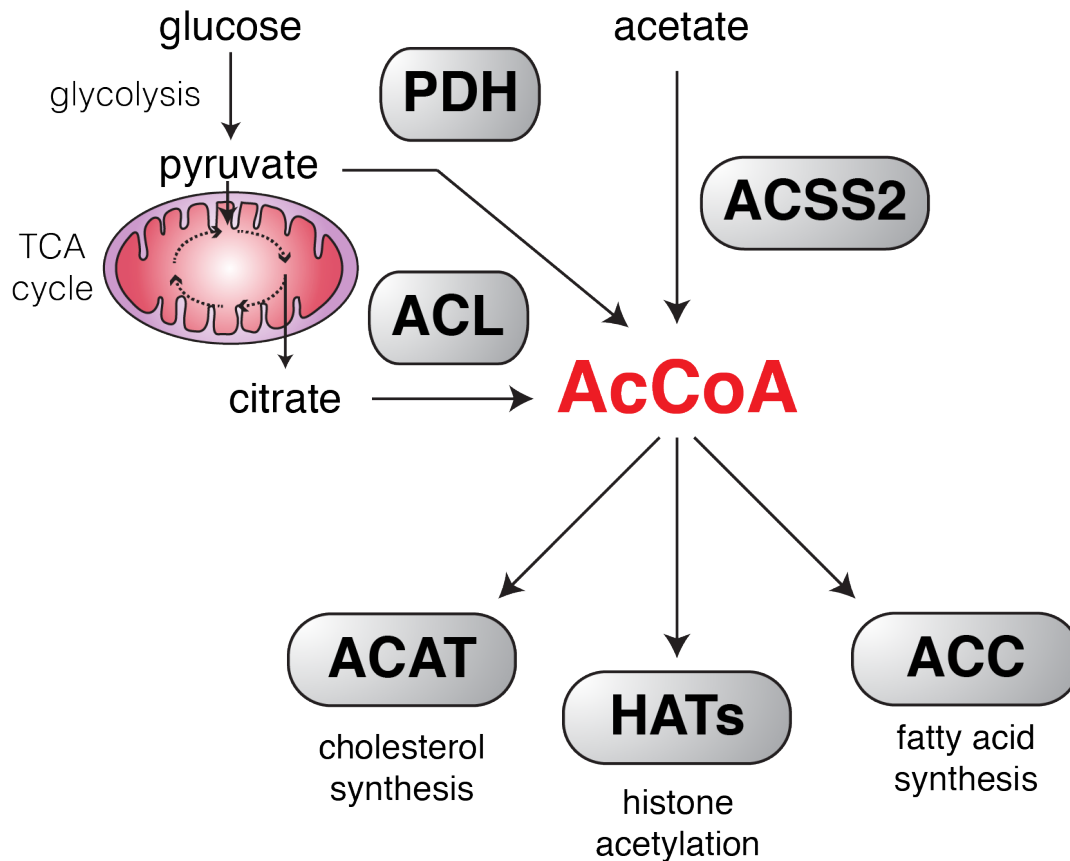


**Figure 1.4: Cytosolic and Nuclear Metabolism of Acetyl-CoA.**

Simplified schematic of pathways involved in acetyl-CoA (AcCoA) synthesis and catabolism in the mammalian cyto/nuclear compartment. For mammalian cells in culture, the main source of cyto/nuclear acetyl-CoA is through TCA-cycle generated citrate that is converted to acetyl-CoA by ACL. The majority of these carbons originate as glucose, but the degradation of fatty acids and amino acids can also contribute (not drawn). Stress-induced PDH translocation out of the mitochondria can bypass the TCA cycle by converting cyto/nuclear pyruvate directly into acetyl-CoA. Acetyl-CoA can also be generated from acetate by ACSS2. Three major pathways utilize cyto/nuclear acetyl-CoA: cholesterol biosynthesis, fatty acid synthesis, and protein acetylation. The enzymes that initiate each pathway are indicated: Acetyl-CoA Acetyltransferase (ACAT), Histone Acetyltransferase (HAT), and Acetyl-CoA Carboxylase (ACC).

under stress the PDH complex could translocate into the nucleus where it would generate acetyl-CoA used for histone acetylation directly from pyruvate, bypassing the mitochondria (Sutendra et al., 2014). As in yeast, acetyl-CoA can also be generated by the cyto/nuclear localized acetyl-CoA synthetase (ACSS2) by charging acetate with free CoA-SH in an ATP-driven reaction. The ACL reaction is favored during energy rich states (Wellen et al., 2009) whereas the ACSS2 reaction is necessary under hypoxic conditions (Comerford et al., 2014).

These two pathways are not mutually exclusive and can complement each other. For example, under conditions of depleted ACL, addition of excess acetate can rescue the levels of histone acetylation in an ACSS2-dependent manner (Wellen et al., 2009). These data suggest that both enzymes feed into the same pool of acetyl-CoA, but that under different growth conditions the dominance of either enzyme changes. My thesis work implicates ACSS2 in the generation of crotonyl-CoA used for histone crotonylation, even in normal growth conditions, suggesting that ACSS2 might have secondary roles in regulating acyl-CoA metabolism under high glucose conditions. Furthermore, aberrant phosphorylation of ACL by constitutively active AKT allows for the continuous production of acetyl-CoA even under nutrient limiting states (Lee et al., 2014), which could explain the epigenomic reprogramming observed in tumors with oncogenic Kras and Akt.

### **Histone Crotonylation**

With high-sensitivity mass spectrometry several groups have profiled the histone acetylation landscape (Choudhary et al., 2009; Kim et al., 2006) demonstrating the general importance of protein acetylation on non-histone substrates.

Thousands of acetylation sites on hundreds of proteins have now been identified, making lysine acetylation a globally important PTM with function outside the nucleus (Choudhary et al., 2014; Verdin and Ott, 2014). Another outcome of these proteomic studies has been the discovery of a range of novel modifications. The major novel class of histone modifications described has been lysine acylations, similar in  $\epsilon$ -amine linkage to lysine acetylation yet distinct in the hydrocarbon chain attached (**Figure 1.5**). Dr. Yingming Zhao, himself a graduate of The Rockefeller University, and his colleagues at The University of Chicago have been at the forefront of identifying these novel histone acylations and have so far identified propionylation, butyrylation (Chen et al., 2007), 2-hydroxyisobutyrylation (Dai et al., 2014), succinylation, malonylation (Xie et al., 2012), and crotonylation (Tan et al., 2011) (**Figure 1.5A**).

The identification of histone lysine crotonylation came out of a systematic approach to identify novel histone PTMs by tandem mass spectrometry (MS/MS) (Tan et al., 2011). The covalent modification of histone protein leads to a characteristic mass shift that can be identified by MS/MS and parsed by computational methods. In their analysis, Zhao and colleagues identified peptides with a mass shift of +68 Da, which did not correspond to any known histone PTM. Through a series of deductions they determined that the additional 68 Da was likely due to the modification of lysine residues by crotonyl (trans-2-butenyl). By comparing peptides extracted from histones with peptides synthesized to include crotonyl-lysine (Kcr), they demonstrated that the two had the same mass spectra and co-eluted off an HPLC column, suggesting that the +68 Da shift they observed was most likely due to crotonyl-lysine.

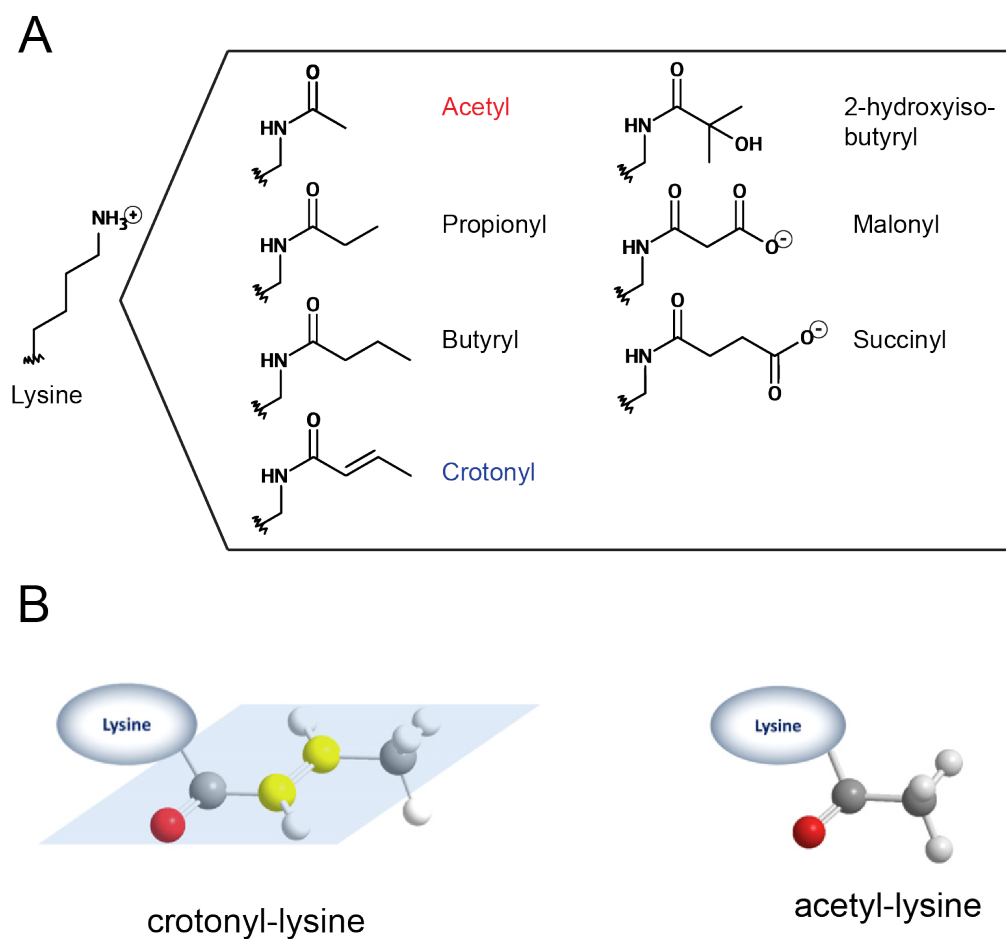


**Figure 1.5: Diversity of Histone Lysine Acylation.**

(A) Chemical structures of all currently identified histone lysine acylations. (B) Three-dimensional representation of crotonyl-lysine and acetyl-lysine. Note that while acetyl-lysine is free to rotate, crotonyl-lysine has a rigid planar orientation (represented by light blue plane) due to the presence of C-C  $\pi$ -bond. Figure 1.5B is adapted from (Tan et al., 2011).

The Zhao group next generated and validated a pan-Kcr antibody, which stained histones extracted from human, mouse, worm, fly, and yeast cells. Furthermore, this immunoblot signal was competed away by a library of Kcr peptides, but not by a library of acetyl-lysine (Kac) peptides, demonstrating that Kcr was a conserved histone modification. Using the pan-Kcr antibody Zhao and coworkers performed ChIP-seq in IMR90, a well-characterized human fibroblast line. Kcr was enriched at promoters and putative enhancer elements of active genes generally coincident with Kac. Like Kac, levels of Kcr generally correlated with gene expression.

To explore the role of Kcr in a biological setting Zhao and colleagues characterized the modification in the highly dynamic spermatogenesis process. They performed ChIP-seq for Kcr in pre-meiotic spermatocytes (Spc) and in post-meiotic round spermatid (RS) and observed a similar patterning of Kcr as in IMR90, marking promoters and enhancers. When they compared levels of Kcr in Spc and RS they observed that the set of genes that had increased Kcr signal through meiosis tended to be highly expressed testis genes, suggesting that Kcr marked testis-specific genes. Furthermore, about a third of these genes resided on the X chromosome, an enrichment not observed with ChIP-seq with pan-Kac. During the transition between Spc and RS, the X-chromosome is known to undergo meiotic sex chromosome inactivation (MSCI), which leads to heterochromatin formation over the sex chromosomes, yet some genes “escape” silencing. Zhao and colleagues’ data suggested that Kcr marked these “escapee” genes. This prompted them to perform immunohistochemistry on tissue enriched for RS, which exhibit MSCI, with pan-Kcr and markers for heterochromatin. This analysis demonstrated that Kcr signal marked small

sections of the heterochromatic X-chromosome. This localization was not observed with Kac staining. They conclude that Kcr may play an important role in epigenetically marking sex chromosomes in the post-meiotic stages of spermatogenesis (Tan et al., 2011). Several manuscripts have been published since the original discovery of histone Kcr in 2011, I will introduce them and discuss their findings within the relevant chapters of my thesis.

The manuscript describing the discovery of Kcr (Tan et al., 2011) was published just as I had joined the Allis lab for my graduate work. I was intrigued by the unique properties reported for Kcr in spermatogenesis and was also excited by the potential for discovery inherent in the novelty of the subject. I was motivated to characterize this novel histone PTM within the paradigm set forth by the studies conducted with histone acetylation. In my Thesis Research Proposal, written at the start of my graduate work, I proposed to study the regulation and function of histone crotonylation by identifying and characterizing the writers (Chapter 2), readers (Chapter 5), and erasers (Chapter 6) of the newly discovered histone PTM. Through these originally proposed experiments I uncovered an unexpected role for acyl-CoA metabolism in the regulation of histone Kcr and its impact of gene activation (Chapters 3 and 4).

Portions of Chapters 2-4 have been published as:

Sabari, et al. (2015). Intracellular Crotonyl-CoA Stimulates Transcription through p300-Catalyzed Histone Crotonylation. *Molecular Cell* 58, 203–215.

Portions of Chapter 5 are currently under review as:

Li, Sabari, Panchenko, et al. (2016). Molecular Coupling of Histone Crotonylation and Active Transcription by AF9 YEATS Domain. *Molecular Cell* (*in review*)

## CHAPTER 2: PURIFICATION OF A HISTONE CROTONYLTRANSFERASE ACTIVITY AND CHARACTERIZATION OF ITS ROLE IN TRANSCRIPTION

### INTRODUCTION

Histones are subject to a vast range of post-translational modifications with specific genomic localizations and well-documented functional roles in the regulation of transcription and other DNA-templated processes. Critical to our understanding of how histone modifications are regulated has been the identification and characterization of enzyme systems that catalyze the covalent modification of specific target residues. Histone lysine acetylation has been particularly well characterized within this paradigm, with the purification and identification of histone acetyltransferases prompting a breakthrough in our understanding of targeted lysine-acetylation's direct role in gene regulation (Brownell et al., 1996). Despite this progress, little is known about the cellular regulation and functional relevance of a rapidly-expanding group of chemically related modifications known as histone acylations, of which acetylation is a well-studied member.

Histone lysine propionylation, butyrylation, malonylation, succinylation, 2-hydroxyisobutyrylation, and crotonylation have all been identified by tandem mass spectrometry (MS/MS) proteomic analysis over the past several years (Chen et al., 2007; Dai et al., 2014; Tan et al., 2011; Xie et al., 2012) (**Figure 1.5**). These discoveries have increased the potential complexity of histone lysine modifications and have prompted interest in the functional consequence of differential acylation, both on histone proteins and non-histone proteins.

Previous ChIP-seq analyses with “pan” acyl-specific antibodies have mapped histone crotonylation and histone 2-hydroxyisobutyrylation to regulatory elements of actively transcribed regions of the genome, generally coincident with the localization of histone acetylation (Dai et al., 2014; Tan et al., 2011). These studies demonstrate that histones flanking active regulatory elements are modified by a number of chemically distinct acylations, suggesting a role for these modifications in transcriptional regulation. Yet, the enzymes responsible for catalyzing crotonylation of histone lysine residues have not been characterized. Here I report the partial purification of a histone crotonyltransferase (HCT) activity from HeLa S3 nuclear extract by column fractionation. I show that the well-studied transcriptional co-activator and histone acetyltransferase (HAT) p300 also possesses histone crotonyltransferase (HCT) activity. In collaboration with Dr. Zhanyun Tang of the Roeder lab, we demonstrate that p300-catalyzed histone crotonylation directly stimulates transcription and does so to a greater degree than p300-catalyzed histone acetylation.

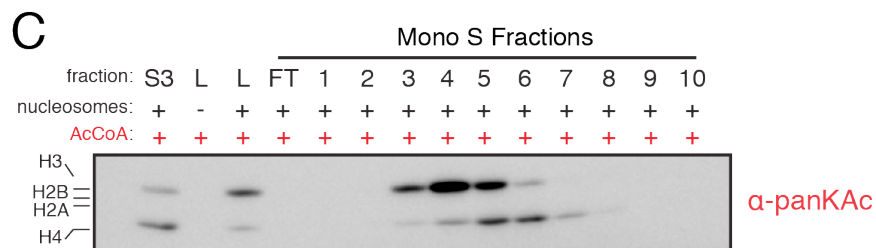
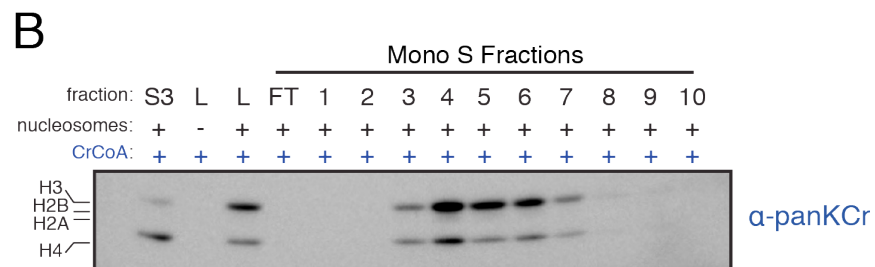
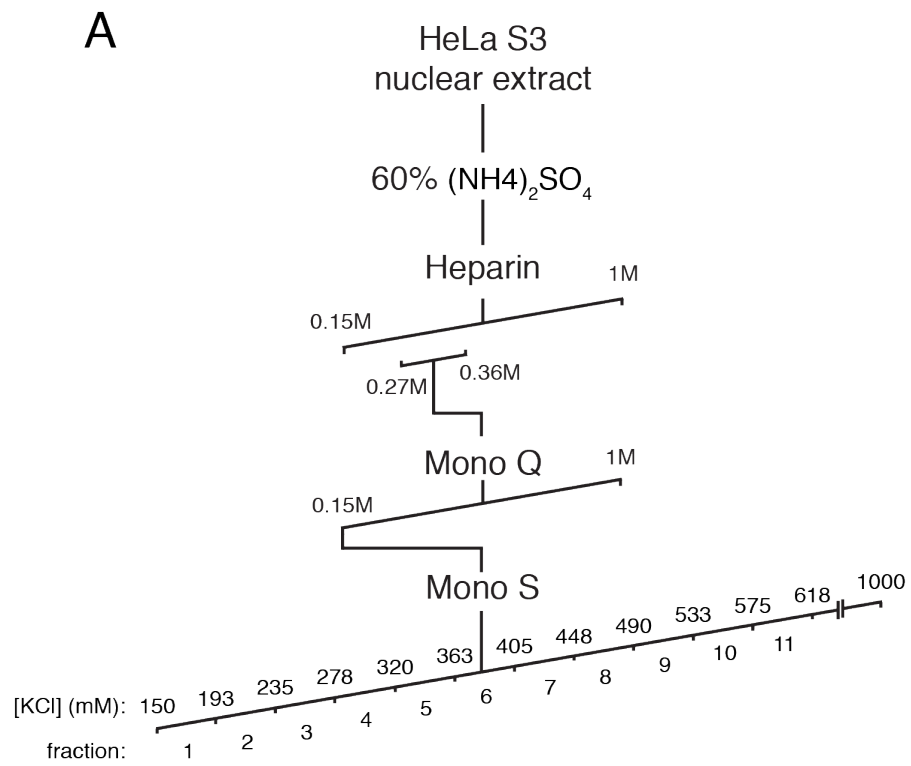
## **RESULTS**

### **HAT and HCT Activities Co-Purify with p300 from HeLa S3 Nuclear Extract**

To identify enzyme(s) capable of catalyzing histone crotonylation, I sought to purify a histone crotonyltransferase (HCT) activity from HeLa S3 nuclear extracts. I employed an HCT assay that mirrors previously described histone acetyltransferase (HAT) assays (Mizzen et al., 1999), except that crotonyl-CoA, rather than acetyl-CoA was used as the high-energy acyl-donor, and

**Figure 2.1: Purification of an HCT Activity.**

(A) HCT purification scheme. (B-C) HCT activity co-elutes with HAT activity. HCT and HAT activities were assayed by panKCr or panKAc immunoblot, respectively, at each round of fractionation and peak HCT activity was followed. The immunoblot readouts for HCT (B) and HAT activity (C) of the final Mono S fractions are shown here. S3 indicates crude unfractionated extract, L indicates the load/Mono S input, and FT indicates the column flow through. Equal volumes of each fraction were used in these assays. For MS/MS analysis of fractions with peak HCT activity (fractions 4, 5, and 6) see Figure 2.2.



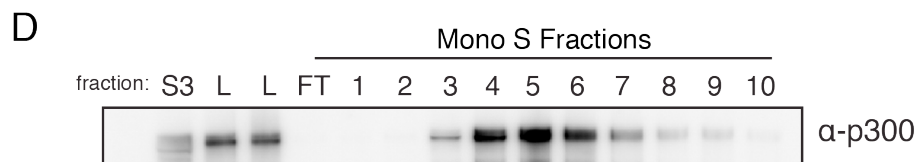
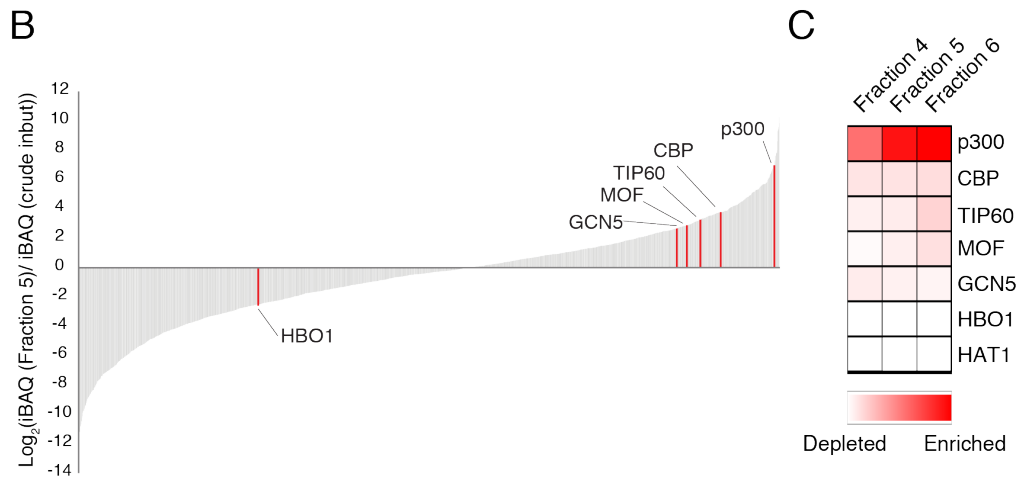
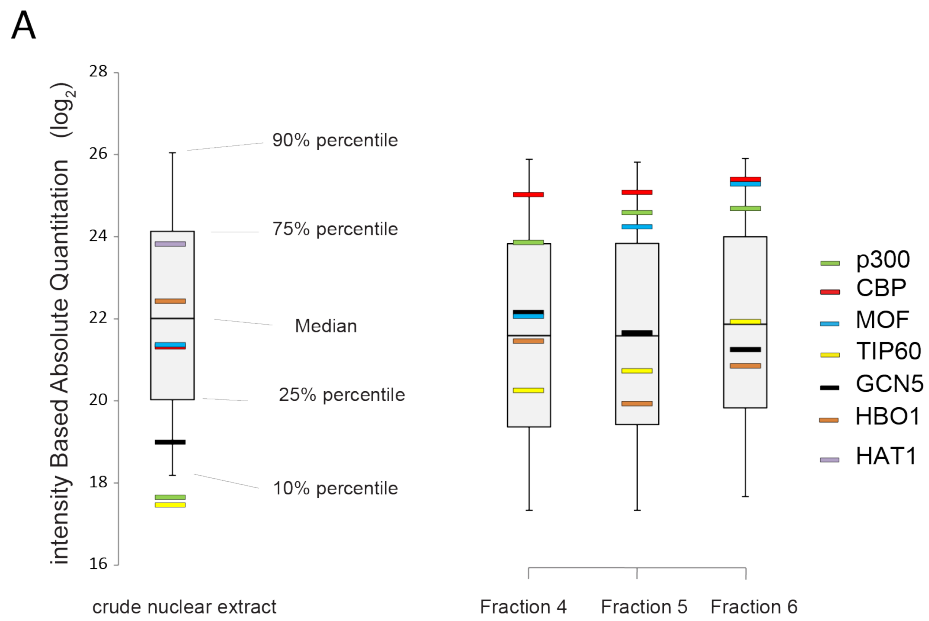
immunoblotting of reaction products with a pan-crotonyl-lysine antibody (panKCr) was used as a measure of HCT activity. In parallel, HAT activity was determined by substituting acetyl-CoA in the reactions and immunoblotting reaction products with a pan-acetyl-lysine antibody (panKAc). Utilizing these assays, HCT activity was detected in crude HeLa S3 nuclear extracts and partially purified by the fractionation scheme outlined in **Figure 2.1A**. Briefly, a soluble nuclear extract was prepared from HeLa S3 cells grown in suspension (see Methods for details), which was subject to a 60%  $(\text{NH}_4)_2\text{SO}_4$  cut, followed by a three step column fractionation over a linear gradient of KCl (0.15M-1M). HCT assays were performed on collected fractions and those presenting HCT activity were pooled and subject to the next round of fractionation. Unexpectedly, HAT activity co-purified with HCT activity through multiple purification steps, including the final step in the partial purification scheme (**Figures 2.1B and 2.1C**). Co-elution of these two activities, albeit with subtle differences toward H3 and H4, suggested either that distinct HAT and HCT activities co-eluted throughout this purification or, unexpectedly, that a “HAT” might be responsible for the observed HCT activity.

To identify proteins that were enriched during the purification of the HCT activity, I worked with Dr. Henrik Molina, the director of The Rockefeller University Proteomics Facility. Dr. Molina subjected peak Mono S fractions 4-6, and the crude nuclear extract (fraction “S3”) to MS/MS analysis (see Methods for details). Our analysis focused on identifying proteins that had been significantly enriched over the course of the purification scheme. Seven previously described HATs were identified with high confidence in the crude nuclear extract, p300, CBP, MOF, TIP60, GCN5, HBO1, and HAT1. Interestingly, five of these HATs

**Figure 2.2: Proteomics Analysis of Partially Purified HCT Activity.**

(A) Box and whisker plot representation of Intensity Based Absolute Quantification (iBAQ) values for all proteins identified in the crude nuclear extract, and in the three Mono S fractions with peak HCT activity (fractions 4, 5, and 6). Calculated iBAQ values for all observed HATs (p300, CBP, MOF, TIP60, GCN5, HBO1, HAT1) are plotted onto the box plots. All shown HATs were confidently matched with between 7 and 46 unique peptides. (B) Enrichments of iBAQ values for Fraction 5 over crude nuclear extract for all observed proteins are plotted as  $\log_2$  values. The observed HATs are highlighted in red. (C) Heatmap representation of the relative iBAQ value enrichment or depletion over crude nuclear extract of the seven observed HATs in Mono S fractions 4, 5, and 6. (D) Immunoblot for p300 in indicated fractions. S3 indicates crude unfractionated extract, L indicates the load/Mono S input, and FT indicates the column flow through. Equal volumes of each fraction were assayed.

The data and analysis presented in Figures 2.2A-2.2C were generated by Dr. Henrik Molina.



were enriched over crude nuclear extract in all three peak-fractions, while HBO1 and HAT1 were depleted. HAT1 went from being the most abundant HAT in crude extract to being below the detection limit in all three peak-fractions. Of all the HATs present in the final fractions, the transcriptional coactivator p300 was the most enriched (**Figure 2.2A**). Based on Intensity Based Absolute Quantitation (iBAQ) values (Schwanhäusser et al., 2011), p300 went from being among the 10% least abundant of all detectable proteins in the crude extract to being among the 20% most abundant of all detectable proteins in the Mono S fraction 5. Utilizing iBAQ values, Dr. Molina assigned an enrichment value for each protein identified in the peak HCT fraction (fraction 5) defined as  $iBAQ(\text{fraction 5}) / iBAQ(\text{crude input})$ . By plotting this enrichment value for all detected proteins, we observed that p300 is among the most enriched proteins and the most enriched HAT in fraction 5 (**Figure 2.2B**). Furthermore, p300 is the most enriched HAT in all three peak-HCT fractions (**Figure 2.2C**). In support of the MS/MS data, immunoblot of the Mono S fractions for p300 showed that the protein is markedly enriched from nuclear extracts through the purification of HCT activity (compare S3 to Mono S fraction 5 in **Figure 2.2D**). These data highlight p300 as a strong candidate for the enzyme responsible for HCT activity observed in my partially purified nuclear extract.

### **p300 has HCT Activity *In Vitro* and In Cells**

To directly test whether p300, or any of the other HATs enriched by our HCT purification, have intrinsic HCT activity, I purified recombinant p300, GCN5, TIP60, and MOF, and assayed their capacity to crotonylate and/or acetylate recombinant histone octamers by our previously described HCT and HAT

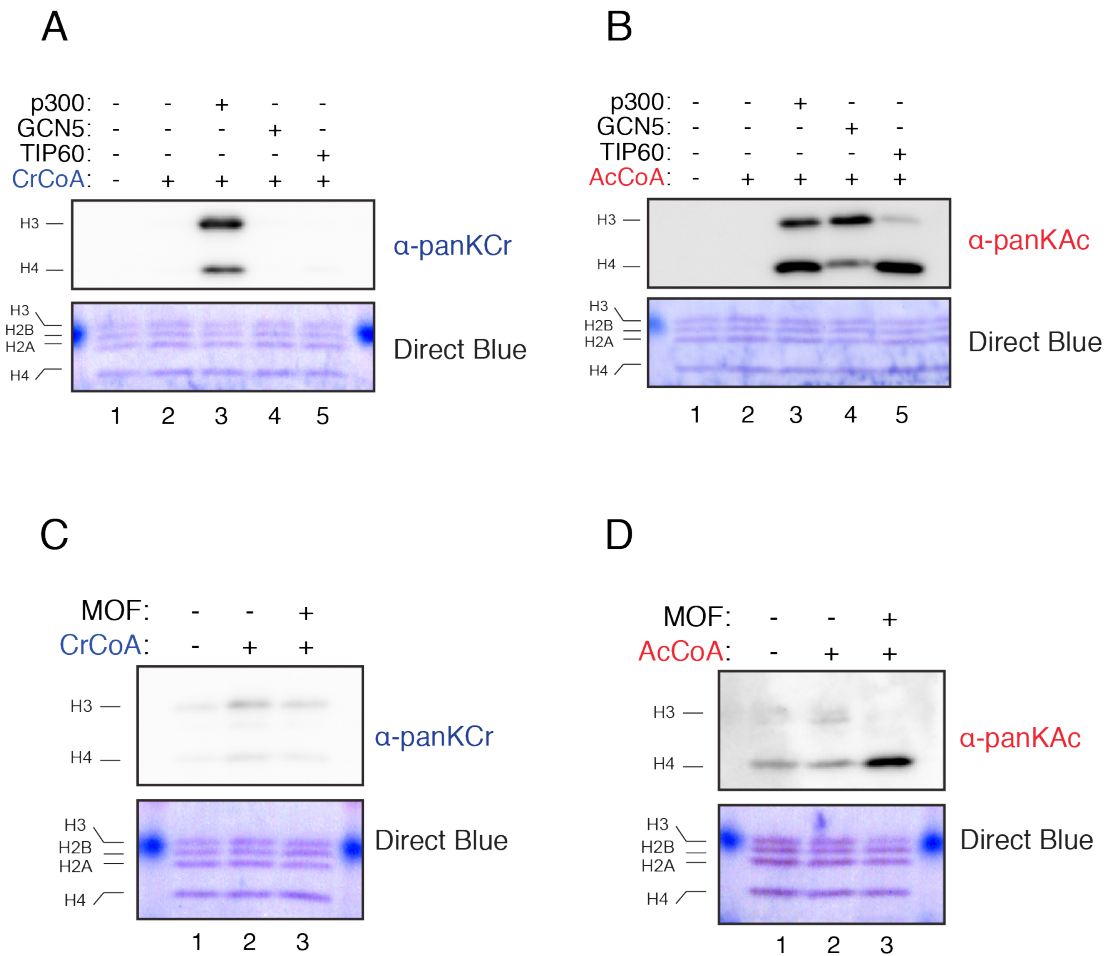


**Figure 2.3: p300 Has Intrinsic HCT activity.**

HATs identified as being enriched during the HCT purification (p300, GCN5, TIP60, and MOF) were purified as recombinant proteins and used as enzyme source in HCT and HAT activity assays. (A) HCT activity assay with purified recombinant p300, GCN5, and TIP60. (B) HAT activity assay with same proteins as in (A). (C) HCT activity assay with purified recombinant MOF. (D) HAT activity assay with purified recombinant MOF. All reactions were performed with recombinant histone octamers as substrate. Reaction products were immunoblotted with the indicated antibodies.

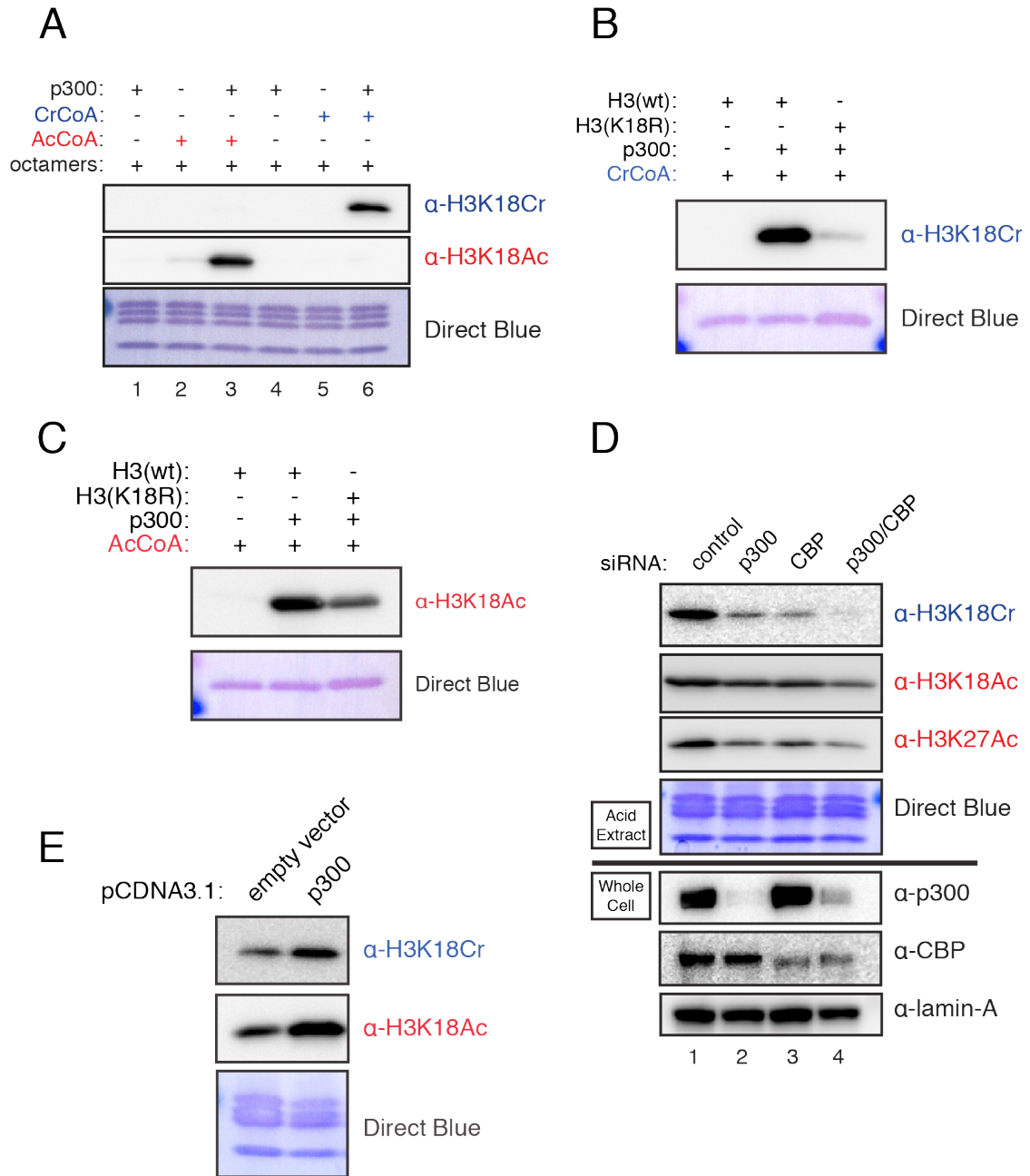
assays. While all of these recombinant enzymes exhibited their well-characterized HAT activities, only p300 showed measurable HCT activity (**Figure 2.3**). Taken together, these data suggest that p300 is most likely the responsible enzyme for the observed HCT activity derived from the purified nuclear extract.

To determine the principal sites of p300-catalyzed crotonylation and acetylation, I worked with Dr. He Huang in Dr. Yingming Zhao's Lab at the University of Chicago, experts in the proteomics of histone acylations. Using semi-quantitative MS/MS analysis of *in vitro* reaction products by spectral counting (Carvalho et al., 2008), they found that H3K18 is the dominant site of both p300 crotonylation and acetylation, under our reaction conditions (data not shown). To confirm activity on H3K18, I made use of available site-specific antibodies against H3K18Cr or H3K18Ac to probe p300-driven HCT and HAT reaction products. Each antibody reacted with its intended target and failed to cross-react with the unintended target, lending support to both our MS/MS data and the acetyl vs. crotonyl specificities of the antibodies (**Figure 2.4A**). To confirm the site-specificity of these antibodies, recombinant H3 with a H3K18R mutation was used as a substrate in p300-driven HAT and HCT assays. Signals from both H3K18Cr and H3K18Ac antibodies were attenuated on the p300-modified H3K18R mutant as compared to the wild type H3, further confirming the antibody site-specificities (**Figures 2.4B and 2.4C**).

I next sought to determine whether p300 regulates H3K18Cr in cells. Knockdown of p300 or its paralog CBP by siRNA reduced the global levels of H3K18Cr, H3K18Ac, and H3K27Ac and double knockdown of p300 and CBP reduced the signals even further, as measured by immunoblot of acid-extracted

**Figure 2.4: p300 Catalyzes H3K18cr.**

(A) p300-mediated HCT and HAT reactions were performed with the indicated reaction conditions. Reaction products were probed with the indicated site-specific antibodies. (B-C) Recombinant H3 with lysine 18 mutated to arginine (K18R) was used, in parallel with wild-type H3 (wt), as substrates in p300-driven HCT (B) or HAT (C) reactions. Products were immunoblotted with the indicated antibodies. (D) HeLa S3 cells were transfected with control or p300- and/or CBP-specific siRNA. 72 hours post-transfection, whole cell lysates and histones were prepared and immunoblotted with the indicated antibodies. Immunoblots of acid extracts are shown above the black line, while immunoblots of whole cell lysates are shown below the black line. (E) Overexpression of p300 in HEK 293T cells increases global levels of H3K18Cr and H3K18Ac. 293T cells were transfected with p300 cDNA. 48 hours post-transfection histones were prepared and immunoblotted with the indicated antibodies.



histones (**Figure 2.4D**). In addition, overexpression of full-length p300 by transient transfection increased both H3K18Cr and H3K18Ac signals (**Figure 2.4E**). Taken together these data support the conclusion that p300 (and its paralog CBP) catalyze both H3K18Cr and H3K18Ac *in vitro* and in cells.

### **p300-Catalyzed Histone Crotonylation Stimulates Transcription in a Cell-Free System**

To directly test whether p300-catalyzed histone crotonylation plays a role in transcriptional regulation, I worked with Dr. Zhanyun Tang. We took advantage of a cell-free transcription assay wherein the presence of either acetyl-CoA or crotonyl-CoA could be experimentally controlled. p300's HAT activity has long been implicated in activator-dependent stimulation of transcription from chromatinized templates in a reaction where maximal RNA synthesis is dependent upon p300 and acetyl-CoA (An et al., 2002). More recently, this assay has been modified to include natural activators, such as p53, and has been exploited to further our mechanistic understanding of transcriptional regulation in the context of chromatin (An et al., 2004; Tang et al., 2013).

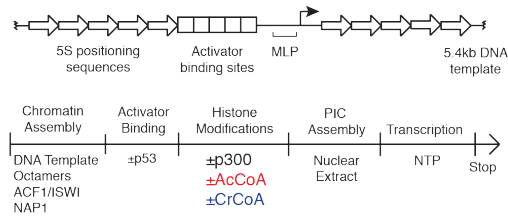
Similar experiments were conducted using a p53-dependent transcription assay, but with acetyl-CoA replaced by crotonyl-CoA (see schematic in **Figure 2.5A**). To ensure the integrity of these assays, I validated the purities of the acetyl-CoA and crotonyl-CoA by HPLC analysis, which showed that both cofactors were pure and showed no traces of cross-contamination (**Figure 2.5B**). Using the H3K18Cr and H3K18Ac antibodies, Dr. Tang confirmed crotonylation of the recombinant chromatin substrate by p300 and its p53-dependence in this system (**Figure 2.5C**). Dr. Tang next performed the transcription assay and

**Figure 2.5: Histone Crotonylation Stimulates Transcription.**

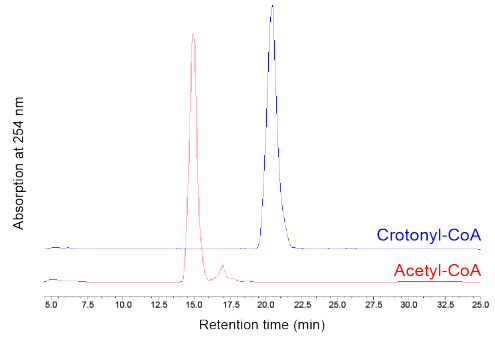
(A) Schematic of the transcription template (top) and the transcription reaction order of addition (bottom). (B) Acetyl-CoA or crotonyl-CoA were injected onto a C18 column and eluted over an acetonitrile gradient as previously described (King and Reiss, 1985). CoA molecules were detected by UV absorbance at 254 nm. (C) p300 HAT and HCT reactions using recombinant chromatin with the indicated additions were analyzed by immunoblot. (D) Transcription assays were performed under the indicated conditions. RNA products were visualized by autoradiography. (E) Densitometry of autoradiographs comparing acetyl-CoA and crotonyl-CoA containing transcription reactions. Data represent mean fold change from three independent experiments  $\pm$  standard deviation, p-value = 0.0013. (F) *In vitro* transcription assays using chromatin reconstituted with recombinant wild-type H3 or with lysine residues 9, 14, 18, 23, 27, 36, and 56 mutated to arginine (K-to-R). RNA products were visualized by autoradiography.

The data presented in Figures 2.5C-2.5F was generated by Dr. Zhanyun Tang.

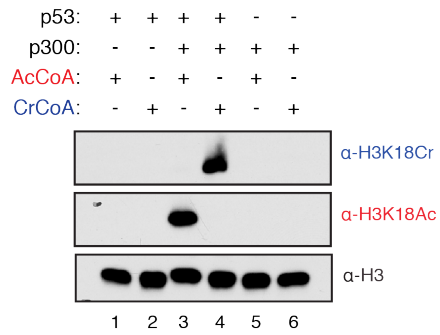
**A**



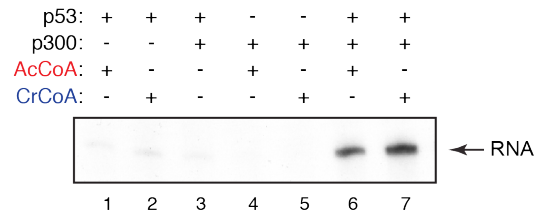
**B**



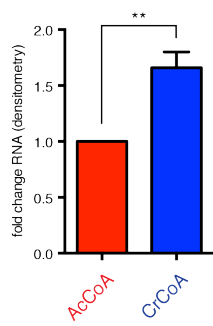
**C**



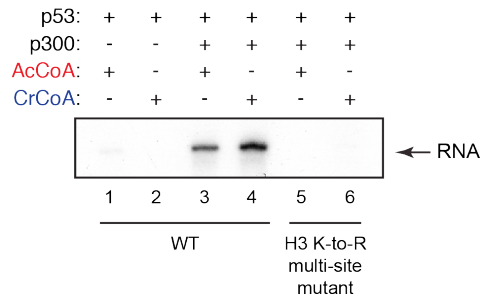
**D**



**E**



**F**



observed that p300-catalyzed crotonylation stimulated transcription in this system to a greater extent than did p300-catalyzed acetylation (**Figure 2.5D**). Under identical assay conditions, crotonyl-CoA containing reactions produced, on average, 1.66-fold greater transcript than did acetyl-CoA containing reactions, as measured by densitometry of autoradiograms from three independent experiments (**Figure 2.5E**).

To confirm that p300's crotonyltransferase activity stimulates transcription by crotonylation of histone proteins and not of auxiliary factors from the added nuclear extract, Dr. Tang reconstituted recombinant chromatin with either wild-type histone H3 or histone H3 with lysine residues 9, 14, 18, 23, 27, 36, and 56 mutated to arginine (K-to-R). For both acetylation and crotonylation, p300-driven RNA production was substantially inhibited when chromatin containing histone H3 K-to-R mutations was used as a template (**Figure 2.5F**), demonstrating that the acetylation or crotonylation of the mutated histone lysine residues is necessary for the production of transcript in this cell-free system. The modest, yet reproducible and statistically significant, difference between histone acetylation and histone crotonylation in the stimulation of transcription provided an early hint that p300-catalyzed histone acetylation and crotonylation are functionally distinct.

## **DISCUSSION**

Here I present data on the purification and characterization of p300 as a histone crotonyltransferase. In collaboration with the Roeder Lab, we demonstrate that p300-catalyzed histone crotonylation directly stimulates transcription. While previous sequencing based studies have shown that histone crotonylation

associates with transcriptionally active regions of the genome (Tan et al., 2011), the studies presented here demonstrate the direct role of histone crotonylation in transcription. Through cell-free experimentation in a controlled environment we were able to make these observations, which would have been difficult in the complex milieu of the cell. For example, early in the investigation of histone crotonylation, I observed that the pan-Kcr antibody exhibited an undefined cross-reactivity with histone acetylation that confounded many early results using this reagent (data not shown). These early observations led to cautious use of this antibody only in cases where it was clear that histone crotonylation was being detected, as in HAT and HCT activity assays where the only source of acetyl or crotonyl is from the added acyl-CoAs. The focus on p300 and the p300-catalyzed H3K18cr led to the adoption of the H3K18cr antibody, which I was able to carefully test and deem acyl-specific (**Figure 2.4A**, and unpublished results). These observations were critical for the next stage of experimentation, which dealt with the cellular regulation and function of p300-catalyzed histone crotonylation.

The HCT activity of p300 is unique among HATs assayed. p300, along with its paralog CBP, occupies a distinct class of HAT proteins based on primary sequence (Lee and Workman, 2007; Roth et al., 2001). Members of the other two major HAT families GNAT (GCN5) and MYST (TIP60 and MOF) exhibited their well-documented HAT activities but did not display HCT activity under the same reaction conditions. Interestingly, p300's HAT domain is structurally unique and utilizes a distinct catalytic method for acetyl transfer (Liu et al., 2008). While it is clear that p300 performs its HAT reaction through a distinct structure and catalytic mechanism, it remains unresolved what specifically allows p300 to

perform the HCT reaction while other HATs cannot. The p300 gene is mutated in a number of developmental disorders and cancers (Gayther et al., 2000; Pasqualucci et al., 2011; Roelfsema et al., 2005), mostly resulting in heterozygous truncation or inactivation. It remains unknown whether a particular mutation could alter p300's preference for acetyl-CoA or crotonyl-CoA, thereby altering its HAT and HCT activities. Another potential for the regulation of p300's HAT versus HCT activity would be conformational change due to signal-induced PTMs. While p300's HAT and co-activator activities are regulated by PTM of various type (auto-acetylation, phosphorylation, and arginine methylation) at various sites (Karanam et al., 2006; Lee et al., 2005; Yang et al., 2001), the effect of these modifications on HCT activity is unknown.

Given that p300 catalyzes both acetylation and crotonylation and barring the identification of a mutant or modified form that only catalyzes one or the other, initial functional characterization of p300's HCT activity was limited to cell-free systems where the presence or absence of acetyl-CoA or crotonyl-CoA could be controlled. The cell-free chromatinized-template transcription assay championed by the Roeder lab (An et al., 2002; 2004; Tang et al., 2013) was an obvious choice. By utilizing this recombinant chromatin template transcription assay, we show that p300-catalyzed histone crotonylation directly stimulated transcription to a greater degree than p300-catalyzed histone acetylation. Our study focused largely on H3K18 because of its identification as the dominant site of p300-driven crotonylation in our *in vitro* assays, the clear regulation of its global levels in mammalian cells by p300/CBP, and the availability of acyl-specific antibodies for this modification. It is currently unknown if one site or a minimal subset of these sites is responsible for the transcriptional stimulation

observed in our cell-free system. Since the multi-site H3 K-to-R mutations ablate this transcriptional response, I conclude that histone crotonylation per se is required for this response; but exactly how that response is mediated and how it may differ mechanistically from the stimulation associated with acetylation remains unclear. While the assays described here utilize purified DNA, histones, activator, and p300, a nuclear extract is added as a source of general transcriptional machinery. Therefore, the precise mechanism by which histone crotonylation is distinct from histone acetylation is not resolved by these experiments. A fully purified system, as detailed in (Guermah et al., 2006) would be necessary for a direct comparison of transcriptional activation observed in crotonyl-CoA containing reactions and acetyl-CoA containing reactions.

Lysine crotonylation, like other acylations, including acetylation, will neutralize the positive charge of the  $\epsilon$ -amino group of lysine, yet the “functional groups” of the various acylations are chemically distinct (**Figure 1.5**). For most acylations, as is the case for histone crotonylation, the difference from acetylation is in increased bulk and rigidity, but for malonylation and succinylation, the modification adds net negative charge to an existing positively charged lysine. It is currently unknown whether there are specific “readers” for crotonyl-lysine or the other histone acylations that take advantage of this increased bulk, rigidity, and/or negative charge, which would add functionality to these modifications through trans-effects. The surprising discoveries that methyl-lysine “readers” can distinguish mono-, di-, and tri-methylated lysines, a comparably small chemical difference compared to the diversity of acylations, provides precedent for such discrimination (Taverna et al., 2007). Identification and characterization of binding modules that selectively prefer crotonyl-lysine, or other acylations,

will be critical to our understanding of the mechanism by which differential histone acylation exerts function. Chapter 5 discusses collaborative work with Dr. Haitao Li (Tsinghua University; Beijing, China) on the characterization of the YEATS domain as a crotonyl-lysine reader.

In addition to the potential recruitment of reader or effector proteins, the cis-effects of various acylations on nucleosome or chromatin structure remains unexplored. Histone acetylation has been shown to directly influence both inter-nucleosomal structure (Robinson et al., 2008; Shogren-Knaak et al., 2006) and intra-nucleosomal structure (Tropberger et al., 2013) by charge neutralization. It is of interest to understand how the additional bulkiness, rigidity, or charge of the various acylations will directly affect nucleosomal or oligonucleosomal structures.

The studies presented in Chapter 2 establish that p300-catalyzes both histone acetylation and crotonylation and demonstrate a role for histone crotonylation in stimulating the transcription reaction. The observations of p300's dual activity immediately suggested that the levels of histone crotonylation would be determined by the concentration of crotonyl-CoA and acetyl-CoA, the subject of Chapter 3.

## CHAPTER 3: THE RELATIVE CONCENTRATIONS OF CROTONYL-COA AND ACETYL-COA REGULATE GLOBAL HISTONE CROTONYLATION

### INTRODUCTION

As described in Chapter 2, I identified that p300, a previously described HAT and transcriptional co-activator, also has HCT activity, yet it remained unclear how histone crotonylation could be regulated differently than histone acetylation. Given that the various histone acylations (acetylation, propionylation, butyrylation, crotonylation, etc.) are derived from their respective charged acyl-CoAs (acetyl-CoA, propionyl-CoA, butyryl-CoA, crotonyl-CoA, etc.), which populate various arms of intermediary metabolism, it has been proposed that differential histone acylation could be regulated by the cellular concentration of these metabolites and thereby act as a potential “integrator” of a cell’s metabolic state (Lin et al., 2012). However, this hypothesis has not been directly tested. With the identification of p300’s dual activity, a simple hypothesis could be proposed: while maintaining p300 (enzyme) and histone (substrate) concentrations, the relative concentrations of either co-reactant (acetyl-CoA or crotonyl-CoA) would determine the rate of either reaction (acetylation or crotonylation), thereby regulating the amounts of either product (acetyl-lysine or crotonyl-lysine). In this model the relative metabolite concentration would determine the state of differential acylation (either acetyl or crotonyl). A number of studies have linked mammalian cellular metabolism to the regulation of histone acetylation (see Chapter 1). An early landmark paper demonstrated that in mammalian cells the enzyme ATP-Citrate Lyase (ACL) was responsible for generating acetyl-CoA used for histone acetylation (Wellen et al.,

2009). Importantly, this study illustrated that the cyto/nuclear concentration of acetyl-CoA could affect histone acetylation and gene expression, providing a precedent for metabolite driven control of transcription mediated through histone modifications.

Here I demonstrate that as a result of p300's dual enzymatic activities, the level of histone crotonylation in the cell is sensitive to the relative cellular concentrations of crotonyl-CoA and acetyl-CoA. I demonstrate that treatment of cells with the neutralized salt of the short chain fatty acid crotonic acid, sodium crotonate (from here on referred to as crotonate), can be used to increase cellular concentrations of crotonyl-CoA. This increase in crotonyl-CoA leads to increased levels of histone crotonylation, which can be "tuned" by treating cells with different concentrations of crotonate. I implicate the cytoplasmic/nuclear metabolic enzyme acyl-CoA synthetase (ACSS2 or AceCS1) in the synthesis of crotonyl-CoA from crotonate in mammalian cells. Furthermore, by depletion of enzymes that produce acetyl-CoA levels of histone crotonylation increase, further demonstrating the balance between acetyl-CoA and crotonyl-CoA for p300's catalytic activity. These data support the conclusion that differential acylation of histones is regulated metabolically, by the relative concentrations of acyl-CoAs.

## **RESULTS**

### **Crotonyl-CoA and Acetyl-CoA Compete for p300's Acyltransferase Activity**

I next sought to gain insights into how differential acylation is regulated in mammalian cells. Given that p300 can catalyze both histone acetylation and crotonylation, I hypothesized that a differentially modified substrate would be

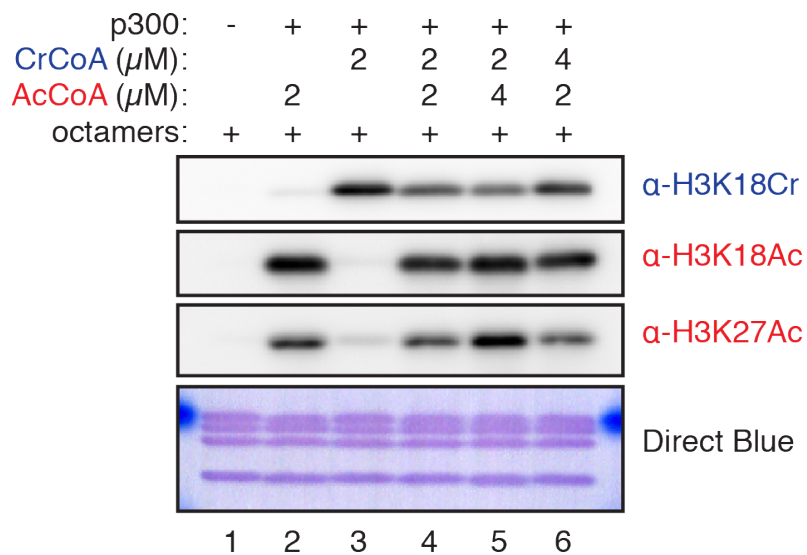


**Figure 3.1: The Relative Concentrations of Acetyl-CoA and Crotonyl-CoA Determine the Reaction Products.**

*In vitro* p300 HAT/HCT reactions were performed with indicated concentrations of crotonyl-CoA and acetyl-CoA. Reaction products were immunoblotted with the indicated antibodies.

the direct result of the cellular concentrations of either acetyl-CoA or crotonyl-CoA that would, in turn, be regulated by extracellular and intracellular sources of these cofactors. To provide a preliminary test of this hypothesis, p300 reactions were performed in which acetyl-CoA and crotonyl-CoA were mixed in varying ratios. Indeed, altering the relative concentrations of these two acyl-CoAs dictated how much of each modification was present in the final reaction product (**Figure 3.1**). I conclude that crotonyl-CoA can compete with acetyl-CoA for p300's activity toward its substrate and, consequentially, the relative concentrations of crotonyl-CoA to acetyl-CoA will determine the enzyme's reaction products. While H3K18 is not the exclusive site of either p300-catalyzed acetylation or crotonylation, the levels of H3K18Cr and H3K18Ac can be used as a surrogate for p300's differential activity *in vitro* and in cell-based assays.

### **LC-MS Measurements of Crotonyl-CoA and Acetyl-CoA**

To investigate the relative cellular concentrations of acetyl-CoA and crotonyl-CoA, I worked with Dr. Justin Cross, Director of Memorial Sloan Kettering's Cancer Metabolism Center, and his colleague Dr. Vladimir Yong-Gonzalez to establish a targeted LC-MS approach that would allow us to extract CoA species from whole cells in culture and measure the abundance of acetyl-CoA and crotonyl-CoA. We assayed HeLa S3 cells growing in full media under exponential growth conditions and observed a small yet measurable pool of crotonyl-CoA, which was approximately 1000x less abundant than acetyl-CoA (**Figures 3.2A and 3.2B**, first column). The pool of crotonyl-CoA was small in comparison to acetyl-CoA, the most abundant CoA-species measured and the product of several major biosynthetic pathways in multiple organelles. The low

basal abundance of crotonyl-CoA places it well below the  $K_m$  of p300 (Meier, 2013), which should allow any fluctuation in its concentration to affect downstream crotonyltransferase reactions.

To test this prediction, I experimentally increased the concentration of crotonyl-CoA in HeLa S3 cells by adding crotonate to the culture media, and observed a dose-dependent increase in both the cellular concentration of crotonyl-CoA and the global levels of H3K18Cr (**Figures 3.2A-3.2C**). The relatively low abundance of cellular crotonyl-CoA allowed for this dramatic fold change in its availability. In contrast, addition of acetate to cells did not dramatically increase the abundance of cellular acetyl-CoA and had little to no effect on global levels of H3K18Ac (**Figures 3.2B and 3.2C**). Here again, I utilized the site-specific and acyl-specific antibodies (H3K18Ac and H3K18Cr) as a tenable surrogate measure for the differential acylation state of histone residues modified by p300/CBP in the cell. Moreover, the increase in histone crotonylation was not specific to H3K18. A dose-dependent signal increase was also observed with the pan-crotonyl-lysine antibody, not only in H3, but also in the other core histones, upon crotonate addition (**Figure 3.2C**). I also observed a similar dose-dependent increase in global histone crotonylation in HEK293T cells, mouse embryonic stem cells, and RAW 264.7 cells, a mouse macrophage cell line, demonstrating that this is not a HeLa S3-specific phenomenon (**Figures 3.2D-3.2E**). These data demonstrate that histone crotonylation is sensitive to fluctuations in crotonyl-CoA concentrations and that crotonate treatment is a general experimental method to specifically increase levels of histone crotonylation.

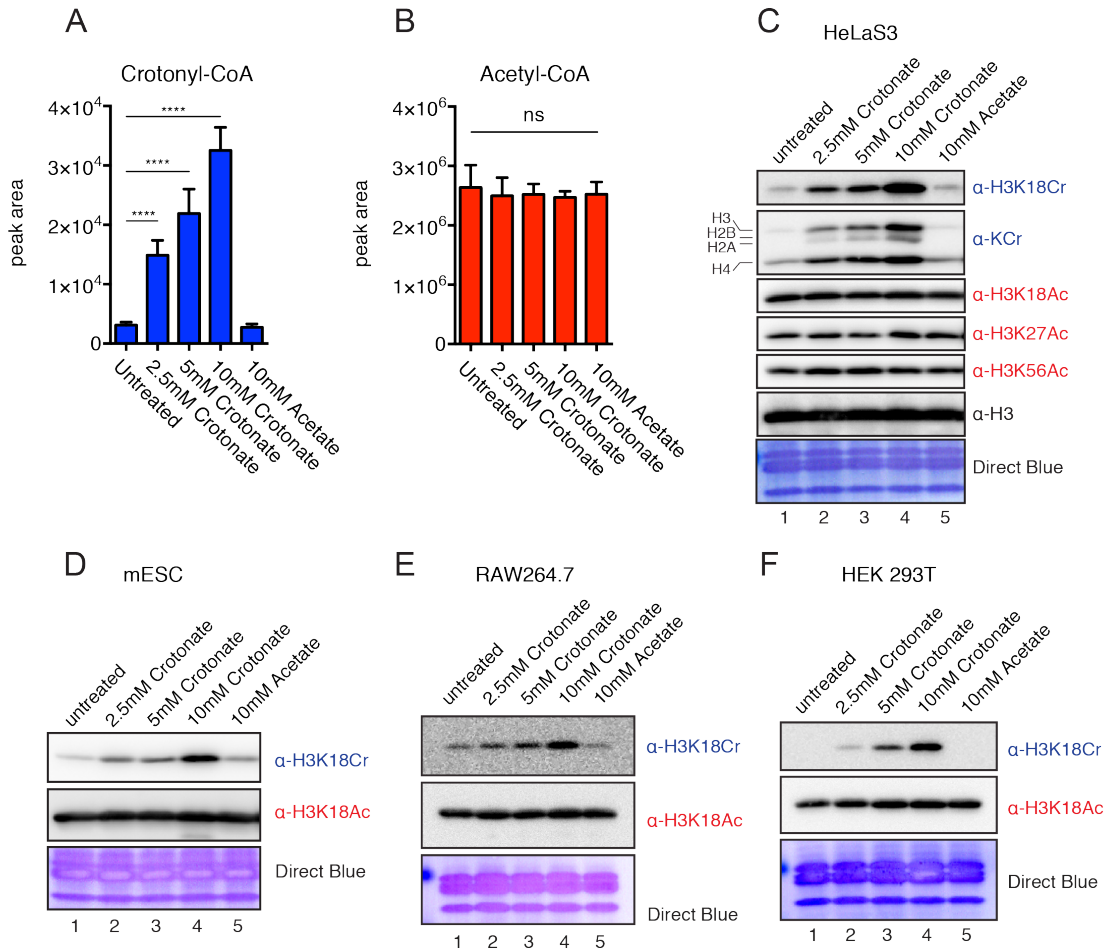


**Figure 3.2: Manipulation of Intracellular Crotonyl-CoA Concentration by Treatment of Cells with Sodium Crotonate.**

(A-B) LC-MS analysis of cellular crotonyl-CoA (A) and acetyl-CoA (B) levels extracted from HeLa S3 cells cultured with the indicated concentration of sodium crotonate (pH 7.4) or sodium acetate (pH 7.4) added to full media for 12 hours. The data represent mean peak area  $\pm$  standard deviation of four independent experiments. Summary of p-value is as follows: ns ( $p > 0.05$ ), \*\*\*\* ( $p \leq 0.0001$ ). (C-F) Histones were acid extracted from HeLa S3 cells (C), mouse embryonic stem cells (mESC) (D), RAW 264.7 cells (E), and HEK293T cells (F) treated as in (B) and immunoblotted by the indicated antibodies.

### Sodium Crotonate Does Not Have HDAC Inhibitor Activity

Given the chemical similarity between crotonate and butyrate, a compound with known histone deacetylase (HDAC) activity (Boffa et al., 1978; Candido et al., 1978), I next sought to ensure that the increase in histone cronylation was not due to the inhibition of an unknown crotonyl-specific HDAC activity. To rule out this possibility I carried out a fluorometric-based HDAC assay with HeLa S3 nuclear extracts as a general source of HDAC activity in the presence of increasing concentrations of crotonate, acetate, or butyrate. While butyrate showed the expected inhibition of HDAC activity, crotonate and acetate showed minimal inhibition (Figure 3.3).

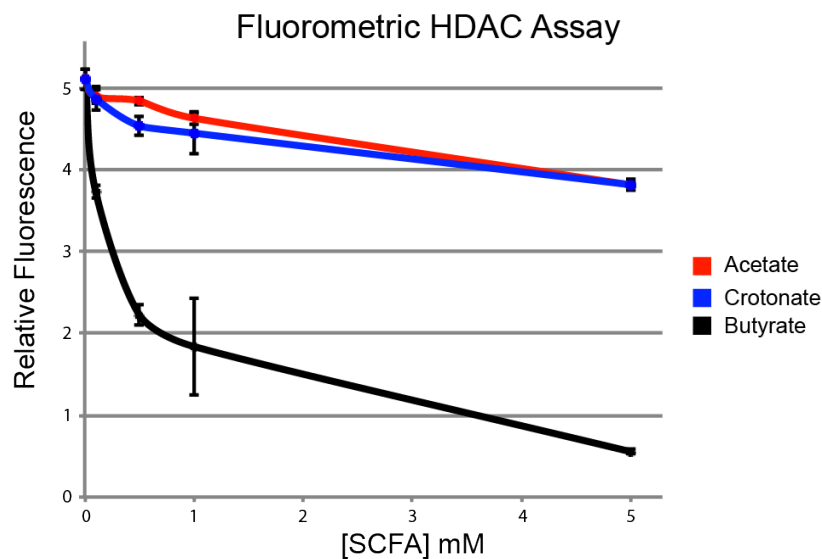


**Figure 3.3: Crotonate is Not an HDAC Inhibitor.**

Increasing concentration of either acetate, butyrate, or crotonate (0, 0.5mM, 1mM, or 5mM) were added to a Fluorometric HDAC assay kit (Active Motif) where fluorescence intensity is an indirect measure of HDAC activity. Butyrate is a known HDAC inhibitor, while Acetate is not considered an HDAC inhibitor. HeLaS3 nuclear extract was used as a general source of HDAC activity.

### **ACSS2 is Responsible for Synthesizing Crotonyl-CoA from Crotonate**

To further demonstrate that addition of crotonate is increasing histone cronylation through the direct production of crotonyl-CoA and not through an indirect mechanism, I asked whether knockdown of the Acyl-CoA Synthetase, ACSS2, would attenuate the increase in histone cronylation. ACSS2 is known to charge acetate with free CoA-SH to form acetyl-CoA in mammalian cells, is known to localize to the cytosol and the nucleus (Wellen et al., 2009), and has been shown to charge longer chain SCFAs *in vitro* (Frenkel and Kitchens, 1977), making it an excellent candidate for the conversion of crotonate to crotonyl-CoA. Supporting this notion, knockdown of ACSS2 prior to addition of crotonate to HeLa S3 cells reduced the amount of crotonyl-CoA produced and the levels of H3K18Cr (**Figures 3.4A and 3.4B**, compare columns/lanes 2 and 4). Intriguingly, I also observed that ACSS2 knockdown reduced the global levels of H3K18Cr in untreated cells (**Figure 3.4B**, compare lanes 1 and 3). This suggests that basal concentrations of crotonyl-CoA used for histone cronylation are synthesized from endogenous sources of crotonate. To further support this observation and to rule out potential complications due to siRNA off-target effects, I tested four separate ACSS2-specific RNAs that all showed a global reduction in H3K18Cr (**Figure 3.4C**). These data suggest that ACSS2 is responsible, at least in part, for the production of crotonyl-CoA to be used for histone cronylation.

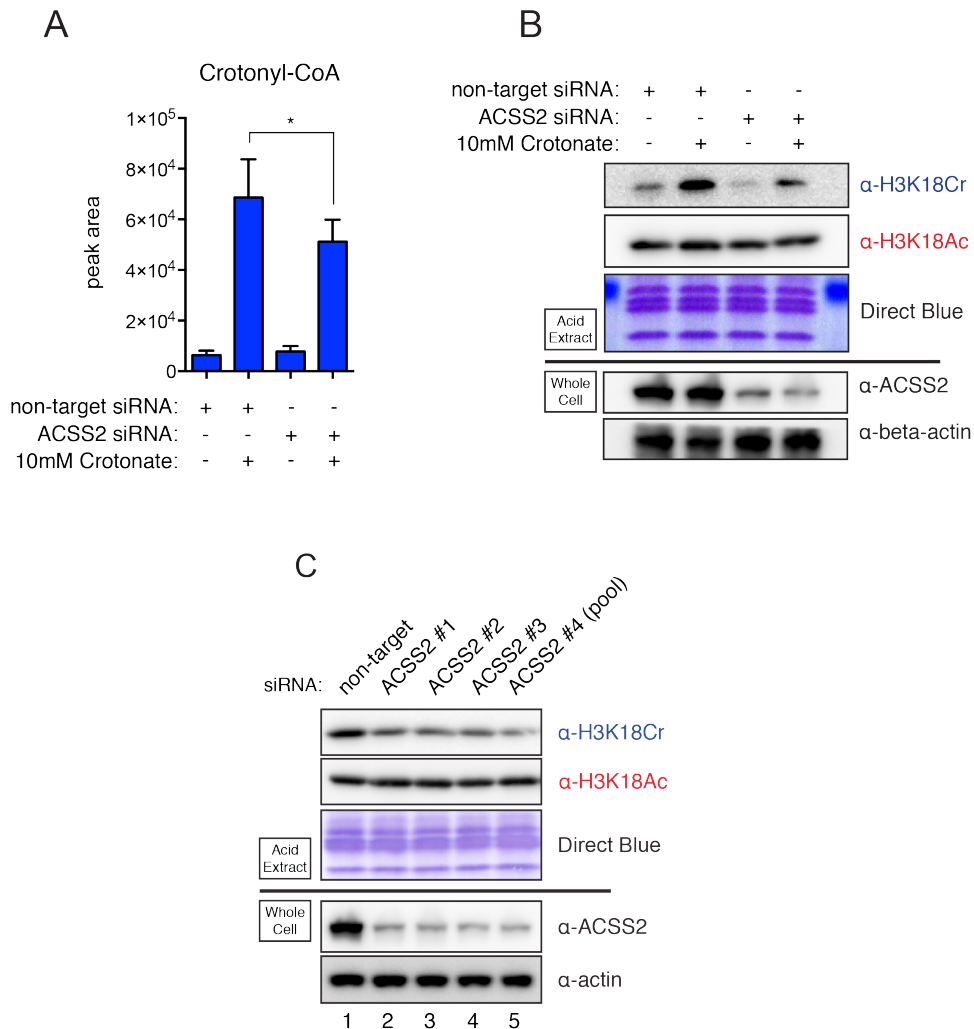


**Figure 3.4: Knockdown of ACSS2 Reduces Cellular Levels of H3K18cr.**

(A) HeLa S3 cells were transfected with control or ACSS2-specific siRNA (pool of 5). 12 hours prior to harvest 10 mM crotonate was added to the media as indicated. 72 hours post-transfection cells were harvested and subject to LC-MS analysis. The data represent mean peak area  $\pm$  standard deviation of four independent experiments. \*, t-test derived p-value < 0.05. (B) Same as (A), except 72 hours post-transfection, histones and whole cell lysates were prepared, and immunoblotted with the indicated antibodies. Immunoblots of acid extracts are shown above the black line, while immunoblots of whole cell lysates are shown below the black line. (C) HeLa S3 cells were transfected with control or specific siRNAs to ACSS2. ACSS2 #1-3 are unique single RNAs, and ACSS2 #4 is the pool of 5 used in (A-B).

## Impairing Acetyl-CoA Synthesis Leads to Higher Levels of Histone

### Crotonylation

I next asked whether impairing acetyl-CoA production would have an effect on histone crotonylation. My *in vitro* reactions would predict that lowering the concentration of acetyl-CoA will lead to an increase in H3K18Cr by reducing the competition for p300/CBP (**Figure 3.1**). A growing literature has shown that the cytoplasmic and nuclear enzyme ATP-Citrate Lyase (ACL) is responsible for producing acetyl-CoA used for histone acetylation in mammalian cells (Lee et al., 2014; Wellen et al., 2009). Knockdowns of ACL by three unique siRNAs resulted in the expected reduction in global levels of H3K18Ac and, as predicted by my *in vitro* experiments, an increase in global levels of H3K18Cr (**Figure 3.5A**). Furthermore, the increase in H3K18Cr can be reversed by the addition of acetate, which has previously been shown to restore histone acetylation levels in the absence of ACL (**Figure 3.5B**) (Wellen et al., 2009).

Recently, the pyruvate dehydrogenase (PDH) complex, which synthesizes acetyl-CoA for the TCA cycle in the mitochondria, has been shown to translocate to the nucleus where it can synthesize acetyl-CoA used for histone acetylation (Sutendra et al., 2014). Upon knockdown of PDHE1 $\alpha$ , a critical subunit of the PDH complex, I observed both the previously reported reduction in H3K18Ac and the predicted increase in H3K18Cr (**Figure 3.5C**). Given the relatively low steady-state levels of crotonyl-CoA to acetyl-CoA in the cell and the decrease in acetyl-CoA observed with ACL knockdown, we do not suggest that crotonyl-CoA is completely replacing acetyl-CoA, but rather that the crotonyl-CoA that is present has less competition for p300 and is therefore more often used for p300-catalyzed histone acylation.

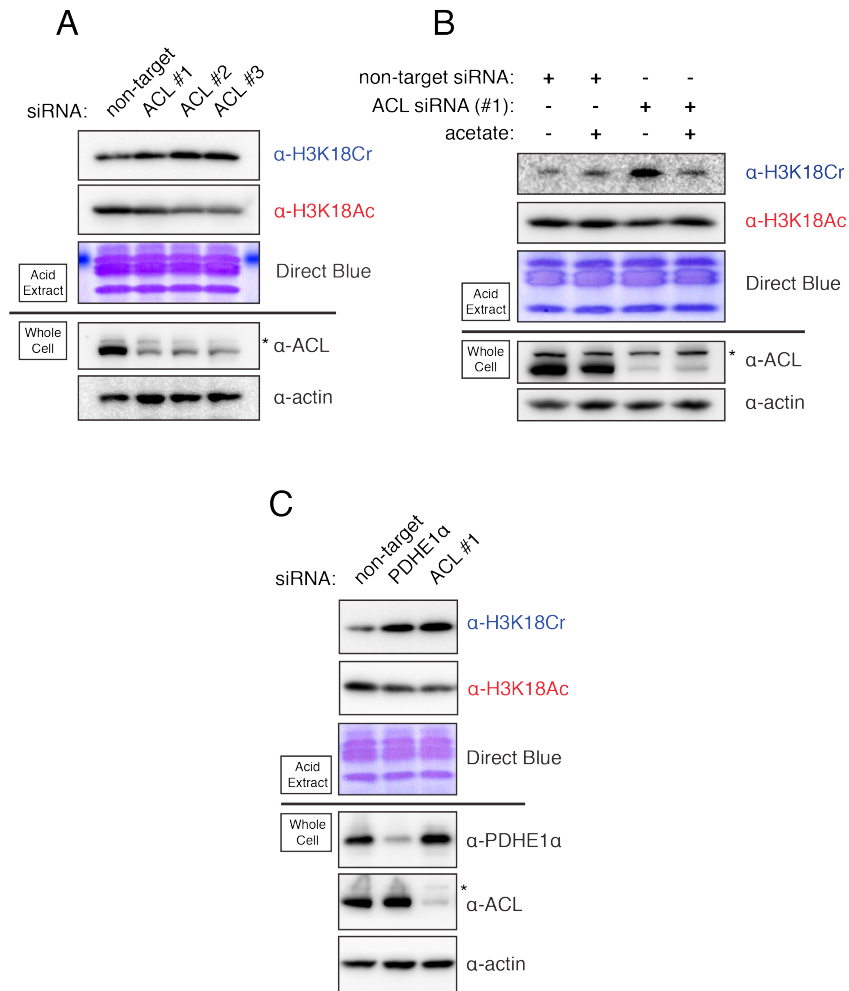


**Figure 3.5: Reducing Acetyl-CoA Leads to an Increase in Histone Crotonylation.**

(A) HeLa S3 cells were transfected with non-target, or one of three unique ACL siRNAs, as indicated. 72hrs post-transfection histone extracts and whole cell lysates were prepared and immunoblotted with the indicated antibodies. Immunoblots of acid extracts are shown above the black line, while immunoblots of whole cell lysates are shown below the black line. Asterisks designate non-specific band in anti-ACL blots. (B) HeLa S3 cells were transfected with either non-target or ACL-specific siRNA (#1) using the same protocol as in (A), except 14 hours prior to harvest 10 mM acetate was added to the media as indicated. Analysis and labeling are as in (A). (C) HeLa S3 cells were transfected with non-target, PDHE1 $\alpha$ , or ACL (#1) specific siRNA, as in (A-B). Analysis and labeling are as in (A-B).

## DISCUSSION

Regulation of histone PTMs by metabolite availability has been proposed as a mechanism for linking chromatin state to metabolism (Donohoe and Bultman, 2012; Gut and Verdin, 2013; Kaelin and McKnight, 2013; Katada et al., 2012; Lu and Thompson, 2012; Meier, 2013). The basic premise is that many chromatin-modifying enzymes utilize products of intermediary metabolism as cofactors essential for their activities. Fluctuations in these metabolites could directly transduce a transcriptional response through the modification of chromatin state either by activating or inhibiting various chromatin-modifying enzymes. This study introduces a new dimension to this paradigm in that fluctuations in both acetyl-CoA and crotonyl-CoA are shown to affect levels of histone acylation. Here I show that crotonyl-CoA can compete with acetyl-CoA for p300's acyl-transferase activity, allowing the relative concentrations of either CoA to determine the reaction products. I implicate the cytoplasmic and nuclear localized metabolic enzyme ACSS2 as a source of intracellular crotonyl-CoA used for histone cronylation. Together these data demonstrate the sensitivity of histone cronylation to acyl-CoA metabolism and provide a toolkit for perturbing histone cronylation in the cell.

I propose that fluctuations in acyl-CoA metabolism and the ratios of these various metabolites will be “translated” by chromatin, through mechanisms described here and through mechanisms yet to be uncovered (**Figure 3.6**). Although I have focused on H3K18, I anticipate that these observations will hold for other enzyme-driven cronylations, and acylations that share enzyme-machineries. The ability to quantitatively measure the cellular concentrations of a

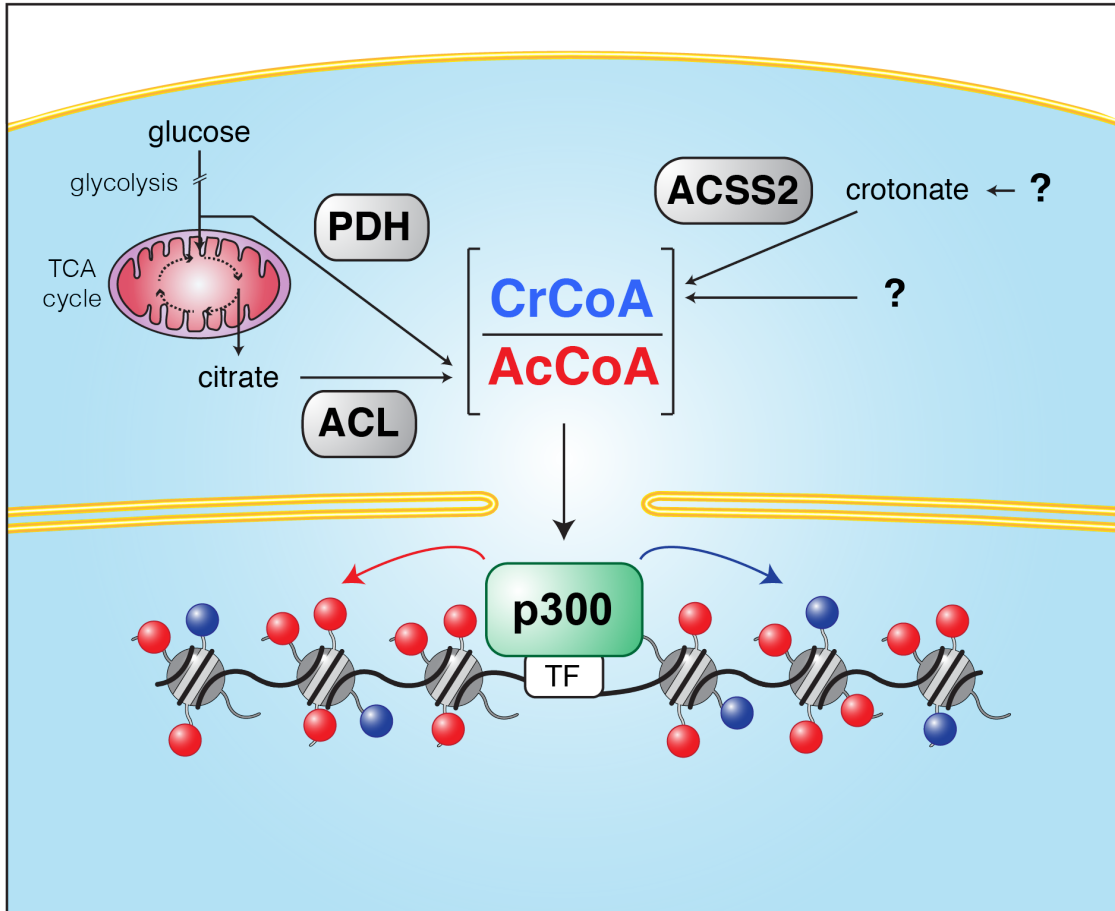


**Figure 3.6: Metabolic Regulation of Histone Crotonylation**

Schematic diagram of the pathways involved in the enzymatic and metabolic regulation of histone crotonylation and histone acetylation (differential acylation). The differential acylation state of chromatin is regulated by the relative concentrations of acetyl-CoA and crotonyl-CoA, which are synthesized through distinct metabolic pathways, diagrammed here. Branches of the diagram that are still unknown are marked by question marks. The PDH (pyruvate dehydrogenase), ACSS2 (Acyl-CoA synthetase), and ACL (ATP Citrate Lyase) reactions occur in both the cytosol and nuclear compartments. We favor the model that DNA-sequence-specific transcription factors (TF) recruit p300/CBP to specific genomic loci where they will “translate” the nuclear/cytosolic acyl-CoA levels by differentially acylating histones.

variety of acyl-CoAs opens up the potential for a new avenue of research. Comparative profiling of acyl-CoAs from a variety of biological materials will be a valuable resource and will allow correlations to be drawn between basal concentrations and function and/or physiological state. For example, ChIP-seq data from developing spermatagonia show an interesting relationship between histone crotonylation and active gene expression programs in the development of male germ cells (Montellier et al., 2013; 2011; Tan et al., 2011). It remains to be tested whether a unique metabolic program underlies these observations or whether similar mechanisms are in play during other developmental or disease pathways. Additionally, it has been long observed that the transformation of cells to a cancerous state requires a rewiring of metabolic pathways (Pavlova and Thompson, 2016; Warburg et al., 1927). Global and local changes in histone acetylation have been observed in a variety of tumors and cancer models (Horwitz et al., 2008; Seligson et al., 2009; 2005). It remains of interest to bridge these two observations and understand whether changes in acyl-CoA metabolism and thereby downstream histone acylations play a significant role in cancer or other aspects of human biology and disease.

These data also suggest that both intra-cellular and extra-cellular concentrations of short chain fatty acids (SCFA), like crotonate, will influence chromatin state through the activity of ACSS2. Fluctuations in the concentration of a variety of SCFAs have been linked to metabolic disorders and diseases. For example, the concentration of 3-hydroxy-butyrate can rise to as high as 25mM in peripheral blood and has been implicated in chromatin regulation (Shimazu et al., 2013). Additionally, differences in the concentrations and makeup of SCFAs from environmental sources have been implicated in a variety of physiological

and disease states ranging from gut microbiota dysbiosis leading to obesity, colitis, and cancer predisposition to the regulation of immune cell development (Lee and Hase, 2014; Tan et al., 2014a). Whether these observed fluctuations in SCFA lead to an increase in their corresponding histone acylation, as we have shown here with crotonate and histone crotonylation, remains untested. Furthermore, it is still unclear how crotonate or crotonic acid, are generated in mammalian cells. Finally, recent reports have highlighted the critical role of ACSS2 in tumor growth (Comerford et al., 2014; Mashimo et al., 2014), yet the role of differential histone acylation in this context was unexplored.

The studies in Chapter 3 establish the metabolic regulation of histone crotonylation and develop tools to specifically perturb histone crotonylation in the cell. With these tools I was now able to ask how increasing or decreasing crotonyl-CoA affects p300-regulated gene activation, the subject of Chapter 4.

## CHAPTER 4: EXPERIMENTAL MANIPULATION OF [CROTONYL-COA] AFFECTS ACTIVATION AND EXPRESSION OF P300 TARGET GENES IN LPS-INDUCED INFLAMMATORY RESPONSE

### INTRODUCTION

Having shown that p300-catalyzed histone crotonylation directly stimulates transcription in a cell-free system (chapter 2) and the metabolic regulation of histone crotonylation in cells (chapter 3), I next sought to investigate whether p300-catalyzed histone crotonylation is involved in the process of gene activation in a cellular context. The LPS-induced inflammatory response in macrophages is a classic model of signal-dependent gene activation, where the role of chromatin and chromatin modifying enzymes are well documented (Smale et al., 2014).

The innate immune system protects an organism from pathogens and other environmental insults through a wide range of mechanisms. While many proteins involved in innate immunity are constitutively expressed other are induced only when needed. This induction is controlled by a series of pattern recognition receptors that specifically recognize pathogen-associated molecular patterns. The presence of receptors on the host cell surface allows the host cell to recognize and respond to specific pathogen-associated signals by activation of signaling cascades generally leading to a specific transcriptional response (Janeway and Medzhitov, 2002; Takeuchi and Akira, 2010).

Lipopolysaccharide (LPS), found on the outer membrane of Gram-negative bacteria, stimulates multiple signaling cascades by engagement with the host receptor, TLR4. While there are transcription-independent responses to TLR4 activation, most of the response is mediated through a signal-dependent

transcriptional cascade (Medzhitov and Horng, 2009; Smale, 2012), which I will refer to as the inflammatory response. The rapid and robust activation of inflammatory response genes provides a model for gene activation where the temporal control of transcription is dependent on the addition of LPS to cells in culture allowing manipulations to crotonyl-CoA concentrations to be made prior to gene activation. Furthermore, the inflammatory response induces the transcription of hundreds of genes through distinct mechanisms dependent on various factors. For example, some genes are primed and their chromatin fully modified before LPS stimulation, while other genes must go through chromatin modification and remodeling before the gene is expressed (Bhatt et al., 2012; Ramirez-Carrozzi et al., 2009). This provides genes that can be experimentally perturbed at the level of chromatin regulation and a series of genes that can act as internal controls that are LPS-responsive but insensitive to chromatin perturbations, as their chromatin is already primed.

The wealth of previously published data profiling the transcriptomic and epigenomic aspects of the inflammatory response also made it an attractive model. Most important to my studies on p300-catalyzed histone crotonylation was a published ChIP-seq data set for p300  $\pm$  LPS (Ghisletti et al., 2010). This p300 ChIP-seq data set provided critical information on which LPS-induced genes are regulated by p300, as demonstrated by ChIP signal at promoter proximal or distal regulatory elements. From these ChIP-seq data I could also determine which p300-regulated genes had p300 localized prior to LPS (primed) and which ones had signal-dependent recruitment of p300. In this chapter, I refer to the former group of genes as “pre-activated” and the latter group of genes as “de novo-activated,” and define these categories based on the p300 ChIP-seq

data. This classification is important because while the genes that are “pre-activated,” meaning they already have p300 bound at their associated regulatory elements, will not be dependent on p300 recruitment and subsequent histone acetylation and/or crotonylation for gene activation, the “de novo-activated” genes will be dependent on this process. This feature of “de novo-activated” genes provides a means to ask whether having more or less p300-catalyzed histone crotonylation affects expression, which can be accomplished through manipulations to crotonyl-CoA concentrations described in Chapter 3.

Here, I show that increasing or decreasing the cellular concentration of crotonyl-CoA prior to LPS-stimulation causes local changes in histone crotonylation, specifically at the histones flanking regulatory elements that show the greatest increase in p300 localization during the inflammatory response (i.e. “de novo-activated” genes). This increase or decrease in crotonyl-CoA concentration also leads to enhanced or diminished levels, respectively, in expression of those specific activated genes.

## **RESULTS**

### **H3K18Cr is Associated with Active Chromatin and Correlates with p300**

#### **Localization**

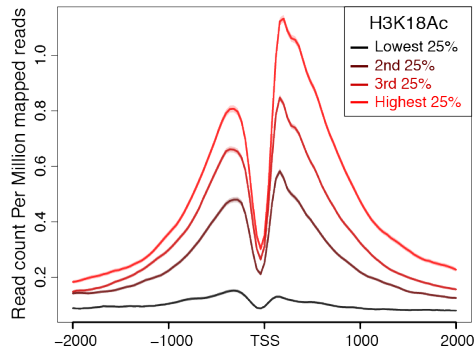
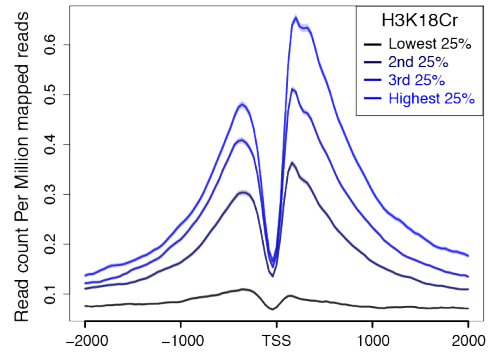
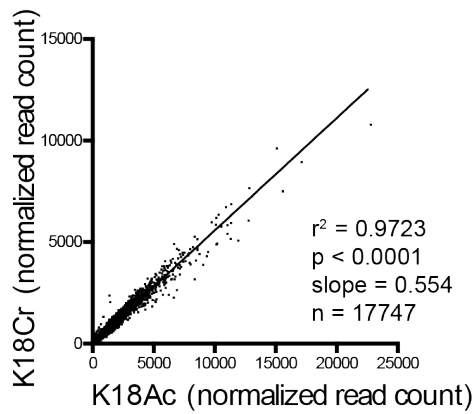
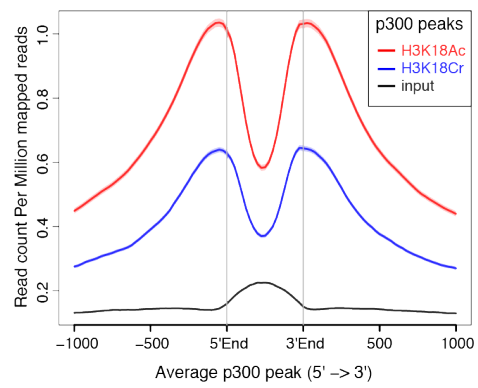
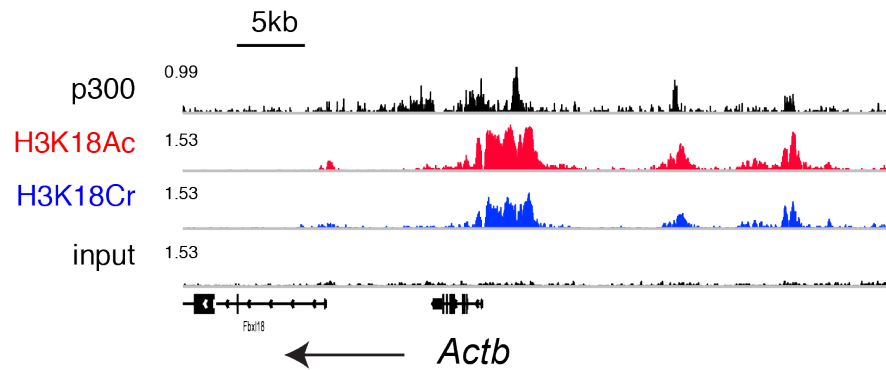
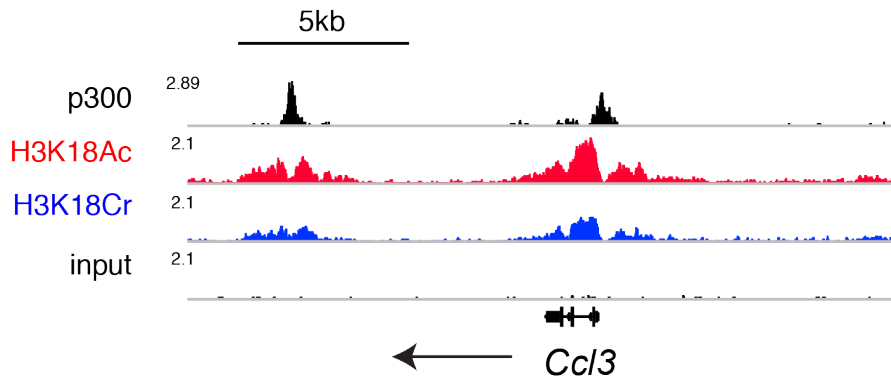
To investigate the role of differential acylation in transcriptional activation within a cellular context, I turned to the LPS-induced inflammatory response in the macrophage cell line RAW 264.7. The macrophage LPS response involves a well-characterized transcriptional program that requires p300 recruitment to many sites of downstream gene activation to facilitate histone acetylation and chromatin remodeling that are critical for the inflammatory response (Ghisletti et

al., 2010; Ramirez-Carrozzi et al., 2009). I performed RNA-seq and ChIP-seq for H3K18Ac and H3K18Cr on cells pre- and post-LPS stimulation (120'). I also made use of published p300 ChIP-seq from macrophages under similar stimulation conditions (Ghisletti et al., 2010).

I first assessed the ChIP-seq data for H3K18Ac and H3K18Cr under unstimulated conditions and observed that both histone modifications map to promoter-proximal and –distal regulatory elements associated with active genes (**Figure 4.1**). By mapping the average profile of both H3K18Ac and H3K18Cr  $\pm$  2kb of the transcription start site (TSS) for four equal groups of genes ranked by expression levels (as determined by RNA-seq), both modifications showed a correlation with gene activity; the group of highest expressed genes exhibited the highest levels of H3K18Ac and H3K18Cr and vice versa (**Figures 4.1A and 4.1B**). Both modifications exhibited the common histone acetylation profile, two peaks flanking a putatively nucleosome depleted regulatory element where p300 is recruited. Levels of H3K18Ac and H3K18Cr followed a significant linear correlation (Figure 4.1C) and were enriched at peaks of p300 across the genome (Figure 4.1D), as predicted by my findings that both modifications are catalyzed by p300. The trends observed by average profiles of H3K18Ac and H3K18Cr reads were also clearly observed at individual genes (Figures 4.1E and 4.1F), where peaks of H3K18Ac and H3K18Cr flanked promoter-proximal and –distal regulatory elements, marked by p300. These data point to a role for p300-catalyzed crotonylation in general transcriptional activation and reaffirm the notion that active regulatory elements are modified by a number of histone acylations.

**Figure 4.1: H3K18Cr, H3K18Ac, and p300 Co-Localize Genome-Wide.**

(A-B) All genes with FPKM >1 were split into 4 equal groups based on their expression levels calculated from RNA-seq of unstimulated RAW 264.7 cells. The average profile of H3K18Ac (A) and H3K18Cr (B) ChIP-seq data from unstimulated RAW 264.7 cells are plotted for each group at TSS  $\pm$  2kb. (C) Correlation between H3K18Ac and H3K18Cr ChIP-seq read counts within all H3K18Cr peaks (17,747). Plotted as normalized read counts (read counts per million mapped reads). (D) Average profile of H3K18Ac, H3K18Cr, and input ChIP-seq data from unstimulated RAW 264.7 around all annotated p300 peaks from unstimulated macrophages. (E-F) Genome browser representation of normalized ChIP-seq reads for p300, H3K18Ac, H3K18Cr, and input from unstimulated macrophages at a “housekeeping” gene (*Actb*) (E) and a lineage specific constitutively expressed (“pre-activated”) gene (*Ccl3*) (F). Normalized to total mapped reads. The y-axis maximum is given at the far left of each track. Arrow below refseq gene track indicates directionality of transcription.

**A****B****C****D****E****F**

## **H3K18Cr and H3K18Ac are Induced at “De Novo-Activated” Regulatory Elements Upon LPS Stimulation**

Stimulation of macrophages by LPS initiates a well-characterized, rapid, and robust transcription program (Bhatt et al., 2012; Ramirez-Carrozzi et al., 2009). For my interests in investigating differential acylation by p300, I focused on two unique classes of LPS-induced genes: I) those showing increased p300 recruitment upon LPS stimulation (fold (reads) > 4), which I will term “de novo-activated”, and II) those showing pre-localized levels of p300 (prior to LPS stimulation) that are not significantly changed upon stimulation ( $-1.3 < \text{fold (reads)} < 1.3$ ), which I will term “pre-activated.” The ChIP-seq traces for p300, H3K18Ac, H3K18Cr, and RNA-seq of genes from both classes  $\pm$  LPS stimulation (120') demonstrate how the chromatin landscape at these two different classes of genes responds to LPS stimulation (**Figure 4.2**). While “de novo-activated” genes (**Figures 4.2A and 4.2B**) showed an induction in both modifications upon LPS stimulation, “pre-activated” genes (**Figures 4.2C and 4.2D**) had peaks of both H3K18Ac and H3K18Cr prior to LPS stimulation. These trends were also observed by average profiles of H3K18Ac and H3K18Cr centered on the TSS of all “pre-activated” and all “de novo-activated” genes (**Figures 4.2E-4.2H**).

## **Increasing Crotonyl-CoA Concentrations by Crotonate Addition Increases H3K18Cr at “De Novo-Activated” Genes and Enhances Gene Expression**

To test whether altering the levels of histone crotonylation would affect gene activation, I asked whether increasing or decreasing the concentration of crotonyl-CoA in RAW 264.7 cells prior to LPS stimulation would alter the differential acylation state at the regulatory elements of “de novo-activated”

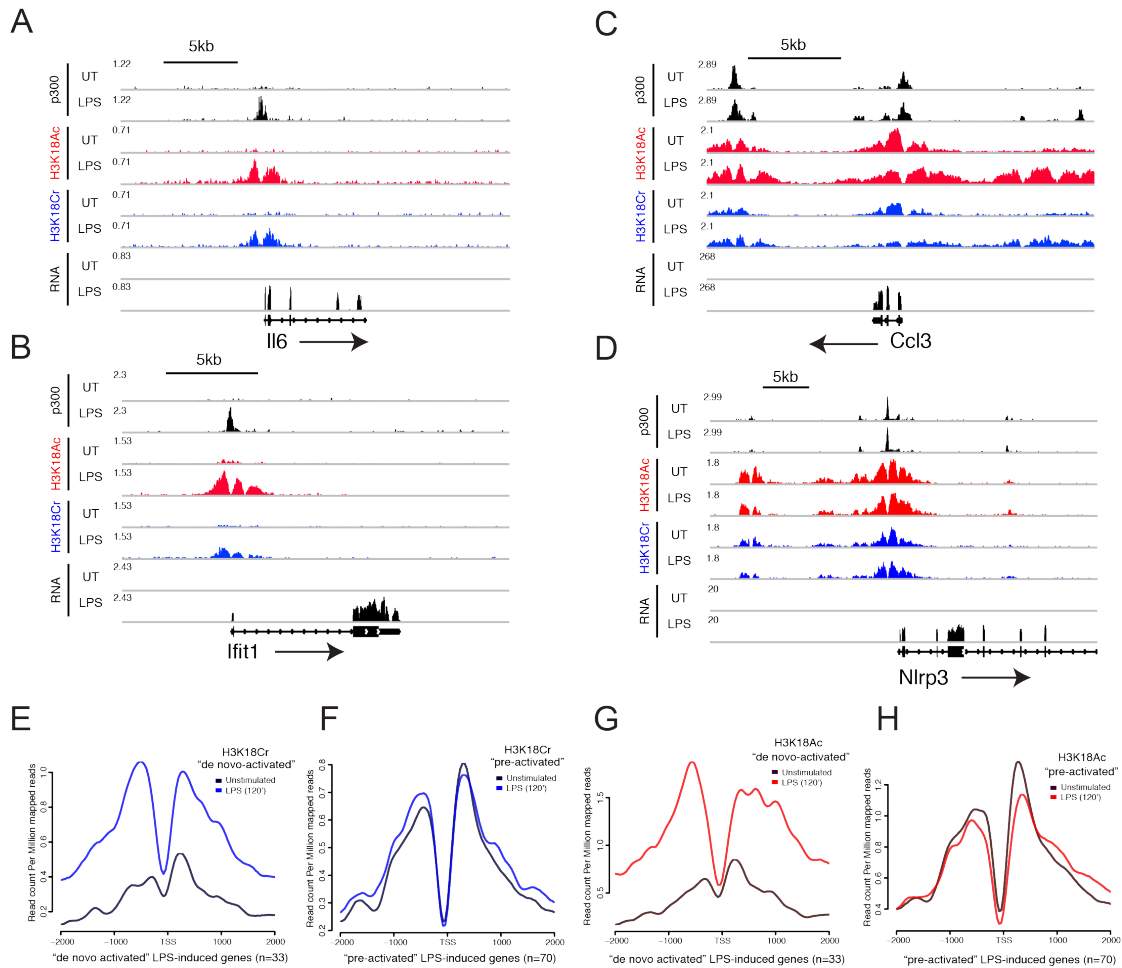


**Figure 4.2: Two Classes of LPS-Stimulated Genes, as Defined by p300 Localization.**

(A-D) Genome browser representation of RNA-seq reads and ChIP-seq reads for p300, H3K18Ac, and H3K18Cr from unstimulated (UT) and 120' LPS-stimulated (LPS) macrophages at two “de novo-activated” genes (*Il6* and *Ifit1*) (A and B) and two “pre-activated” genes (*Ccl3* and *Nlrp3*) (C and D). Normalized to total mapped reads. The y-axis maximum is given at the far left of each track. Arrow indicates directionality of transcription. (E-H) The average profile of H3K18Cr (E and F) and H3K18Ac (G and H) ChIP-seq data plotted at the TSS ± 2kb of either all “de novo-activated” genes (E and G) or all “pre-activated” genes (G and H) with or without LPS stimulation.

genes. I focused on the “de novo-activated” genes because the above data suggest that for these genes the p300-catalyzed acylation of histones was a rate-limiting step in the transcription reaction. I hypothesized that “de novo-activated” genes would be more responsive to changes in the concentrations of crotonyl-CoA than the “pre-activated” genes, which are both acetylated and crotonylated prior to LPS stimulation.

RAW 264.7 cells were first treated with varying concentrations of sodium crotonate followed by LPS stimulation. The crotonate pretreatment increased the concentration of crotonyl-CoA within the cell in a dose-dependent manner without impacting the concentration of acetyl-CoA, as measured by LC-MS (Figure 4.3). After 2 hours of LPS stimulation, I performed ChIP for H3K18Cr

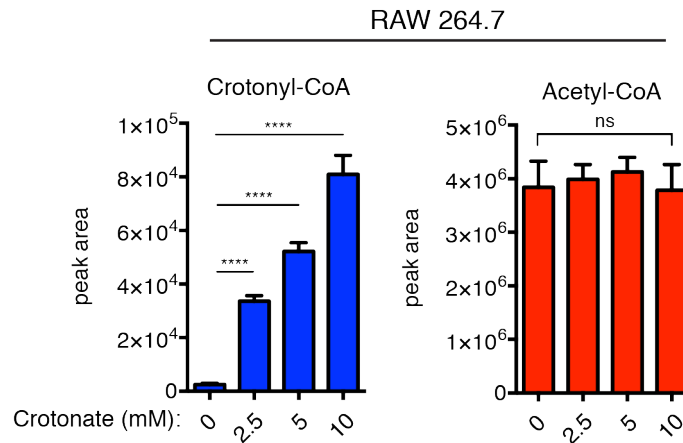
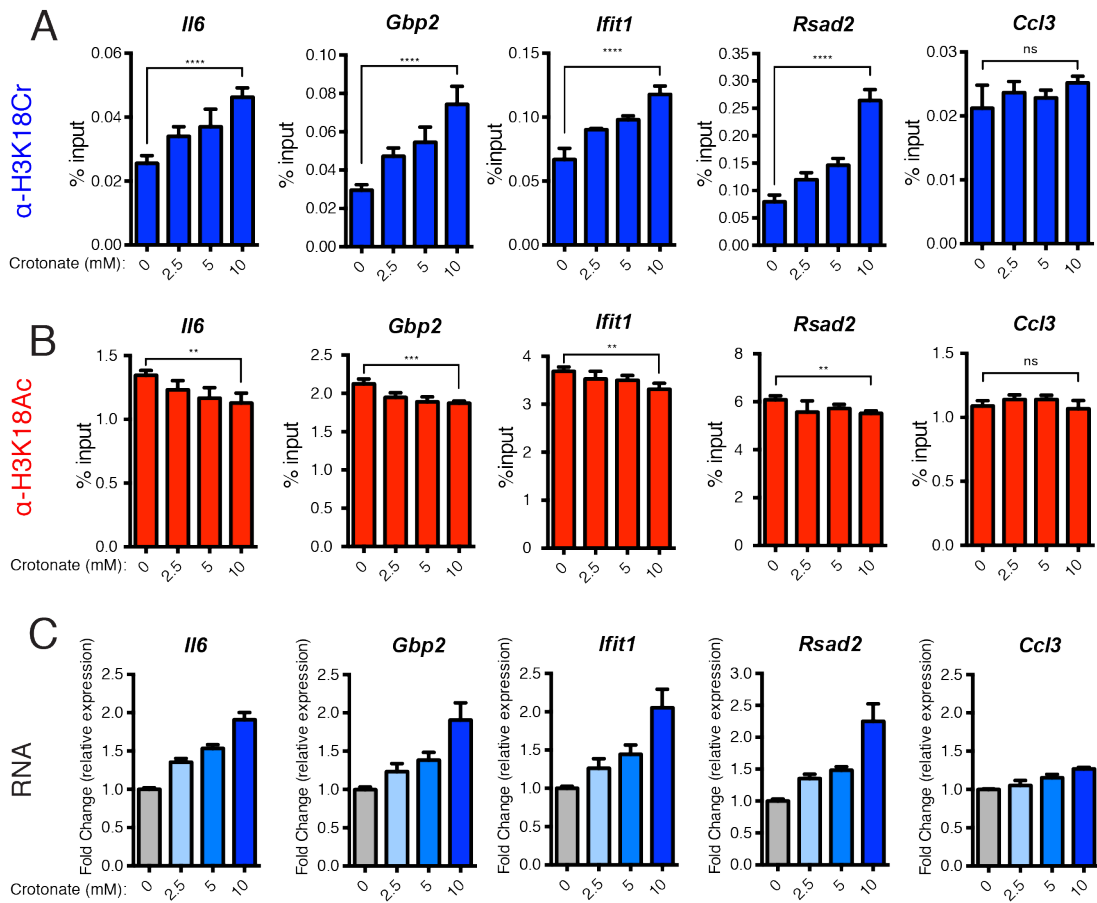


**Figure 4.3: LC-MS Measurements of Crotonyl-CoA and Acetyl-CoA in RAW264.7 Cells.** LC-MS measurements of crotonyl-CoA (left) and acetyl-CoA (right) from RAW 264.7 cells pretreated with the indicated concentration of sodium crotonate, pH 7.4, for 12 hours. The data represent mean peak area  $\pm$  standard deviation of four independent experiments. Summary of unpaired t-test p-value: ns ( $p > 0.05$ ) and \*\*\*\* ( $p \leq 0.0001$ ). These experiments were conducted by Drs. Justin Cross and Vladimir Yong-Gonzalez.

**Figure 4.4: Crotonate Treatment Correlates With Increased H3K18Cr, Decreased H3K18Ac and Increased Gene Expression.**

(A) qPCR analysis of H3K18Cr ChIP products from RAW 264.7 cells pre-treated with the indicated concentration of sodium crotonate (pH 7.4) (mM) for 6 hours prior to a 2-hour LPS stimulation. Primers were designed for TSS-proximal ChIP-seq peaks of H3K18Ac and H3K18Cr. ChIP-qPCR results for four “de novo-activated” genes (*Il6*, *Gbp2*, *Ifit1*, and *Rsad2*) and one “pre-activated” gene (*Ccl3*) are shown. Data are represented as mean of % input  $\pm$  standard deviation of technical replicates. Summary of p-value is as follows: ns ( $p > 0.05$ ), \*\* ( $p \leq 0.01$ ), \*\*\* ( $p \leq 0.001$ ), \*\*\*\* ( $p \leq 0.0001$ ). (B) Experiment and analysis are same as (A), except ChIP was performed with H3K18Ac antibody. (C) RT-qPCR analysis of LPS-stimulated (120') RAW 264.7 cells pre-treated with the indicated concentration of sodium crotonate (pH 7.4) (mM). Relative expression is normalized to *Gapdh*. RT-qPCR data for the same set of genes as in (A-B). Data are represented as the mean fold-change in relative expression due to crotonate addition from three independent experiments  $\pm$  standard deviation.



and H3K18Ac. In support of our hypothesis, I observed a dose-dependent increase in H3K18Cr at the promoters of four “de novo-activated” genes (*Il6*, *Gbp2*, *Ifit1*, and *Rsad2*) and no significant change in H3K18Cr at a “pre-activated” (pre-acetylated) gene (*Ccl3*) (**Figure 4.4A**). Furthermore, I observed an associated dose-dependent decrease in H3K18Ac at the promoters of the “de novo-activated” genes tested and no significant change in H3K18Ac at the “pre-activated” gene (**Figure 4.4B**).

With the ability to fine tune the amount of H3K18Cr present on the promoters of “de novo-activated” genes, I next measured mRNA by RT-qPCR from cells treated with varying concentrations of sodium crotonate prior to a 2 hour LPS stimulation. Gene expression of the “de novo-activated” genes was increased in a dose-dependent manner, while the “pre-activated” gene was only minimally affected (**Figure 4.4C**). Additional tested genes (“de novo-activated:” *Cmpk2*, *Cxcl10*, *Ifnb*, and *Ccl5*, and “pre-activated:” *Pim1*) followed the same trend (**Figure 4.5**). These data provide evidence correlating the abundance of H3K18Cr at the proximal regulatory elements of a gene to its expression, supporting the notion that the balance between histone crotonylation and histone acetylation (i.e. differential acylation) plays a functional role in gene expression.

To explore the scope of LPS-induced genes that are further induced due to crotonate pre-treatment, I next performed RNA-seq on LPS stimulated (120') cells with and without pre-treatment of crotonate (10mM). Consistent with the RT-qPCR data of select genes, “de novo-activated” genes were on average further stimulated by crotonate pre-treatment with a mean fold increase of 2.4 over LPS-induction, whereas “pre-activated” genes were on average unaffected with a mean fold change of 1.0 (**Figure 4.6A**). I next asked whether all crotonate-

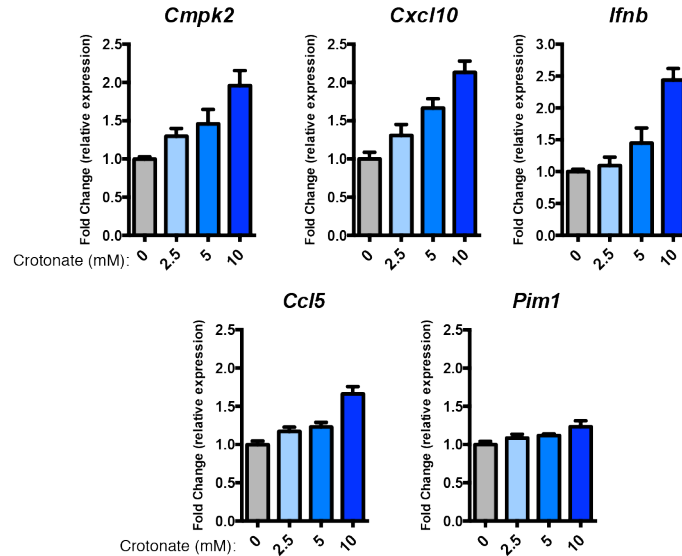


**Figure 4.5: De Novo-Activated Genes Are Further Stimulated By Crotonate Pre-Treatment.** RT-qPCR analysis of LPS-stimulated (120') RAW 264.7 cells pre-treated with the indicated concentration of sodium crotonate (pH 7.4) (mM) for the indicated genes. Relative expression is normalized to *Gapdh*. Data are represented as the mean fold-change in relative expression due to crotonate addition from three independent experiments  $\pm$  standard deviation.

responsive genes (>2-fold increase over LPS stimulation) also show a greater than average recruitment of p300 upon LPS stimulation. To do this, I compared the fold-change of p300 reads ( $\pm$  2kb from TSS) of a list of all genes whose expression was induced >2-fold ("All LPS-induced", n=850) to a subset of that list of genes that were further induced >2-fold over LPS-stimulation due to crotonate pre-treatment ("Further induced by crotonate", n=48). Notably, I observed a significantly greater than average fold-change in p300 recruitment to crotonate-responsive genes (**Figure 4.6B**). I also observed a statistically significant positive correlation between the fold-change in p300-localization upon LPS and the fold-change in mRNA abundance due to crotonate treatment

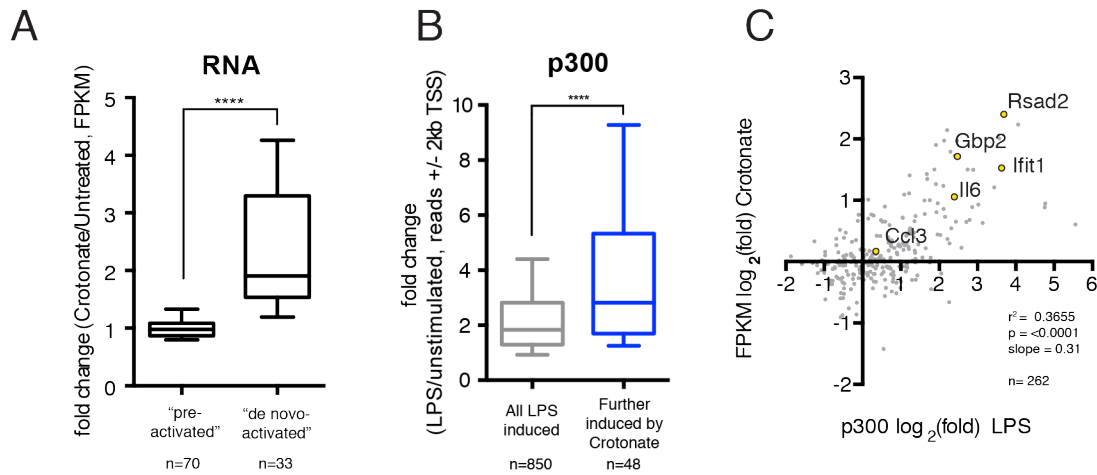


**Figure 4.6: RNA-seq Analysis of Crotonate Pre-Treatment.**

(A) The fold changes in FPKM over LPS-stimulation due to crotonate pre-treatment, as measured by RNA-seq, are represented as a box and whisker plot (10<sup>th</sup> - 90<sup>th</sup> percentile) for both “pre-activated” and “de novo-activated” genes. \*\*\*\*, p-value < 0.0001. (B) Box and whisker plot representation (10<sup>th</sup> - 90<sup>th</sup> percentile) of the fold change in p300 read counts, due to LPS stimulation,  $\pm$  2kb from the TSS of two sets of genes, (1) all LPS induced genes (fold change (FPKM)  $\geq$ 2 upon LPS stimulation, n=850) and (2) a subset of (1) whose expression was further induced  $\geq$ 2-fold due to pre-treatment with crotonate (n=48). \*\*\*\*, p-value < 0.0001. (C) Scatter plot representation of all LPS-stimulated genes with annotated p300 peaks  $\pm$  500bp from TSS (n=262), plotting fold change in p300 read counts due to LPS by fold change in expression (FPKM) over LPS-induction due to crotonate pre-treatment; both are plotted as  $\log_2$  values. Four “de novo-activated” gene (*Il6*, *Gbp2*, *Ifit1*, and *Rsad2*) and one “pre-activated” gene (*Ccl3*) are highlighted in yellow.

(**Figure 4.6C**), further establishing the link between p300-mediated transcriptional activation and differential histone acylation.

### **Increasing Cellular Concentrations of Crotonyl-CoA Prior to LPS Stimulation Enhances Cytokine and Chemokine Secretion Upon LPS Stimulation**

To test whether the effects observed in gene expression led to changes in the functional arm of the inflammatory response, I measured how pre-treating cells with crotonate affected cytokine and chemokine secretion upon LPS stimulation. I first performed an LPS time-course with or without crotonate treatment (10mM), collected supernatants 0, 3, 6, and 16 hours post LPS-stimulation, and observed a greater concentration of secreted Il6 in cells pre-treated with crotonate at every time point post-LPS-stimulation, as measured by a standard ELISA (**Figure 4.7A**). I next employed a multiplex bead-based immunoassay (see Methods for detail) to more broadly analyze the effect of crotonate treatment on cytokine and chemokine secretion. I collected supernatant from cells pre-treated with increasing concentrations of sodium crotonate followed by a 16hr LPS stimulation and measured the concentrations of a variety of LPS-induced chemokines and cytokines (Il6, Cxcl10, Cxcl1, Ccl5, and Ccl3). In agreement with the standard ELISA assay, I observed a dose-dependent increase in Il6 secretion due to crotonate addition (**Figure 4.7B**). I also observed a dose-dependent increase in Cxcl10, Cxcl1, and Ccl5 secretion, all of which are products of “de novo activated” genes (**Figure 4.7B**). Furthermore, Ccl3, a secreted factors expressed from a “pre-activated” gene, did not show a significant change in protein secretion due to addition of crotonate (**Figure 4.7C**).

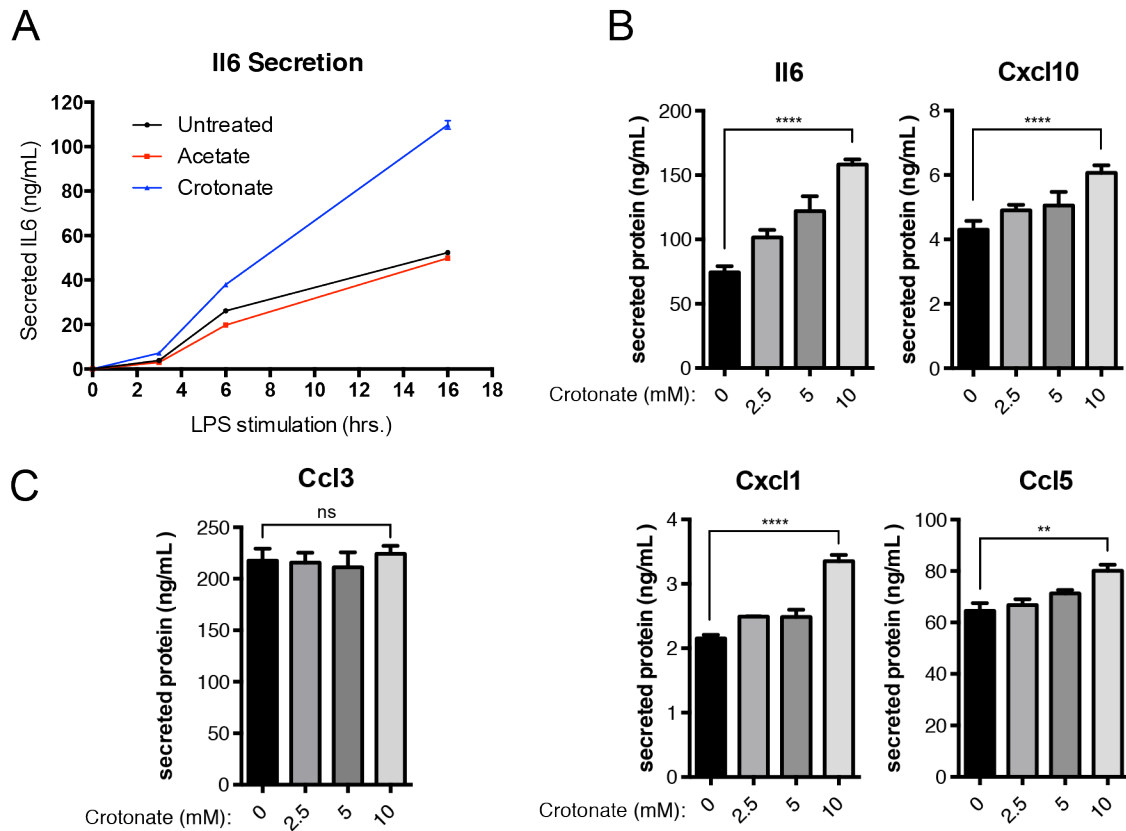


**Figure 4.7: Increased Cellular Crotonyl-CoA Concentration Prior to LPS Stimulation Leads to Enhanced Cytokine and Chemokine secretion Upon LPS Stimulation.**

(A) RAW 264.7 cells were treated with either 10mM Acetate or 10mM Crotonate, or left untreated for 6 hours prior to LPS stimulation. Supernatants were collected at 0, 3hr, 6hr, or 16hr after LPS stimulation and the concentration of IL6 was measure by standard ELISA. Data are presented as mean of technical replicates  $\pm$  standard deviation. (B-C) Chemokine and cytokine protein abundance in supernatants from LPS-stimulated (16hr) RAW 264.7 cells pre-treated with the indicated concentration of sodium crotonate. Data for four “de novo-activated” chemo/cytokines (IL6, Cxcl10, Cxcl1, and Ccl5) (B) and one “pre-activated” chemokine (Ccl3) (C) are represented here as the mean of two independent experiments  $\pm$  standard deviation. Summary of p-value is as follows: ns ( $p > 0.05$ ), \*\* ( $p \leq 0.01$ ), \*\*\* ( $p \leq 0.001$ ), \*\*\*\* ( $p \leq 0.0001$ ).

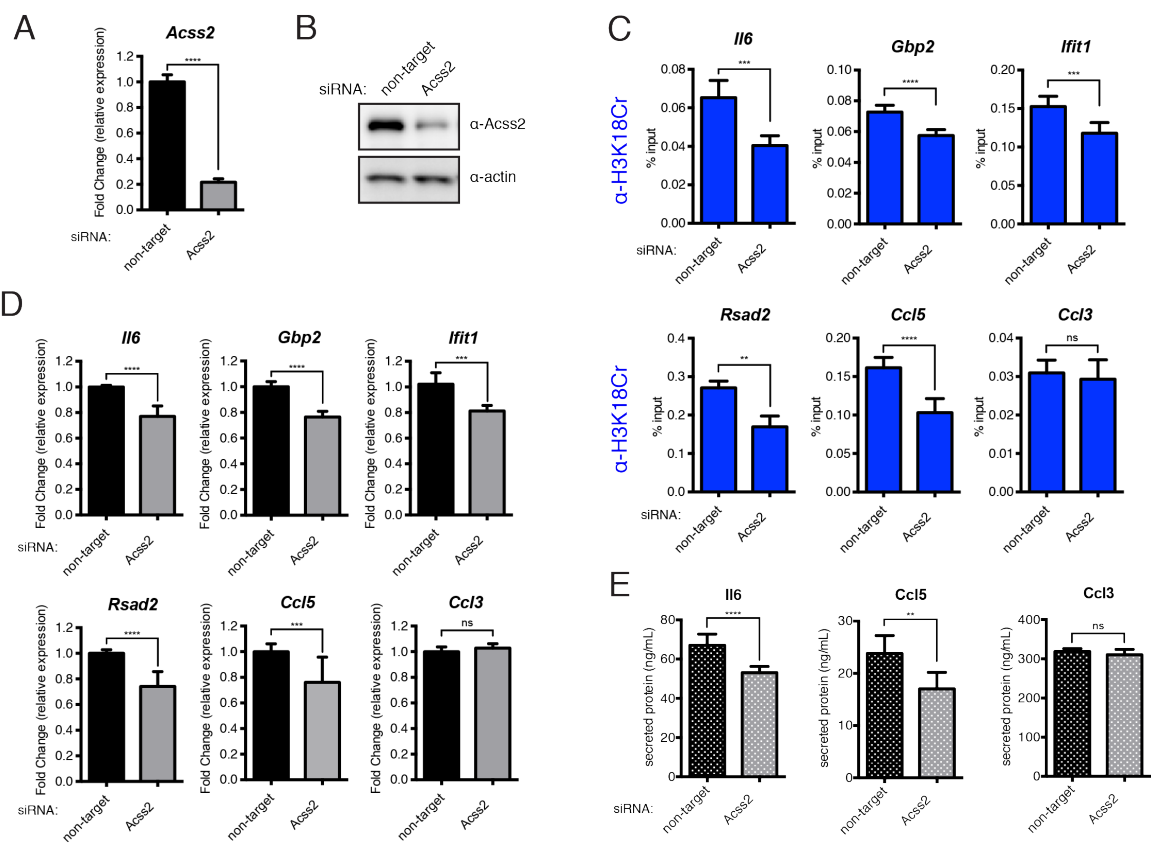
### **Knockdown of *Acss2* Reduces H3K18Cr at the Promoters of “De Novo-activated” Genes and Attenuates Gene Expression**

To test whether decreasing crotonyl-CoA available for histone crotonylation prior to LPS-stimulation would have a negative effect on “de novo-activated” genes, I performed siRNA knockdown of *Acss2* in RAW 264.7 cells prior to a 120' LPS stimulation. I confirmed knockdown of *Acss2* both at the RNA level by RT-qPCR (**Figure 4.8A**) and at the protein level by immunoblot (**Figure 4.8B**). I next performed ChIP for H3K18Cr in LPS-stimulated (120') cells that had been transfected with either non-target or *Acss2*-specific siRNA. As expected, I observed significant decreases in H3K18Cr due to *Acss2* knockdown in five “de novo-activated” genes (*Il6*, *Gbp2*, *Ifit1*, *Rsad2*, and *Ccl5*) and no significant change in the “pre-activated” gene (*Ccl3*) (**Figure 4.8C**). I next performed RT-qPCR under the same experimental conditions with three independent replicates and observed a reduction in mRNA abundance for the five “de novo-activated” genes tested (*Il6*, *Gbp2*, *Ifit1*, *Rsad2*, and *Ccl5*) and no change for the “pre-activated” gene (*Ccl3*) (**Figure 4.8D**). Furthermore, under similar experimental conditions I observed a reduction in the LPS-induced secretion of *Il6* and *Ccl5*, but no significant change in *Ccl3* secretion, upon knockdown of *Acss2* (**Figure 4.8E**). These data support the notion that the cellular concentrations of crotonyl-CoA regulates the levels of histone crotonylation, which in turn impacts the rate of gene activation.

Based on these findings, I conclude that differential histone acylation (crotonylation vs. acetylation) at specific lysine residues (H3K18, in this study, and likely other histone sites) is regulated metabolically by a previously unappreciated balance in cellular levels of crotonyl-CoA and acetyl-CoA. I favor

**Figure 4.8: Knockdown of *Acss2* Prior to LPS Stimulation Leads to a Decreased Induction of H3K18Cr at, and Decreased Stimulation of, “De Novo-Activated” Inflammatory Genes Upon LPS Stimulation.**

(A-B) RAW 264.7 cells were transfected with control or *Acss2*-specific siRNAs, 72 hours post-transfection cells were harvested for either RT-qPCR analysis (A) or immunoblot analysis (B) to assess knockdown efficiency. For (A) data is presented as mean fold change due to *ACSS2* knockdown of technical replicates  $\pm$  standard deviation. (C) qPCR analysis of H3K18Cr ChIP products from LPS-stimulated (120') RAW 264.7 cells that had been transfected with either control siRNA or siRNAs specific for *Acss2* 72 hours prior to stimulation. ChIP-qPCR results for five “de novo-activated” genes (*Il6*, *Gbp2*, *Ifit1*, *Rsad2*, and *Ccl5*) and one “pre-activated” gene (*Ccl3*) are shown here. Data are represented as mean of % input of technical replicates  $\pm$  standard deviation. (D) RT-qPCR analysis of LPS-stimulated (120') RAW 264.7 cells previously transfected with either control or *Acss2*-specific RNAs, as in (C). Relative expression is normalized to *Gapdh*. RT-qPCR data are shown for the same set of genes as in (C). Data are represented as the mean fold-change in relative expression due to *Acss2* knockdown from three independent experiments  $\pm$  standard deviation. (E) Chemokine and cytokine protein abundance in supernatants from LPS-stimulated (16hr) RAW 264.7 cells transfected with the indicated RNAs, as in (C). Data for two “de novo-activated” chemo/cytokines (*Il6* and *Ccl5*) and one “pre-activated” chemokine (*Ccl3*) are represented here as the mean of two independent experiments  $\pm$  standard deviation. Summary of p-value is as follows: ns ( $p > 0.05$ ), \*\* ( $p \leq 0.01$ ), \*\*\* ( $p \leq 0.001$ ), \*\*\*\* ( $p \leq 0.0001$ ).



the view that the concentrations of crotonyl-CoA and acetyl-CoA (and likely other short-chain acylations) are “translated” by the co-activators p300 and CBP into the differential acylation states of local chromatin influencing transcriptional activation by mechanisms that remain unclear. These findings lend support to emerging studies linking metabolism to the alteration of chromatin landscapes and thereby the regulation of gene expression.

## **DISCUSSION**

Regulation of histone modifications, and thereby regulation of chromatin structure, by metabolite availability has been proposed as a potential mechanism for gene regulation under the premise that many chromatin-modifying enzymes utilize products of intermediary metabolism as cofactors essential for their activities (Gut and Verdin, 2013; Kaelin and McKnight, 2013; Meier, 2013). Our study introduces a new dimension to this paradigm in that fluctuations in both acetyl-CoA and crotonyl-CoA are shown to affect global and local chromatin landscapes leading to distinct functional outputs. While our study clearly establishes that the concentration of crotonyl-CoA influences transcriptional activation through its effects on differential acylation, it remains unclear whether the physiological concentrations of crotonyl-CoA are as dynamic as they are in our cell culture experiments where crotonate addition to media was used to experimentally alter the cellular concentration of crotonyl-CoA.

The data presented here illustrate that the intra-and inter-cellular metabolic state of the cell can directly influence the local chromatin landscape by causing fluctuations in metabolite/cofactor concentrations required for histone crotonylation and acetylation. I put forward a proof-of-concept for the

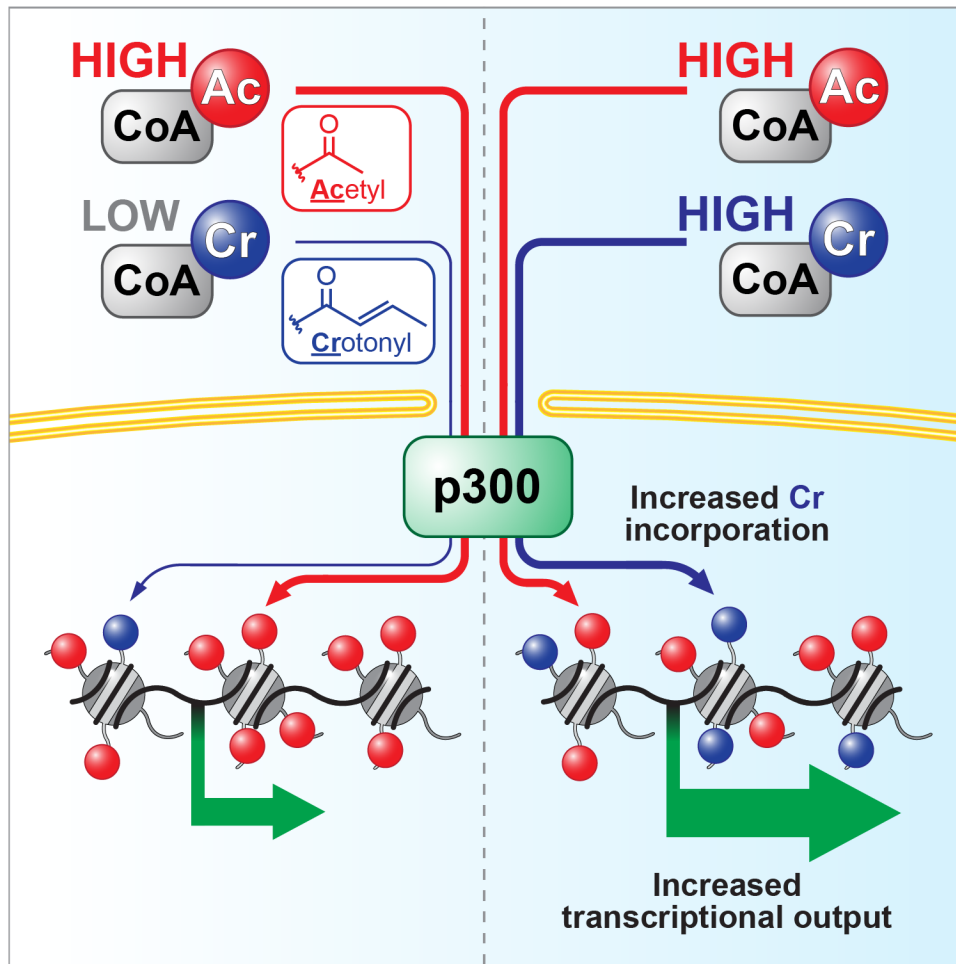


**Figure 4.9: Metabolic Regulation of Transcription Through Differential Acylation.**

A schematic of how acyl-CoA metabolism can impact transcription is presented here. The concentration of acyl-CoAs in the nucleus determines the state of differential acylation at p300-targetted genes, which in turn impacts transcriptional potential. The illustration was designed by Dr. Alexey Soshnev.

functional connection between acyl-CoA metabolism and transcriptional activation, operating through the differential acylation of histones (**Figure 4.9**). Future work as to the physiological range of acyl-CoA concentrations in a variety of cell-types, environments, and stress conditions will be critical to understand specifically how and for what biological process nature exploits this hitherto unexplored mechanism of gene regulation.

These data corroborate the cell-free transcription assays presented in Chapter 2 and demonstrate that the amount of histone crotonylation at a given regulatory element correlates with transcription. While the direct mechanism by which histone crotonylation stimulates transcription is not resolved by these studies, a cell-based model of crotonylation-dependent transcription is established. This cell-based model is utilized in Chapter 5 to demonstrate the relevance of the AF9 YEATS domain interaction with crotonyl-lysine in the context of gene expression.

As discussed in Chapter 2 and the General Introduction, there are two main mechanisms by which histone PTMs function, namely in *cis* (e.g. biophysical modulation of the chromatin fiber) or in *trans* (e.g. recruitment or repulsion of “readers”). Current work in the lab led by Dr. Tanya Panchenko is exploring the role of histone crotonylation on chromatin fiber compaction, yet this work is too preliminary to discuss here. In collaboration with Dr. Haitao Li, major inroads have been made into the *trans* effects of histone crotonylation with the identification and characterization of the YEATS domain as a “reader” module for crotonyl-lysine, the subject of Chapter 5.

## CHAPTER 5: MOLECULAR COUPLING OF HISTONE CROTONYLATION AND ACTIVE TRANSCRIPTION BY AF9 YEATS DOMAIN

### INTRODUCTION

While I have demonstrated that histone crotonylation at the promoters of genes stimulates transcription (Chapter 4), the underlying mechanism(s) responsible for bringing this about remained unclear. As discussed in the general introduction (Chapter 1), there are two major mechanisms by which histone modifications exert their function: through biophysical modulation of the chromatin fiber or through the recruitment or occlusion of effector modules, often termed “readers.” For example, histone acetylation negates the positive charge of the modified lysine residue leading to the destabilization of both inter-nucleosomal and intra-nucleosomal interactions. Histone acetylation also acts as a platform for the binding of reader modules, most famously bromodomains, which tend to be associated with protein and complexes involved in transcriptional regulation (Filippakopoulos et al., 2012). In principle, histone crotonylation could be working through both mechanisms in a similar fashion to histone acetylation, yet little is known about the biophysical consequences of histone crotonylation and a reader of crotonyl-lysine has not been identified. Furthermore, studies have demonstrated that bromodomain proteins bind with lower affinity to acyl chains more complex than acetyl and show minimal to no binding to crotonyl-lysine (Flynn et al., 2015; Vollmuth and Geyer, 2010). In this chapter I describe the identification and characterization of the YEATS domain as a reader of histone crotonylation.

The YEATS domain was identified as a conserved protein domain in proteins associated with transcriptional regulation (pfam accession: PF03366) and named as an acronym of the founding proteins from yeast and human (Yaf9, ENL, AF9, Taf14, and Sas5) (Le Masson et al., 2003). While only four human proteins contain a YEATS domain (AF9, ENL, GAS41, and YEATS2), they are all members of chromatin-modifying complexes associated with transcriptional activation (Schulze et al., 2009) (**Figure 5.1A**). GAS41 and YEATS2 are subunits within two multi-subunit HAT complexes, NuA4 and ATAC, respectively (Doyon et al., 2004; Suganuma et al., 2008). AF9 and ENL are paralogs and interchangeably inhabit two distinct nuclear complexes, the super elongation complex, thought to regulate RNAPII elongation, and the DOT1L complex, responsible for catalyzing methylation at H3K79, a modification associated with active transcription (Lin et al., 2010; Yokoyama et al., 2010) (**Figure 5.1B**). Human YEATS domain proteins are also implicated in cancer. GAS41 is amplified in both glioma and astrocytoma (Fischer et al., 1997; 1996) and recurrently mutated in serous endometrial tumors (Le Gallo et al., 2012). AF9 and ENL are the most recurrent translocation partners of MLL in MLL-rearranged leukemias, a pediatric acute leukemia with poor prognosis and poor response to conventional therapies (Krivtsov and Armstrong, 2007). The majority of this chapter will focus on the YEATS domain of AF9.

The studies described in this chapter were conducted in close collaboration with Dr. Haitao Li and his group at Tsinghua University in Beijing and with Dr. Tanya Panchenko, a colleague in the Allis lab. Dr. Haitao Li's group

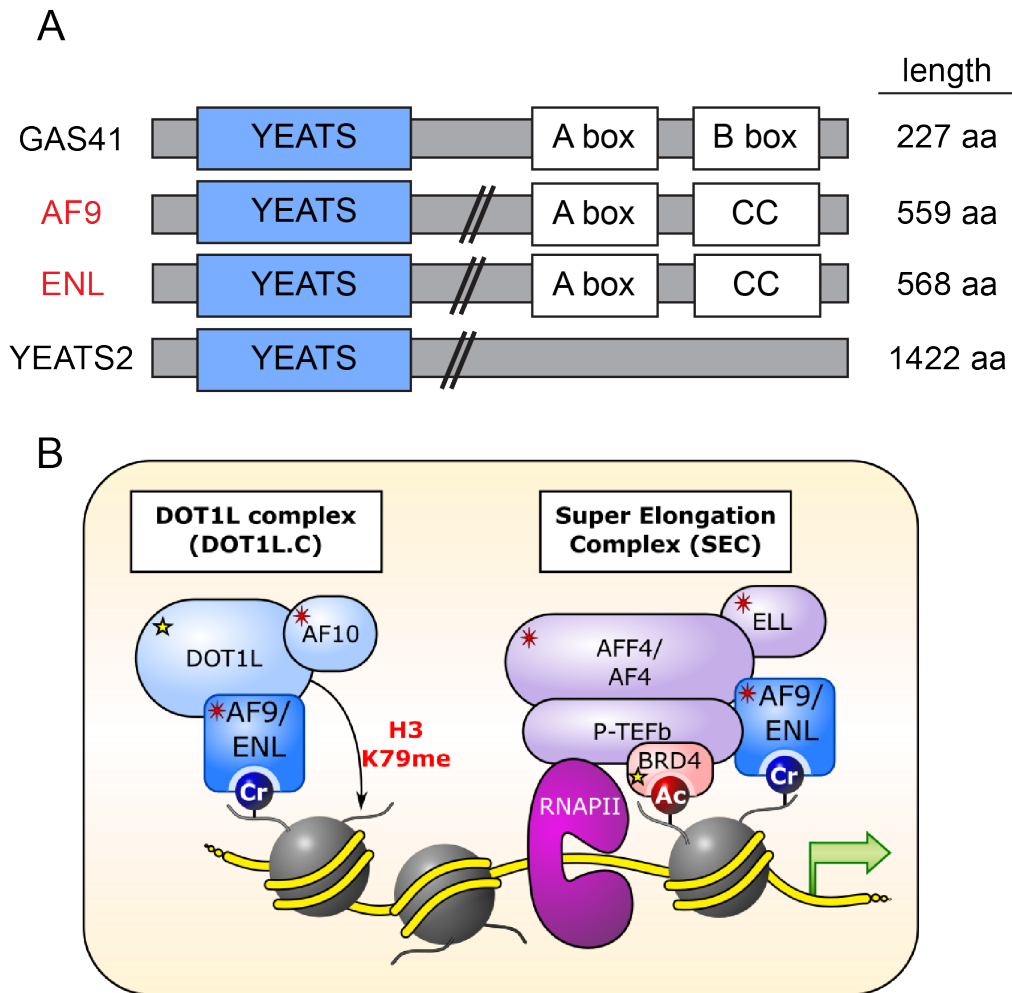


**Figure 5.1: YEATS Domain Proteins are Associated with Transcriptional Regulation.**

(A) Protein domain representation of the four human YEATS domain proteins. The coiled-coil domain (CC) in the c-terminus of AF9 and ENL is their interaction domain with both AFF4 and DOT1L. Not drawn to scale. Adapted from (Schulze et al., 2009). (B) Complex subunit composition for the two AF9 and ENL containing complexes. Red asterisk designates MLL fusion partner and yellow star indicates proteins with small-molecule inhibitors currently in clinical trial. The illustration in Figure 5.1B was designed by Dr. Tanya Panchenko.

(from here on referred to as the Li group) has expertise in the structural biology of epigenetic factors, with a focus on reader domains. As such, the Li group conducted all the structural and biophysical experimentation and analysis. I performed the functional studies in close collaboration with Dr. Tanya Panchenko. This work has recently been submitted for publication and is currently under review at *Molecular Cell*.

Recognition of histone post-translational modifications (PTMs) by histone-binding effectors constitutes a major mechanism for epigenetic regulation (Jenuwein and Allis, 2001). A wide-range of so-called “reader” modules has been characterized for type- and site-specific readout of histone PTMs (Musselman et al., 2012; Patel and Wang, 2013; Taverna et al., 2007). Following the groundbreaking discovery of bromodomain (BrD) as an acetyl-lysine “reading” module (Dhalluin et al., 1999; Sanchez and Zhou, 2009), therapeutic applications of small-molecule inhibitors that block BrD:ligand interactions are currently in clinical trials and show promise for the treatment of various cancers (Filippakopoulos and Knapp, 2014). With the application of mass spectrometry-based proteomics, novel histone PTMs have been documented, including various types of non-acetyl histone lysine acylations, such as propionylation, butyrylation, crotonylation, and succinylation among others (Huang et al., 2014; 2015). Alternations in cellular metabolism that, in turn, lead to shifts in the steady-state balance of non-acetyl histone acylations may function in coordinating particular transcription programs that govern cell growth and development. However, the downstream readout of histone acylations such as crotonyl-lysine is poorly understood in comparison to a wealth of knowledge on histone acetylation.

Like histone acetylation, histone lysine crotonylation has been detected from yeast to human and is primarily associated with active transcription (Tan et al., 2011). As well, crotonylation occurs on the  $\epsilon$ -amino group of lysine, but distinguishes itself from acetylation by its planar orientation and four-carbon length. Histone crotonyl-lysine (Kcr) but not acetyl-lysine (Kac) was found to preferentially mark “escapee genes” during post-meiotic sex inactivation in mouse testis, providing an early indication for a unique role of histone crotonylation distinct from histone acetylation (Montellier et al., 2013; Tan et al., 2011). Similarities between histone acetylation and crotonylation also exist blurring distinctions. For example, Kcr and Kac sites overlap in histones and are catalyzed by p300/CBP, a well-known histone acetyltransferase (HAT). Like histone acetylation, p300/CBP-mediated crotonylation directly stimulates transcription *in vitro* and *in vivo* albeit to varying degrees (Sabari et al., 2015). Moreover, Sirtuin family members (e.g. SIRT1-3), well-studied histone deacetylases (HDACs), remove Kcr in a site-specific manner (Bao et al., 2014; Feldman et al., 2013). A subset of bromodomains, such as BRD9 and TAF1, can tolerate Kcr but with compromised affinity as compared to that of Kac recognition (Flynn et al., 2015). Given these contrasting findings, a clear distinction between histone acetylation and histone crotonylation is lacking and structural and functional consequences between the two are poorly understood.

Previously, the Li group has reported that YEATS domains constitute a novel family of histone acetylation readers (Li et al., 2014). Here, through a combination of structural, biochemical/biophysical binding, and cell-based transcription activation studies, we define the evolutionarily conserved YEATS domain as a family of Kcr-favorable readers that directly link histone

crotonylation to active transcription. Crystal structural studies of AF9 YEATS bound to H3K9cr and H3K18cr peptides revealed an extended aromatic sandwiching cage for crotonyl-specific readout. By contrast, structure analysis of BRD3 bromodomain bound to H3K18ac peptide revealed that the bulkier and more rigid Kcr would be occluded due to steric clash. By experimentally perturbing histone crotonylation levels, we show that AF9 co-localizes with H3K18cr and positively regulates gene expression in a YEATS-dependent manner. Furthermore, we show a previously unappreciated role of AF9 in the rapid gene activation in the context of the immune response. Collectively, our work describes a new epigenetic mechanism to regulate gene activity through the establishment and readout of histone crotonylation, highlighting a functional significance of non-acetyl histone acylations.

## RESULTS

### **The YEATS Domain Has Histone Crotonyl-lysine Binding Activity**

Recently the Li group characterized the YEATS domain as a novel Kac reader module (Li et al., 2014). Based on their structural studies of AF9 YEATS bound to H3K9ac, they defined a serine-lined aromatic sandwiching cage for specific readout of Kac. The long Kac side chain is sandwiched by bulky aromatic residues with the flat acetyl group snugly clamped, well-oriented in position. Interestingly, although the Kac-binding channel is long and flat, it contains a clear opening at the end where the acetyl group protrudes (**Figure 5.2A, pink arrow**). Based on this observation, we hypothesized that this opening might permit the recognitions of bulkier and longer acyl-chain hydrocarbon lengths.

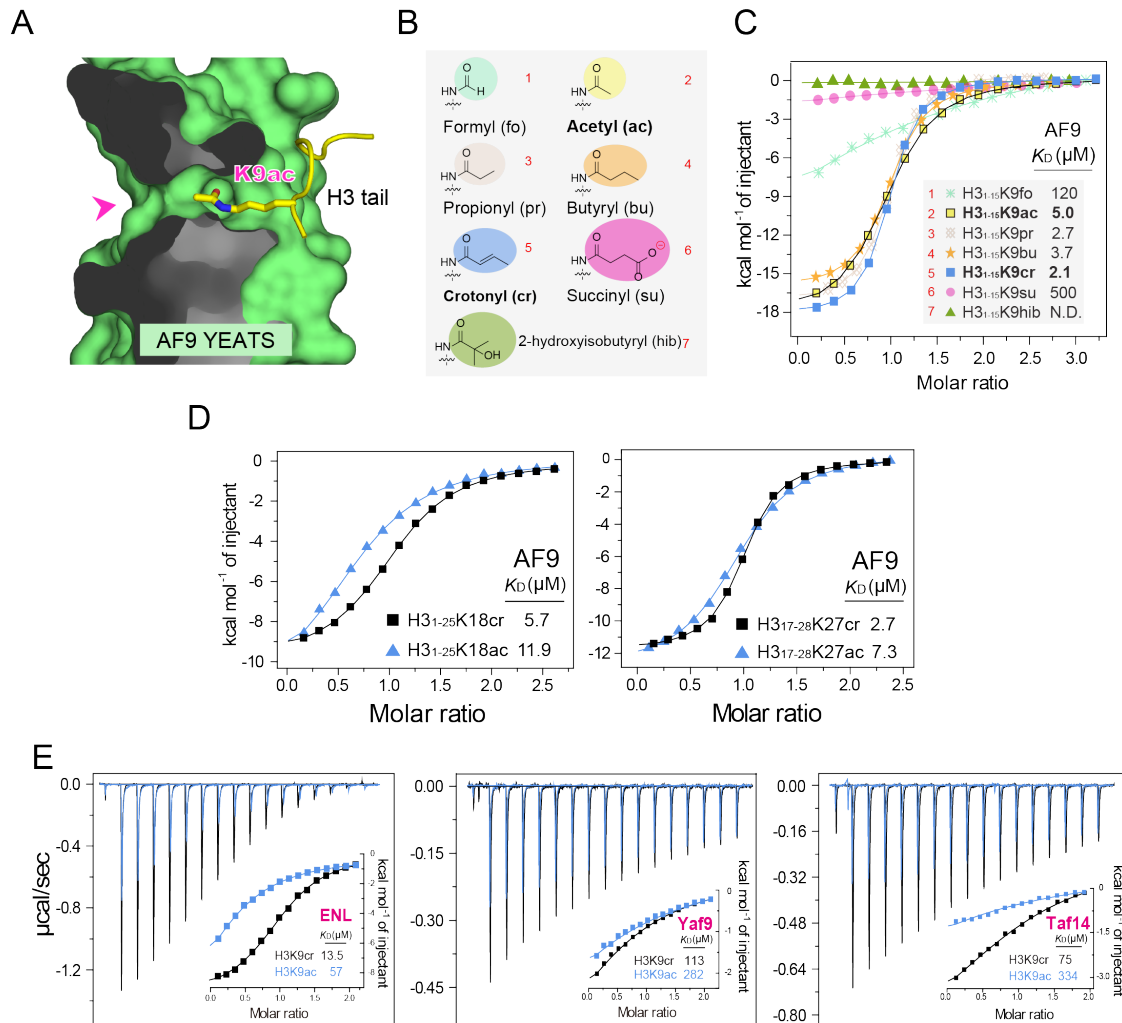


**Figure 5.2: Identification of AF9 YEATS Domain as a Histone Crotonyl-Lysine Reader.**

(A) Cut-away view of AF9 YEATS in complex with H3K9ac peptide. AF9 YEATS is represented as green surface and histone peptide is shown as yellow stick. Pink arrow denotes the wide opening of Kac-reader pocket. (B) Chemical structures of known histone lysine acylations. Abbreviations and numbers correspond to data shown in (C). (C) Isothermal titration calorimetry (ITC) fitting curves of wild type AF9 YEATS titrated by a series of H3<sub>1-15</sub> peptides containing K9 acylations shown in (B). (D) ITC fitting curves comparing Kcr and Kac binding preference at sites H3K18 (left) and H3K27 (right). (E) ITC titration and fitting curves of H3K9ac or H3K9cr bound by YEATS domains from human ENL, and yeast Yaf9 and Taf14. The data and analysis presented in Figure 5.2 were generated by the Li group.

To test this hypothesis, the Li group synthesized a series of acylated histone H3<sub>1-15</sub>K9 peptides including formylation (fo), acetylation (ac), propionylation (pr), butyrylation (bu), crotonylation (cr), succinylation (su) and 2-hydroxyisobutyrylation (hib) (**Figure 5.2B**), and performed isothermal titration calorimetry (ITC) using purified AF9 YEATS domain. Calorimetric titrations revealed that AF9 YEATS binds to lysine acylations in an order of K9cr (2.1  $\mu$ M) > K9pr (2.7  $\mu$ M) > K9bu (3.7  $\mu$ M) > K9ac (5.0  $\mu$ M) > K9fo (120  $\mu$ M) > K9su (500  $\mu$ M) > K9hib (N.D.) ( $K_d$  values shown in parenthesis, **Figure 5.2C**). Remarkably, the linear extension of the hydrocarbon chain beyond Kac resulted in 2.4-, 1.9-, 1.4-fold binding enhancement for Kcr-, Kpr- and Kbu-modified peptides, respectively. By contrast, shortened (Kfo), acidified (Ksu) or branched (Khib) K9 acylations caused a significantly reduced or complete loss of binding. These quantitative binding studies confirm that AF9 YEATS favors a subset of bulkier acyl-lysines with the strongest preference for the planar, four-carbon crotonylation (**Figure 5.2C**).

Based on previous observations made with Kac peptides (Li et al., 2014), the Li group next tested the binding preference of AF9 YEATS for two other sites on the H3 tail, H3K18, and H3K27. For both sites AF9 YEATS bound with higher affinity to Kcr than to Kac (**Figure 5.2D**), suggesting that crotonylation can generally enhance the AF9 YEATS-H3 interaction as compared to acetylation, regardless of the site of modification.

Crotonylation has been identified in budding yeast as well as human (Tan et al., 2011). In order to test if Kcr preference is conserved in YEATS across species, the Li group expressed and purified recombinant YEATS domains of human ENL and of yeast Yaf9 and Taf14. Calorimetric titrations using H3<sub>1-15</sub>K9cr

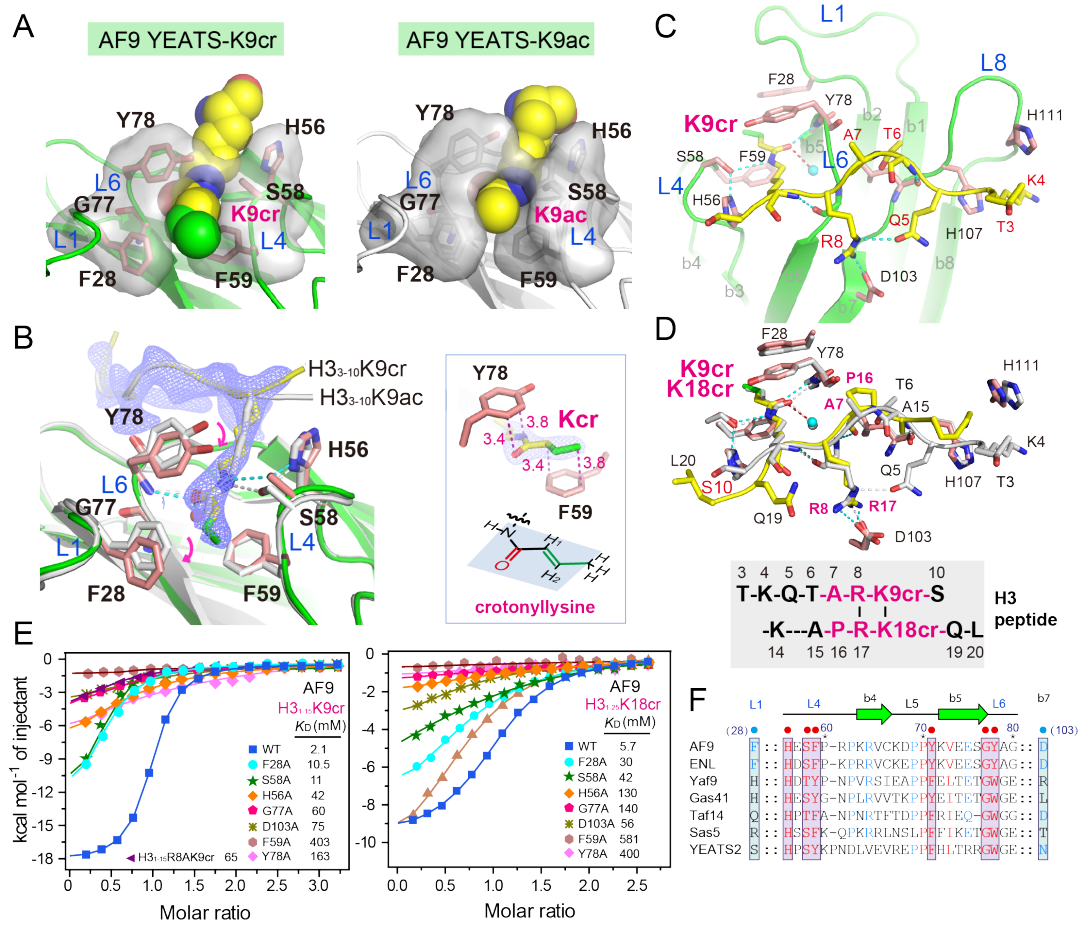
vs H3<sub>1-15</sub>K9ac peptides revealed 2.5- to 4.5-fold binding enhancement for Kcr than Kac (**Figure 5.2E**). Collectively, these results suggest that favorable Kcr readout is a common function of YEATS conserved from yeast to mammals.

### **Structural Basis for Crotonyl-Lysine Recognition by AF9 YEATS**

To explore the molecular basis underlying Kcr readout by AF9 YEATS, the Li group first determined the co-crystal structure of AF9 YEATS bound to H3<sub>1-15</sub>K9cr peptide at 2.7 Å resolution. In the complex structure, AF9 YEATS uses the same Kac-binding aromatic sandwich cage for Kcr recognition; and the crotonyl group takes on a trans-conformation with the extended hydrocarbon chain snugly stacking against F59 aromatic ring (**Figure 5.3A**). Comparison of Kcr-bound and Kac-bound AF9 YEATS binding pocket revealed nearly identical overall pocket arrangements except for slight conformational adjustments of aromatic residues Y78 and F28 (**Figure 5.3B**, left panel). The crotonylamide group is characteristic of a planar feature due to  $\pi$ -electron conjugation (**Figure 5.3B**, right panel). Besides the relayed hydrogen bonding interactions conserved in both Kac and Kcr amide recognition, preferential binding to Kcr is notably contributed by  $\pi$ -aromatic interactions of the planar crotonylamide group with F59, Y78 aromatic rings, as evidenced by interplanar distances between 3.4-3.8 Å (**Figure 5.3B**, right panel). Moreover, additional hydrophobic contacts introduced by hydrocarbon chain extension further stabilize Kcr-AF9 recognition. Even though a 15 amino acid long H3<sub>1-15</sub> peptide was used for crystallization, only H3 T3-S10 could be modeled around a surface formed by loops connecting the core  $\beta$ -strands of AF9

**Figure 5.3: Molecular Basis for H3K9cr and H3K18cr Readout by AF9 YEATS Domain.**

(A) Crystal structure of AF9 YEATS domain shows the insertion of the H3K9 containing crotonyl-lysine (left) and acetyl-lysine (right) into its aromatic sandwich cage. K9ac and K9cr are depicted as space-filling spheres with the two additional hydrocarbon atoms of the crotonyl group highlighted green. (B) Left, detailed interaction map of the K9cr readout by AF9 YEATS shows a rotation of Y78 and F28 when compared to K9ac (pink arrows). For comparison, K9cr-bound structure (green, with key residues highlighted in light pink) was superimposed with K9ac-bound structure (white). Hydrogen bonds are shown as dashes. K9cr peptide is covered by 2Fo-Fc omit map (blue meshes) contoured at  $2.5 \sigma$ . A sharpening B-factor of 75 was applied to obtain the most informative maps. Right, details of  $\pi$ -aromatic stacking between planar H3K9 crotonylamide and F59 phenyl ring with distances denoted in magenta. (C) Overall structure of H3K9cr bound to AF9 YEATS. AF9 YEATS is depicted as green ribbons with key residues highlighted in pink. Histone H3 peptide is shown as yellow sticks. (D) Superimposition of H3K9cr- and H3K18cr-bound complexes. H3K9cr complex is colored white as a reference and H3K18cr peptide is shown as yellow sticks. Structure-based sequence alignment between H3K9cr and H3K18cr is shown below. (E) Mutagenesis and ITC titration assays using mutant and wild type AF9 YEATS with H3K9cr (left) or H3K18cr (right) peptides. (F) Sequence conservation analysis of YEATS reader pocket residues from yeast to human. The data and analysis presented in Figure 5.3 were generated by the Li group.



YEATS (**Figure 5.3C**). Importantly, K9cr is stapled into a pocket formed by L1, L4 and L6 loops of AF9, and the K9cr-flanking H3 residues are recognized by extensive polar or hydrophobic contacts including a signature “H3R8-AF9D103” hydrogen bonding pair (**Figures 5.3C**), demonstrating the critical importance of the -1R on the histone peptide.

AF9 YEATS binds to H3K18cr with an affinity of 5.7  $\mu\text{M}$ . Therefore, we next determined the co-crystal structure of histone AF9 YEATS bound to H3<sub>1-20</sub>-K18cr peptide at 2.8 Å resolution. In the complex structure, H3 K14-L20 was modeled with K18cr anchored and was recognized essentially in the same mode as described above for K9cr (**Figures 5.3D**). H3K18cr peptide binds to AF9 YEATS in the same orientation as H3K9cr such that residue H3R17 at -1 position interacts with acidic residue D103, recapitulating the importance of an “R-Kcr” signature motif for AF9 YEATS recognition (Li et al., 2014). Structural alignment of H3K18cr- and H3K9cr-bound AF9 complexes revealed that H3 segment “P16-R17-K18cr” overlapped well with “A7-R8-K9cr”, while H3 K14-A15 and Q19-L20 displayed large discrepancy (**Figure 5.3D**). Nevertheless, crotonylation brings H3K18cr binding by AF9 YEATS to single digit micromolar order - an affinity fairly strong compared to other known histone mark-reader pairs (Patel and Wang, 2013).

### **Mutagenesis and Binding Studies**

We next performed mutagenesis and ITC titration studies to verify the importance of key Kcr binding residues. As summarized in **Figure 5.3E**, alanine mutation of pocket residues F28, H56, S58, F59, G77, and Y78 resulted in 5- to 192-fold binding reduction for H3K9cr and 5- to 102-fold binding reduction for

H3K18cr peptides, respectively. Strikingly, F59A led to the most dramatic binding loss, highlighting its critical role in lysine crotonylation-specific readout by providing aromatic stacking interactions.. D103 plays an important role in “-1” arginine recognition within the “R-Kcr” motif. In support, AF9 D103A mutation caused 36- and 10-fold binding loss for H3K9cr and H3K18cr peptides. Consistently, histone H3 R8A mutation caused a binding loss of 31-fold for H3K9cr readout (**Figure 5.3E**, left panel), further validating the contribution of “H3R8-D103” hydrogen bonding pair. Sequence alignment reveals that all the pocket residues from L4 and L6 loops tested above are highly conserved among YEATS domains (**Figure 5.3F**), consistent with the conserved Kcr reader activity observed for YEATS from yeast to human.

### **YEATS Domain Is a Crotonyl-Lysine Reader in the Cellular Context**

To confirm the AF9 YEATS-Kcr interaction in a cellular context, Dr. Tanya Panchenko performed immunoprecipitation (IP) of AF9 to determine whether crotonylated nucleosomes would co-IP. Using HeLa cell lines expressing FLAG-tagged constructs of AF9 or AF9 with the F59A point mutant shown to ablate YEATS-Kcr binding (**Figure 5.3E**), Dr. Panchenko generated mono-nucleosome containing nuclear extracts by MNase digestion and performed FLAG-IPs in this context. Immunoblot analysis of IP material revealed that while ELL2 and AFF4 (complex component members with mapped interaction domains in the C-terminus of AF9) were insensitive to the F59A mutation, both H3K9cr and H3K18cr nucleosomes only co-IP with the wild-type AF9 (**Figure 5.4A**). These data demonstrate that AF9 binds nucleosomes marked by H3K9cr and H3K18cr and that this interaction is YEATS-dependent.

Dr. Panchenko next performed nucleosome pulldowns with pre-modified nucleosomes generated *via* amber suppression. Recombinant pre-modified H3K9ac, H3K9cr, H3K18ac, and H3K18cr histones were generated by amber suppression, as previously described (Gattner et al., 2013; Kim et al., 2012). The modification statuses of these pre-modified histones were validated by MS/MS analysis, which showed the expected modification at >90% purity (**Figure 5.4B**). These pre-modified H3 histones, in conjunction with unmodified recombinant core histones, were assembled into nucleosomes by standard salt dialysis (Dyer et al., 2004) with a biotinylated 601 DNA template, allowing the nucleosomes to be immobilized by streptavidin. The immobilized nucleosomes either unmodified, acetylated, or crotonylated (at either H3K9 or H3K18) were then incubated in HeLa nuclear extract and interacting proteins were affinity purified. Immunoblot analysis of pulldown material, focusing on the YEATS domain proteins AF9 and ENL, revealed that while the acylated nucleosomes at either site pulled down more AF9 and ENL than unmodified nucleosomes or control pulldowns, nucleosomes bearing H3K9cr and H3K18cr purified more AF9 and ENL from extract than nucleosomes bearing H3K9ac or H3K18ac (**Figure 5.4C**). These data corroborate the biophysical data that the YEATS domain of AF9 has a stronger preference for Kcr than Kac.

### **Bromodomains Do Not Exhibit YEATS-Like Preference for Crotonyl-lysine**

Bromodomains constitute a major family of histone acetylation readers (Filippakopoulos et al., 2012). To explore whether bromodomains have crotonyl-lysine reader activity, the Li group expressed a variety of bromodomains and compared their binding affinity to Kac- and Kcr-containing peptides. Based on

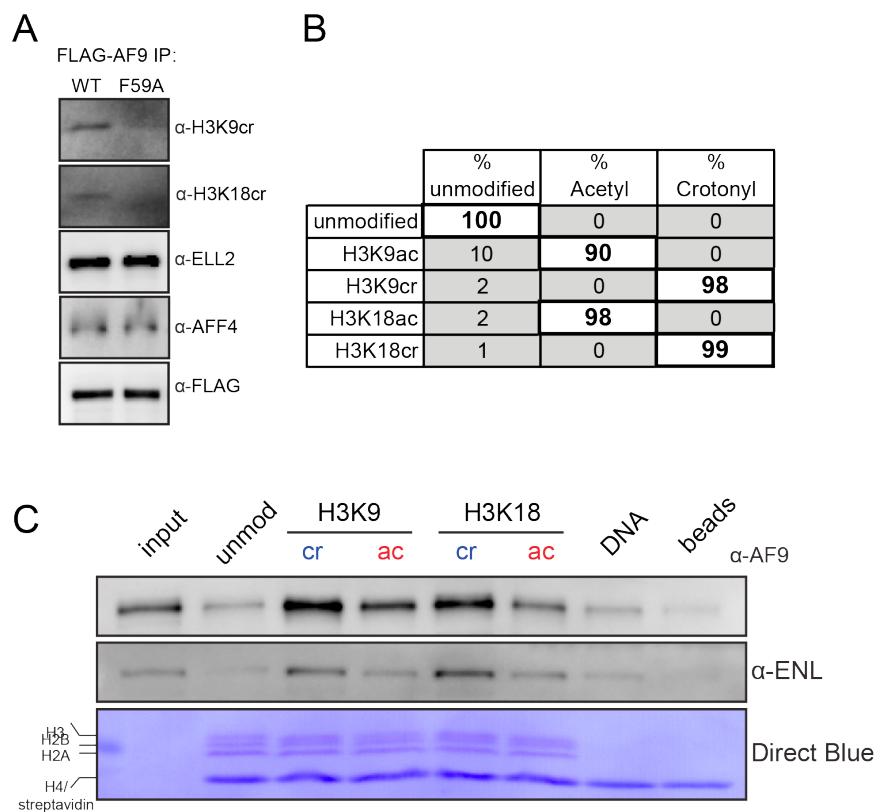


**Figure 5.4: The YEATS Domain Prefers Kcr to Kac Marked Nucleosomes.**

(A) AF9 co-immuno-precipitates nucleosomes marked by H3K9cr and H3K18cr in a YEATS-dependent manner. MNase nuclear extracts were derived from HeLa cells expressing either a wildtype FLAG-tagged AF9 construct (FLAG-AF9-WT) or a F59A mutant FLAG-tagged AF9 (FLAG-AF9-F59A). Immunoblot analysis with the indicated antibodies was performed on the IP eluate of WT and F59A AF9 constructs. (B) MS/MS analysis of recombinant histones pre-modified via amber suppression demonstrates the purity of the expected product. (C) Immunoblot analysis for AF9 and ENL of indicated pulldowns. Site-specific pre-acetylated or pre-crotonylated H3-containing nucleosomes were used as bait in pulldown assays. Direct Blue staining of the membrane documents comparable input material. The streptavidin monomer co-migrates with histone H4 at this resolution. The data and analysis presented in Figure 5.3 were generated by Dr. Tanya Panchenko.

the classification of bromodomains (Filippakopoulos et al., 2012), representative members from seven major BrD sub-families were chosen for ITC titration assay. While all the bromodomains tested here exhibited reported Kac binding activity at their respective target sites, cognate Kcr binding was not detected for most bromodomains (**Figures 5.5A**). Though the second bromodomain of TAF1 (abbreviated TAF1<sub>BrD2</sub> and in an analogous manner hereafter for other multi-bromodomain proteins) displayed an H4K5crK8cr binding activity, its binding affinity was three times weaker than the H4 acetylation counterpart (117  $\mu$ M *vs* 52  $\mu$ M, **Figure 5.5A**).

The Li group next synthesized a series of histone acylation peptides bearing Kac, Kpr, Kbu, and Kcr marks (**Figure 5.5B**) at sites H4K8, H3K14, and H3K18, and performed quantitative ITC titrations for BRD4<sub>BrD1</sub>:H4K8ac/pr/bu/cr, BAZ2A-H3K14ac/pr/bu/cr, BRD3<sub>BrD2</sub>-H3K18ac/pr/bu/cr, as well as AF9<sub>YEATS</sub>-H3K18ac/pr/bu/cr pairs. Interestingly, all bromodomains exhibited reduced binding following chain extension from acetylation to crotonylation (**Figure 5.5C**), suggesting that bromodomains are primarily evolved towards Kac readout with restricted tolerance to Kpr, Kbu and Kcr. By contrast, AF9-YEATS exhibited enhanced binding following chain extension with tightest binding for Kcr (**Figures 5.5C**). The above observations on BrD acyl-lysine readout are in agreement with a recent profiling study, in which 49 bromodomains tested displayed compromised binding to non-acetyl acylations (Flynn et al., 2015). Collectively, these data suggest that bromodomains do not exhibit YEATS-like preference for non-acetyl acylation, especially crotonyl-lysine.

## Structural Basis for Differential Recognition of H3K18 Acylation by BRD3 and AF9

The above data suggest that BRD3 and AF9 recognize H3K18 acetyl versus crotonyl with distinct acylation type preference. To better explore the underlying structural basis, the Li group determined the co-crystal structure of BRD3<sub>BrD2</sub> bound to H3<sub>10-24</sub>-K18ac peptide at 2.6 Å resolution. In the complex structure, H3 “A15-P16-R17-K18ac-Q19-L20-A21-T22” could be modeled with K18ac inserted into the well-established Kac reader pocket formed by loops L<sub>ZA</sub> and L<sub>BC</sub> (**Figures 5.5D**). Interaction analysis revealed that Kac is notably stabilized by hydrophobic contacts and hydrogen bonding interactions involving an invariant asparagine N391 as well as Y348 and P333 (mediated by water) (**Figures 5.5D**). Moreover, H3K18ac flanking sequences contributed multiple hydrogen bonding and hydrophobic contacts with BRD3<sub>BrD2</sub>. Notably, histone H3R17 at -1 position formed a hydrogen-bond with D394 and histone H3L20 at +2 position is inserted into a hydrophobic pocket formed by W332, P333, H395, V397 and M400, collectively accounting for H3K18 site preference (**Figures 5.5D**).

It is interesting to note that both BRD3<sub>BrD2</sub> and AF9 adopt a similar strategy to recognize a signature “R-K” motif around H3K18ac/cr, in which the “-1R” is stabilized by an aspartate residue (D394 in BRD3 and D103 in AF9), while K18ac/cr is inserted into an adjacent reader pocket (**Figures 5.5E and 5.5G**). The Kac pocket of BRD3<sub>BrD2</sub> is formed at the center of the four-helical bundle of the bromodomain (**Figures 5.5D and 5.5E**). This configuration, with its tight network of hydrogen bond stabilized water molecules (**Figure 5.5E, blue balls**) is perfectly suited for Kac binding, but would be restrictive to any further extension of the hydrocarbon chain. Conceivably, in order to fit into the reader pocket,

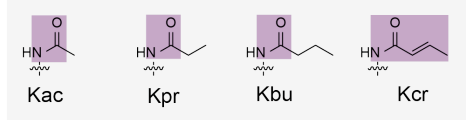
**Figure 5.5: Bromodomains Do Not Exhibit Crotonyllysine Preference and the Underlying Molecular Basis.**

(A) Summary of Kcr- and Kac-binding affinities by select bromodomains from seven phylogenetic families (Filippakopoulos et al., 2012). Cognate modification sites are listed in the last column of the table. (B) Comparison of chemical structures of lysine acetylation (Kac), propionylation (Kpr), butyrylation (Kbu) and cronylation (Kcr). The planar part due to  $\pi$ -conjugation is box-shaded. (C) ITC fitting curves comparing Kac, Kpr, Kbu and Kcr binding affinities of H4K8 readout by the first bromodomain of BRD4 (BRD4<sub>BrD1</sub>), of H3K14 readout by BAZ2A bromodomain, of H3K18 readout by the second bromodomain of BRD3 (BRD3<sub>BrD2</sub>) and AF9 YEATS. (D) Histone H3K18ac binding by BRD3<sub>BrD2</sub>. BRD3<sub>BrD2</sub> is presented as ribbon covered by its half-transparent surface. H3K18ac peptide is shown as yellow sticks. Water molecules are shown as cyan balls. (E) Recognition of H3 “R17-K18ac” by BRD3<sub>BrD2</sub>. BRD3<sub>BrD2</sub> is shown as surface view. Note the spatial restraints around the K18 acetylamide group caused by the side-open pocket. (F) Steric clash between F334 of BRD3<sub>BrD2</sub> and a modeled K18cr. The experimental K18ac group is shown in yellow and overlaid for reference. The extended hydrocarbon group of cronylation is colored green. Red disk indicates steric clash. (G) Recognition of H3 “R17-K18cr” by AF9 YEATS. Note the position of crotonylamide group in the extended and end-open pocket. The data and analysis presented in Figure 5.5 were generated by the Li group.

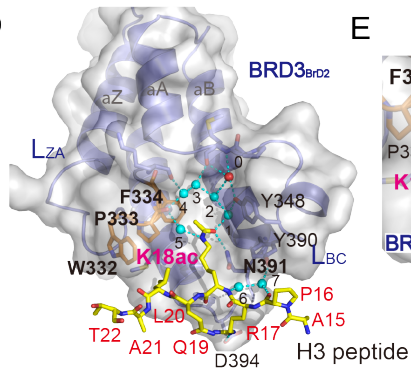
A

Bromo protein	Kcr-binding $K_D$ ( $\mu$ M)	Kac-binding $K_D$ ( $\mu$ M)	Bromo family	Modified site
GCN5	N.D.	100	I	H4K16
BPTF	N.D.	100	I	H4K16
BRD4 <sub>BrD1</sub>	>3,000	270	II	H4K8
BRD3 <sub>BrD2</sub>	N.D.	45	II	H3K18
p300	N.D.	70	III	H4K12
BDR9	N.D.	350	IV	H3K27
BAZ2A	N.D.	20	V	H3K14
TAF1 <sub>BrD2</sub>	117	52	VII	H4K5K8
PB1 <sub>BrD2</sub>	N.D.	330	VIII	H3K14

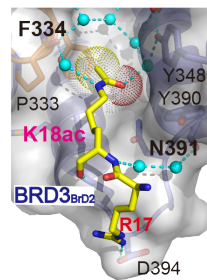
B



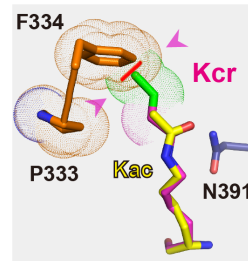
D



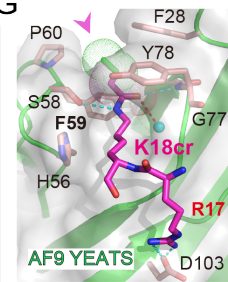
E



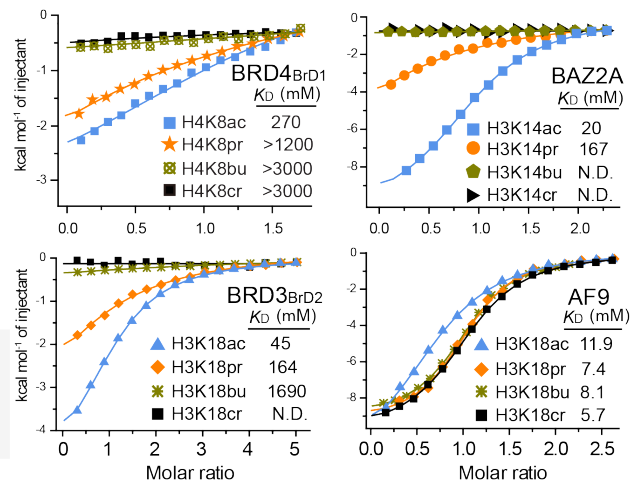
F



G



C



bulkier acylations such as propionylation and butyrylation have to adopt a bent conformation at the cost of binding energy. This may account for about 4- and 38-fold reduced affinity for H3K18pr and H3K18bu readout by BRD3<sub>BRD2</sub>, respectively. Furthermore, given the planar feature of crotonylation, H3K18cr may be too rigid and bulky to fit into the BRD3<sub>BRD2</sub> reader pocket, thus causing total loss of binding. In support, the modeled Kcr hydrocarbon chain directly clashes against the phenyl ring of F334, a residue highly conserved in bromodomains (**Figures 5.5F**) (Filippakopoulos et al., 2012). In contrast, the extended AF9 YEATS reader pocket is a flat and open ended, ideal dimension for acyl chains bulkier than Kac, especially Kcr (**Figure 5.5G**).

### **Kcr and AF9 YEATS Co-Localize Genome-Wide**

To assess the functional role of the AF9 YEATS-Kcr interaction I returned to the lipopolysaccharide (LPS)-induced inflammatory response as a model of gene activation. In Chapter 4, I describe a role for p300-catalyzed H3K18cr in inflammatory gene activation by studying the macrophage-like cell line RAW264.7 (Sabari et al., 2015). To assess the role of AF9 in LPS-driven gene activation I first compared cells pre and post LPS stimulation by chromatin immunoprecipitation followed by high throughput sequencing (ChIP-seq) for AF9 and in parallel generated a RAW264.7 cell line expressing a FLAG-tagged AF9 and performed FLAG ChIP-seq under the same conditions. Both ChIP-seq data sets showed that AF9 is recruited to LPS-induced genes upon LPS stimulation, demonstrating that AF9 is involved in the process of inflammatory gene activation (**Figures 5.6A and 5.6B**). Both datasets showed that AF9 peaks 3'

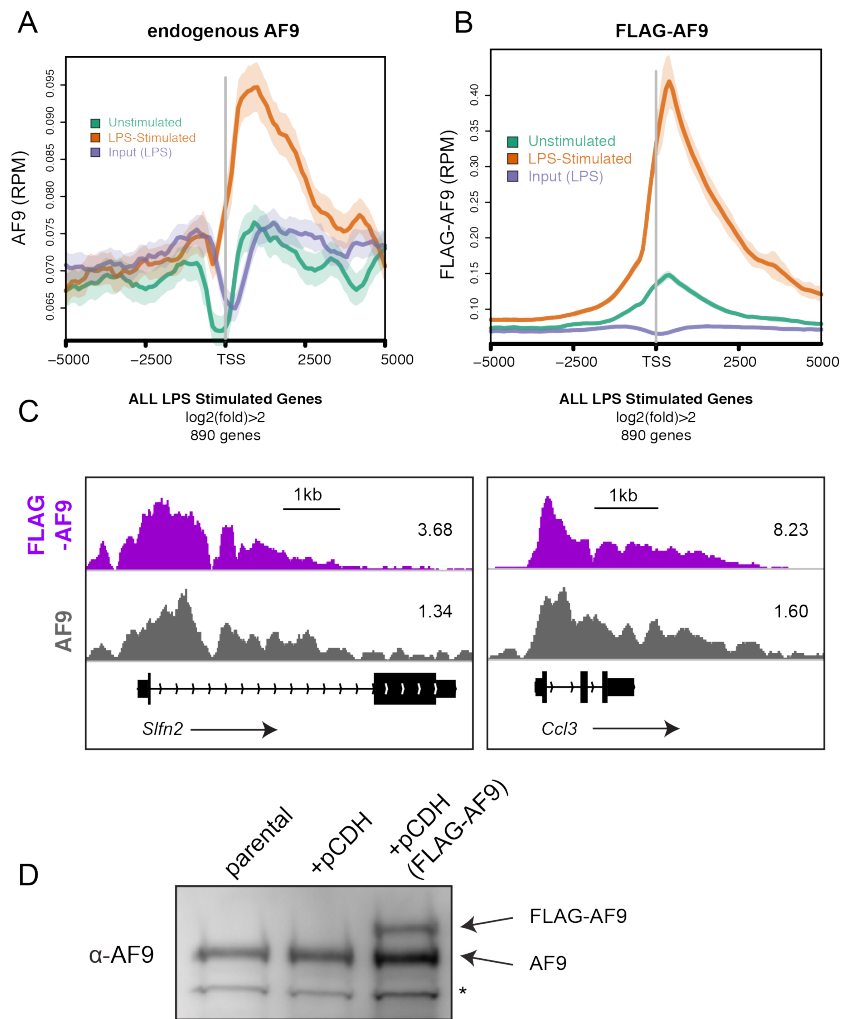


**Figure 5.6: ChIP-Seq for AF9 and FLAG-AF9.**

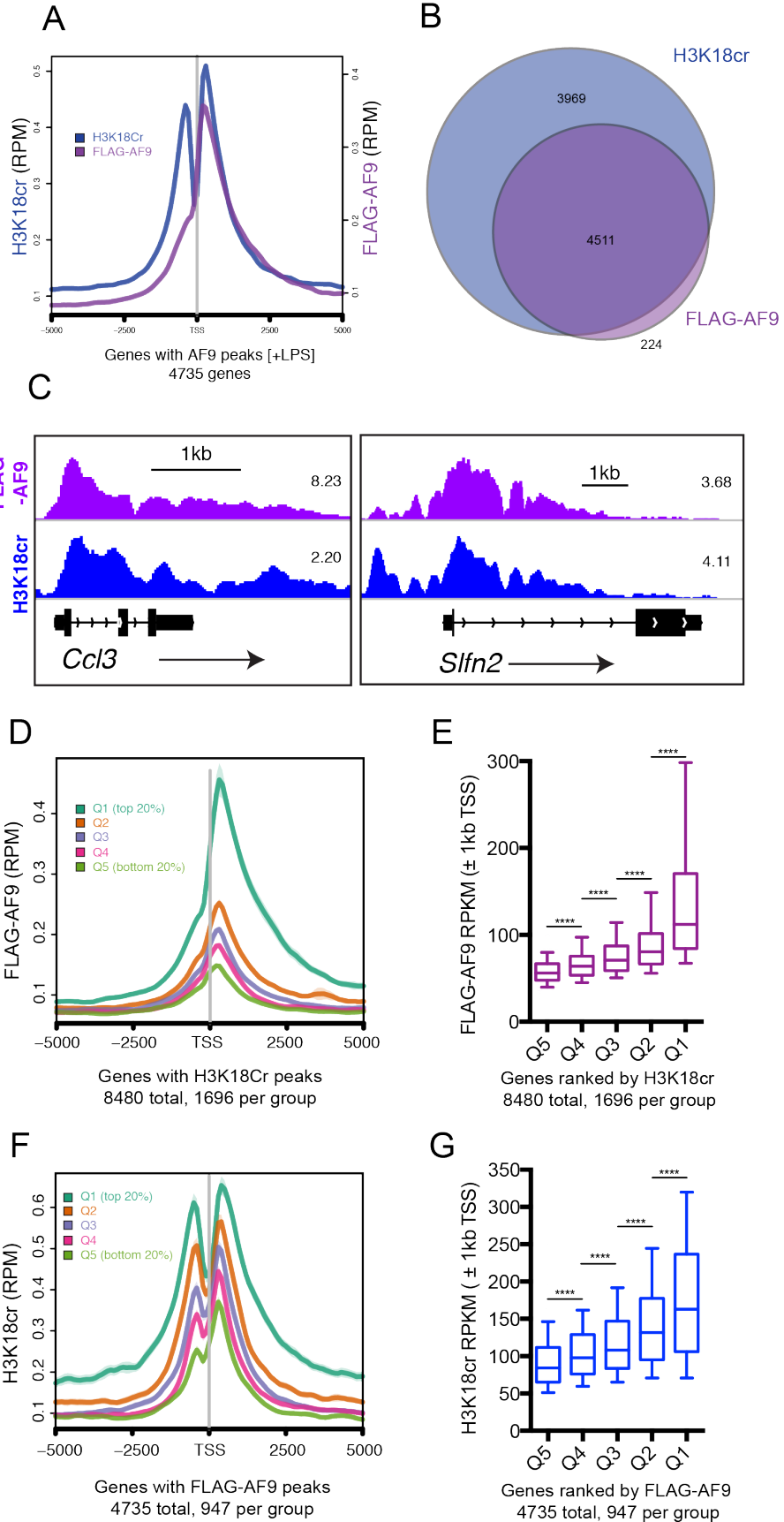
(A-B) AF9 is recruited to LPS stimulated genes. Average profile of (A) AF9 ChIP-seq and (B) FLAG-AF9 ChIP-seq data from unstimulated or LPS-stimulated RAW264.7 cells plotted  $\pm 5\text{kb}$  TSS of LPS-stimulated genes ( $\log_2(\text{fold}) > 2$ ; 890 genes). (C) Comparison of endogenous AF9 (grey) and FLAG-AF9 (purple) ChIP-Seq from RAW264.7 cells at two genes with endogenous AF9 peaks, *Slfn2* and *Ccl3*. (D) The FLAG-AF9 transgene is expressed at levels lower than endogenous AF9. Whole cell lysates from the indicated RAW 264.7 cell lines were resolved by SDS-PAGE and subject to immunoblot with an antibody against AF9. The FLAG tagged AF9 migrated slower due to increased molecular weight. The asterisk denotes a non-specific band.

of the transcription start site (TSS) and exhibited a tail that stretches into the gene body, as can be observed in average profiles of genes (**Figures 5.6A and 5.6B**) or at specific loci (**Figure 5.6C**). While ChIP-seq for the endogenous AF9 exhibited the same trends as the FLAG ChIP-seq, the endogenous AF9 data set suffered from high levels of background signal. Furthermore, the FLAG-AF9 protein was expressed at levels comparable to, if not lower than endogenous AF9 (**Figure 5.6D**), mitigating concerns about artifactual localization due to hyper over-expression. For these reasons the remainder of the analysis was performed with the higher-quality FLAG-ChIP-seq data.

I next asked whether AF9 and H3K18cr co-localize across the genome. Using ChIP-seq data for FLAG-AF9 from LPS-stimulated cells I generated a list of 4735 genes with high confidence AF9 peaks  $\pm$  1kb from their TSS and plotted FLAG-AF9 and H3K18cr (Sabari et al., 2015) at these genes around the TSS (**Figure 5.7A**). From this global analysis, the 3' peak of H3K18cr co-localized with the peak of AF9. Additionally, 95% of AF9 bound genes were also marked by H3K18cr (4511 out of 4735) (**Figure 5.7B**). The co-localization of AF9 and H3K18cr can be further appreciated locally at representative genes *Ccl3* and *Slfn2* (**Figures 5.7D**). Having shown that H3K18cr co-localizes with AF9 across genes marked by AF9, I next asked whether the levels of H3K18cr correlate with the levels of AF9. To do this I ranked genes marked by H3K18cr by number of read bases normalized to total reads (RPKM)  $\pm$  1kb TSS (8480 genes) and grouped these genes into quintiles Q1-Q5, with Q1 genes exhibiting the most reads for H3K18cr and Q5 the lowest (1696 genes per group). FLAG-AF9 data was then plotted for these quintiles around TSS and the highest FLAG-AF9 signal was

**Figure 5.7: Genome-Wide Co-Localization of H3K18cr and AF9.**

(A) H3K18cr and AF9 co-localize at genes marked by AF9. Average profile of FLAG-AF9 and H3K18cr ChIP-seq data from LPS-stimulated cells plotted +/- 5kb TSS of genes occupied by AF9 (4735 genes). (B) Venn diagram showing the overlap of AF9 occupied (purple) and H3K18cr marked (blue) genes. H3K18cr marks 95% of genes occupied by AF9. (C) Genome-browser view of FLAG-AF9 (purple) and H3K18cr (blue) at three representative AF9-occupied genes. (D) Venn diagram showing the overlap of FLAG-AF9 occupied (purple), H3K18cr marked (blue), and H3K18ac marked (red) genes.



found on genes with the highest H3K18cr and vice versa (**Figure 5.7D**). In a similar analysis, RPKM values  $\pm$  1kb for genes in Q1-Q5 were counted for FLAG-AF9 and then graphed in box and whisker plots (**Figure 5.7E**). Each successive group of ranked genes exhibited significantly higher FLAG-AF9 reads demonstrating the correlation between AF9 and H3K18Cr levels at active genes. The same trend was observed by plotting and counting RPKM values for H3K18cr for groups ranked by levels of FLAG-AF9 (**Figures 5.7F and 5.7G**). These data demonstrate the co-localization of AF9 and H3K18Cr across the genome and specifically 3' of the TSS of active genes.

### **The AF9-Kcr Interaction Positively Regulates Gene Expression in a YEATS-Dependent Manner**

Having shown that AF9 is recruited to LPS-stimulated genes and that AF9 co-localizes and correlates with H3K18cr genome-wide, I next asked whether this co-localization is H3K18cr- and/or YEATS-dependent. I have previously reported that by increasing the cellular concentration of crotonyl-CoA prior to LPS stimulation I could directly increase the levels of H3K18cr thereby increasing expression of a number of p300-targetted genes (Sabari et al., 2015) (see Chapter 4). Based on our findings that the YEATS domain exhibits preferential binding to Kcr, I hypothesized that this interaction and subsequent recruitment of YEATS-containing complexes could be the molecular mechanism driving the enhanced stimulation capacity of Kcr. To understand the impact of increasing H3K18cr on AF9 recruitment I performed ChIP-seq for FLAG-AF9 from cells pre-treated with crotonate (10mM) followed by LPS stimulation. Utilizing previously published RNA-seq data sets (Sabari et al., 2015), I generated two groups of LPS-stimulated

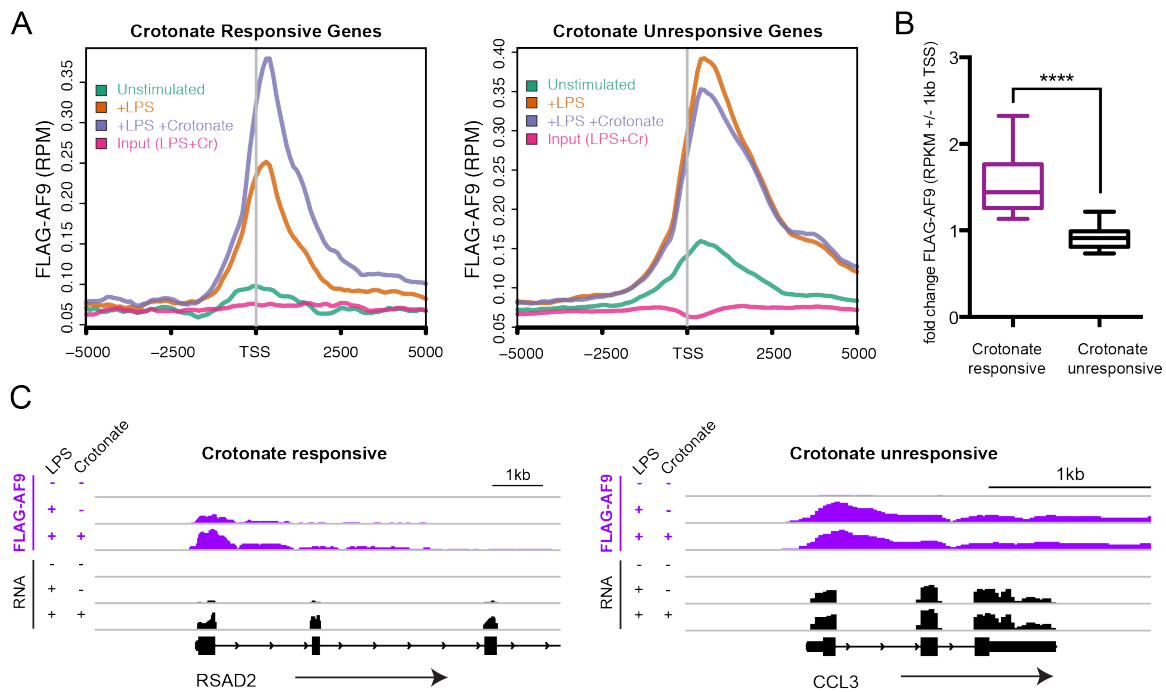


**Figure 5.8: FLAG-AF9 ChIP-Seq.**

(A) AF9 is further recruited to genes transcriptionally responsive to increased crotonyl-CoA concentration by crotonate pre-treatment. FLAG-AF9 ChIP-seq data from RAW264.7 cells unstimulated (green), LPS-stimulated (orange), or pre-treated with 10mM sodium crotonate and then LPS-stimulated (purple)  $\pm 5$ kb TSS of genes either responsive to crotonate ( $\log_2(\text{fold-FPKM}) > 1.0$ ; 52 genes) shown in left panel, or genes unresponsive to crotonate ( $\log_2(\text{fold-FPKM}) < 0.01$ ; 233 genes) shown in right panel. Sequenced input from crotonate treated and LPS stimulated cells is plotted in pink. (B) Box and whisker plot (10-90<sup>th</sup> percentile) of fold change due to crotonate pre-treatment in FLAG-AF9 RPKM  $\pm 1$ kb TSS of crotonate responsive and crotonate unresponsive genes. \*\*\*\*: t-test derived p-value < 0.0001. (C) Genome-browser view of FLAG-AF9 ChIP-seq (purple) and RNA-seq (black) data from cells unstimulated, LPS-stimulated, or crotonate pre-treated and LPS-stimulated for a representative responsive gene (*Rsad2*) and representative unresponsive gene (*Ccl3*).

genes ( $\log_2(\text{fold}) > 1.0$ ;  $\pm$  LPS), those that were crotonate responsive ( $\log_2(\text{fold}) > 1.0$ ; LPS  $\pm$  crotonate) and those that were unresponsive to crotonate ( $\log_2(\text{fold}) < 0.01$ ; LPS  $\pm$  crotonate). FLAG-AF9 ChIP-seq data from unstimulated, LPS-stimulated, and LPS-stimulated plus crotonate pre-treatment conditions were plotted around the TSS of these two sets of genes (**Figure 5.8A**). Consistent with a role for AF9 in crotonate-responsiveness, FLAG-AF9 signal was higher with crotonate treatment only at crotonate responsive genes. By comparing FLAG-AF9 RPKM  $\pm$  1kb TSS of genes in each group and calculating the fold change induced by crotonate pre-treatment for each gene, I observed a mean fold-change in AF9 of 1.58 for responsive genes compared to 0.92 in unresponsive genes (**Figure 5.8B**). The increase in AF9 localization due to increased Kcr by crotonate treatment can be seen at *Rsad2*, a representative crotonate responsive gene, whereas at *Ccl3*, a representative unresponsive gene, there was no change to AF9 localization (**Figure 5.8C**). Together these data support a role for enhanced AF9 localization at genes that have enhanced H3K18cr levels and expression.

To test whether the increase in AF9 upon increased Kcr is dependent upon the YEATS-Kcr interaction Dr. Panchenko generated a RAW264.7 cell line expressing FLAG-AF9(F59A), a point mutation which ablates H3K18cr binding *in vitro* and in cells (**Figures 5.3E and 5.4C**), and I compared this line to FLAG-AF9(WT) by FLAG-ChIP under pre-treatment of increasing concentrations of sodium crotonate. The two transgenes were expressed at equivalent levels, as demonstrated by immunoblot and qRT-PCR (**Figures 5.9A and 5.9B**). Using primers designed at AF9 peaks, ChIP-qPCR analysis at a number of crotonate-responsive genes (*Rsad2*, *Il6*, *Ifit1*, *Cmpk2*, and *Gbp2*) showed that while AF9 signal increased with increasing concentrations of crotonate, the F59A mutant

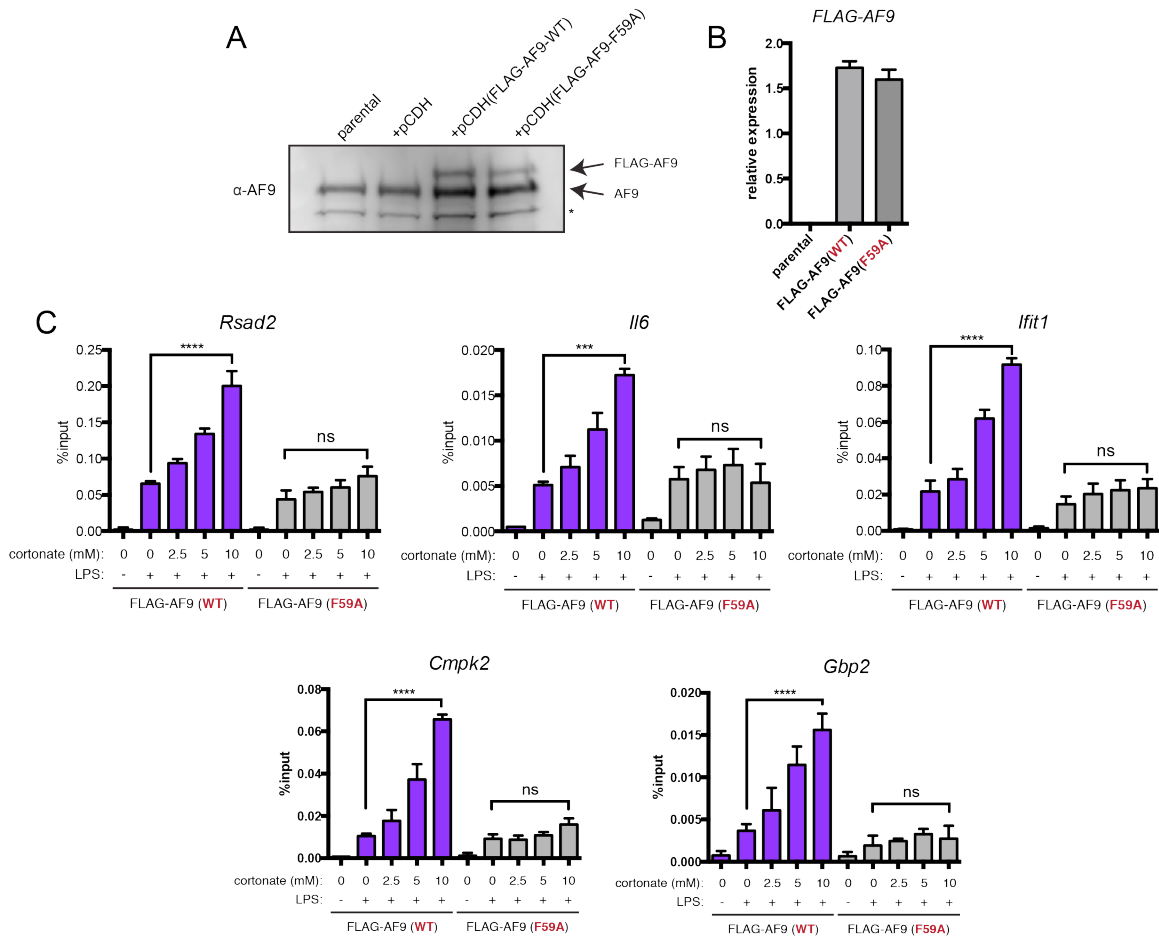


**Figure 5.9: The Increased Recruitment of AF9 Due to Crotonate Pre-Treatment is YEATS-Kcr Dependent.**

(A) Immunoblot analysis for AF9 protein levels of whole cell lysates from the indicated cell lines. Top band is the FLAG-tagged AF9, the middle band is endogenous AF9, and the band marked by an asterisk is a non-specific protein. (B) qRT-PCR analysis of FLAG-AF9 expression in the indicated cell lines. Data is presented as mean relative expression with standard deviation. (C) FLAG-ChIP was performed from RAW264.7 cells expressing a wild type AF9 (FLAG-AF9(WT)) construct or an AF9 construct with the YEATS-Kcr abrogating F59A mutation (FLAG-AF9(F59A)) under the conditions indicated followed by qPCR analysis of ChIP product and appropriate inputs. Data are plotted as mean percent input + standard deviation. \*\*\*: t-test derived p-value = 0.0001; \*\*\*\*: <0.0001; ns >0.05.

was unresponsive (**Figure 5.9C**). Together these data support the model that the AF9-YEATS interaction with H3K18cr is capable of enhancing AF9 recruitment.

Interestingly, the F59A mutant was recruited to tested loci upon LPS stimulation to comparable levels as the wild-type protein suggesting that it was integrated into its associated complexes and recruited by YEATS-independent means, yet it lost the capability to “read” H3K18cr and was not further recruited upon crotonate treatment (**Figure 5.9C**).

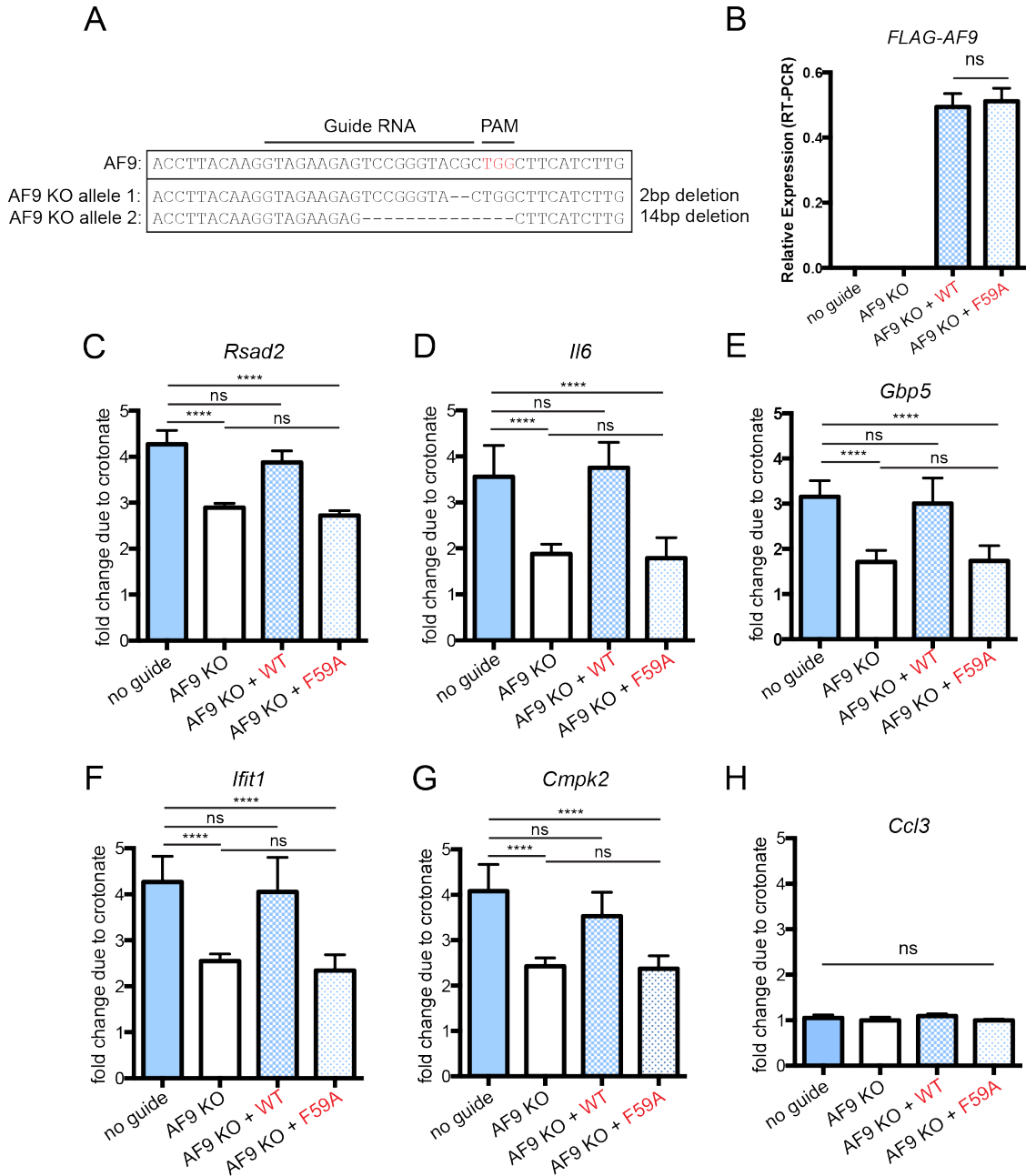
The increase in H3K18cr by crotonate pre-treatment is associated with increased gene expression. To test whether AF9 is responsible for crotonate-enhanced expression, Dr. Panchenko engineered a RAW264.7 cell line with genetic knockout of AF9 by CRISPR-Cas9 (**Figure 5.10A**) and I tested whether previously described genes were still crotonate responsive in this genetic context. By pre-treatment of parental cells with crotonate, the crotonate-responsive genes tested (*Rsad2*, *Il6*, *Ifit1*, *Cmpk2*, and *Gbp5*) exhibited between a 3 to 4-fold increase in gene expression over LPS-induction, while cells lacking AF9 demonstrated a significantly reduced response, as measured by qRT-PCR (**Figures 5.10C-5.10G**). Importantly, this reduction could be rescued by addback of wildtype AF9 but not by AF9 (F59A), demonstrating the gene selectivity of the phenotype and the functional importance of the YEATS-Kcr interaction in this process (**Figures 5.10C - 5.10G**). *Ccl3*, as a representative non-responsive gene, was unaffected by crotonate pre-treatment (**Figure 5.10H**). Both the AF9 and AF9 (F59A) transgenes were expressed at the same level (**Figure 5.10B**). Taken together these findings establish a functional role for the YEATS-Kcr interaction in the positive regulation of gene expression.

**Figure 5.10: The Transcriptional Response to Increased Crotonyl-CoA is Dependent on AF9 and the YEATS-Kcr Interaction.**

(A) Sequence verification of AF9 knockout by CRISPR-Cas9. The guide RNA used to target AF9 is indicated. Nucleotide deletions leading to a frameshift mutation are observed on both alleles at the predicted cut site.

(B) qRT-PCR analysis of FLAG-AF9 expression in the indicated cell lines. Data is presented as mean relative expression with standard deviation.

(C-H) The fold change in mRNA abundance, as measured by qRT-PCR, due to crotonate pre-treatment under 120' LPS stimulation was compared across four RAW264.7 cell lines: 1) wild type control (no guide), 2) CRISPR-Cas9 mediated AF9 genetic knockout (AF9 KO), 3) AF9 KO expressing a wild type construct of FLAG-AF9 (AF9KO + WT), and 4) AF9 KO expressing a F59A mutant construct of FLAG-AF9 (AF9KO + F59A). Data for five crotonate responsive genes (C-G) and one crotonate unresponsive gene (H) are presented. Data are plotted as mean fold change of two biological replicates + standard deviation. \*\*\*\*: t-test derived p-value < 0.0001; ns: >0.05.



## DISCUSSION

Although a variety of histone lysine acylations have been identified, diverse in both chemical structure and site of modification, it remains unclear how they are functionally distinct from acetylation, the archetypal histone acylation. Focusing on Kcr, we have previously reported the enzymatic and metabolic means by which Kcr is regulated independently of Kac and the enhanced transcriptional response when the balance is shifted towards Kcr (Sabari et al., 2015). Driven by insights gleaned from the co-crystal structure of AF9 YEATS domain in complex with H3K9ac (Li et al., 2014), we postulated that the YEATS binding pocket would prefer Kcr. This hypothesis was confirmed by ITC with purified components as well as by the “designer nucleosomes” pulldowns. The underlying molecular basis for YEATS-Kcr recognition was further revealed by co-crystal structural studies. In addition, utilizing a cell-based model of transcriptional activation wherein histone crotonylation levels can be perturbed, we showed that AF9 positively regulates gene expression in a YEATS-Kcr dependent manner. Collectively, our work reported here establishes that the YEATS domain, originally annotated as a novel family of Kac effector proteins, exhibits an evolutionarily conserved preference for Kcr over Kac. This provides the mechanism by which Kcr stimulates transcription, further highlighting the functional distinction between Kcr and Kac.

### **YEATS Possesses a Unique Mechanism for Preferential Crotonyl-lysine Readout**

Crotonyl-lysine sets itself apart from other acylation marks by its  $\pi$ -electron conjugation of its crotonylamide group, thus being rigid and planar in shape

(**Figure 5.3B**). Structural analysis of AF9 YEATS domain bound to H3K9cr or H3K18cr demonstrates the crotonylamide plane is sandwiched by aromatic residues Y78 from the top and F59 from the bottom, and  $\pi$ -aromatic stacking and hydrophobic contacts contribute to preferential crotonylation readout (**Figure 5.3B**). Among them, Y78 is primarily responsible for the amide group recognition, while F59 provides critical stacking contacts with the extended crotonyl hydrocarbon chain. An aromatic feature at positions 59 and 78 is highly conserved among YEATS domain proteins from yeast to human (F and Y at position 59, or Y and W at position 78) (**Figure 5.3F**), accounting for the conserved crotonyl-lysine reader activity among YEATS family members. Following crotonyl-lysine insertion, AF9 F28 from the L1 loop displayed adaptive side chain flip, suggesting a role of F28 in sensing the tip part of the longer chain acylations. Thus, the occurrence of F28 may partly account for the binding loss observed for the branched Khib and acidified Ksu marks. Interestingly, residues at position 28 displayed large discrepancy across species, ranging from small side chain residue serine in YEATS2 to basic residue arginine in Sas5 (**Figure 5.3F**), which suggests that different YEATS domains may display fine-tuned acylation type sensitivity in addition to the common Kcr preference.

Comparison between the co-crystal structures of BRD3-H3K18ac and AF9-H3K18cr highlights the ways in which YEATS is distinct from bromodomains. The reader pocket of bromodomain is generated at the center of a four-helical bundle and side-open (**Figure 5.5D**). Acetyl-lysine is perpendicularly inserted into the pocket positioned in such a way that any extension of the acylation chain would be restricted by the pocket dimension (**Figure 5.5E**). As supported by previous structural studies (Flynn et al., 2015; Vollmuth and Geyer, 2010), longer

acylation chains such as propionylation and butyrylation, must be rotated to protrude out of the pocket from the side opening, compromising affinity. Crotonyl-lysine, due to its bulky and planar feature cannot be rotated and is therefore occluded from binding most bromodomains. By contrast, the reader pocket of YEATS is elongated and open ended, being ideal to positively sense a large repertoire of acyl-lysine marks with extended acylation chains (**Figure 5.5G**).

### **AF9 YEATS Regulates the Response of Inflammatory Genes to Histone Crotonylation**

We demonstrate here that AF9 is recruited to activated genes in the LPS-induced inflammatory response. AF9 is a member of two distinct transcription-associated complexes, the Super Elongation Complex (SEC) and the Dot1L complex (DOT1LC) (Lin et al., 2010; Yokoyama et al., 2010). While this is the first direct demonstration that AF9 is recruited to LPS stimulated genes, it is not entirely surprising given that the inflammatory response requires the recruitment and activity of multiple remodeling and elongation complexes (Medzhitov and Horng, 2009; Smale et al., 2014). Furthermore, it has been previously demonstrated that components of the SEC (ELL2 and AFF4) are recruited to regulatory elements of activated genes in the context of EGF-stimulation (Lai et al., 2015). AF9 localization is enhanced beyond levels attained by signal-induced recruitment by crotonate pre-treatment. This crotonate enhanced AF9 localization is dose-dependent and occurs specifically at genes that have been previously shown to exhibit dose-dependent increases in H3K18cr, decreases in

H3K18ac, and increases in gene expression under the same crotonate pre-treatment and stimulation conditions (Sabari et al., 2015). AF9 is recruited to sites of gene activation in a YEATS-independent manner (**Figure 5.9C**, compare 0 mM crotonate,  $\pm$  LPS), likely driven there by its known interactions with multiple components of the DOT1LC or SEC. The interaction of AF9 with its complex members is known to be YEATS independent, with mapped interaction domains in AF9's C-terminus (Biswas et al., 2011; He et al., 2011; 2010; Li et al., 2014; Yokoyama et al., 2010). These observations suggest that robust and coordinated signal-induced recruitment can override the need for the YEATS-Kcr/Kac interaction, yet still the YEATS domain allows AF9 to “read” the chromatin landscape and respond to increases in histone crotonylation. (**Figure 5.9C**, compare increasing crotonate treatment WT vs. F59A). Furthermore, the enhanced expression observed with crotonate pre-treatment is dependent on AF9 and a fully functional YEATS domain (**Figure 5.10C - 5.10G**).

Our data support a role for the AF9 YEATS-Kcr interaction in the positive regulation of gene expression, but also suggest that Kcr exerts its function through other pathways as well. CRISPR-mediated knockout of AF9 significantly reduces the crotonate response in our model system, but does not abolish it completely (**Figure 5.10**). This residual response could be due to another YEATS domain protein (ENL, GAS41, or YEATS2) or another as of yet unidentified Kcr reader domain (trans-effects). Histone Kcr could also cause changes to nucleosome stability or inter-nucleosomal interactions, thereby promoting transcription in a reader-independent manner (cis-effects). In support of potential cis-effects, a recent study demonstrated that H3-H4 tetrasomes

comprised of H3K122cr were less stable in solution than tetrasomes with unmodified H3 (Suzuki et al., 2015). As such, we anticipate that future studies will uncover other pathways mediated by Kcr.

In this Chapter, in close collaboration with the Drs. Haitao Li and Yuanyuan Li from the Li group, and Dr. Tanya Panchenko, my colleague in the Allis lab, I demonstrate that the YEATS domain has an expanded acyl-binding repertoire with highest binding to Kcr. This Kcr preference prompted us to focus on the functional role of the YEATS-Kcr interaction within the context of gene activation. The enhanced affinity for Kpr or Kbu as compared to Kac for the YEATS domain is likely functional and we anticipate that perturbations to these histone modifications will impact YEATS domain localization proportional to the measured binding affinities. The preferential binding of YEATS to Kcr as compared to Kac, reported here, makes YEATS unique among acetyllysine readers, so far tested, demonstrating that specific protein folds have evolved to functionally exploit the diversity of lysine acylations. This work supports the general view that the wide range of lysine acylations being uncovered in histone proteins function to expand the cell's repertoire of transcriptional responses through the selective engagement of acyl-specific reader proteins.

## CHAPTER 6: IDENTIFICATION AND CHARACTERIZATION OF DEACETYLASE ACTIVITIES

### INTRODUCTION

The steady-state balance of a PTM is regulated by the counteracting activities of the catalytic addition and removal of the modification. For histone acetylation this balance is regulated by the activities of the HATs and HDACs. For mammals, four classes of HDACs have been described. Classes I, II, and IV represent HDACs 1-11, which all share a similar Zn<sup>2+</sup>-dependent catalytic mechanism. These are considered the “classic” HDACs with homology to the yeast Rpd3, the first characterized HDAC (Taunton et al., 1996). Class III HDACs represent the sirtuin proteins (SIRT1-7), NAD<sup>+</sup> dependent deacetylases with catalytic domain homology to the yeast sir2, described as a deacetylase by Guarente and colleagues (Imai et al., 2000). The sirtuin enzymes are catalytically and structurally distinct from the classic HDAC enzymes and for the purposes of this thesis we will consider the two major classes of HDACs as classic HDACs and sirtuins.

The classic HDACs are the enzymes inhibited by butyrate and other HDAC inhibitors that demonstrate intriguing cancer-specific toxicities. The NAD<sup>+</sup> dependency of the sirtuins has sparked interest in how these enzymes could be used as sensors of the metabolic redox state of the cell. Many intriguing observations have been made about the sirtuins role in DNA-damage, cancer, and aging (Guarente, 2007). Given the interesting biology of both classes, these proteins have been the subject of pharmacological interest for discovery of both inhibitors and activators. A small molecule inhibitor of Class I and II HDACs,

SAHA/Vorinostat was the first epigenetic therapy to be approved for clinical trial and is currently used in the treatments of T cell lymphoma. Several other HDAC inhibitors have been approved or are in clinical trial for the treatment of various malignancies (Falkenberg and Johnstone, 2014). As the sirtuin proteins have been implicated as anti-aging factors (Guarente, 2007; 2012) , efforts have been focused on developing sirtuin activators for the treatment of aging and age-related diseases (Sinclair and Guarente, 2014).

Several findings led me to focus on the sirtuin enzymes as potential decrotonylases. SIRT1, 2, and 3 were shown to have depropionylase and debutyrylase activities (Smith and Denu, 2007). SIRT5 was shown to have highly specific de-succinylase and de-malonylase activity *in vitro* and *in vivo* (Du et al., 2011). These studies suggested that the sirtuin family of enzymes might have acyl-specific roles. During the time of my thesis work other papers were published to further demonstrate the unique capacity of sirtuin enzymes to remove various acylations. SIRT6 was shown to have activity for long-chain acylations, specifically lysine palmitoylation (16 carbon) and myristoylation (14 carbon) (Jiang et al., 2013). SIRT5 was shown to have activity on glutarylation (Tan et al., 2014b). While these studies focused on non-histone substrates, they suggested a role for the sirtuin enzymes in removal of acylation more complex than acetyl-lysine.

During the time of my thesis work two independent studies have shown that sirtuins have decrotonylase activity. The first study from John Denu's lab carried out a systematic screen for the capacity of the sirtuin enzymes to remove a large variety of lysine acylations from histone peptides (Feldman et al., 2013). This study assayed all seven mammalian sirtuins against twelve different

acylations from short-chain to long-chain at position H3K9, and included crotonyl-lysine. This study provided quantitative rate measurements for all reactions assayed. In relation to crotonyl-lysine, they showed that both SIRT1 and SIRT2 have broad deacylation activity, which includes decrotonylation. They did not detect any decrotonylation activity from the other five sirtuins assayed and they do not observe any activity from SIRT7 (Feldman et al., 2013). The second study utilized a peptide crosslinking strategy to purify proteins interacting with crotonyl-lysine and isolated SIRT1, SIRT2, and SIRT3 from nuclear extracts. Although previous reports have demonstrated SIRT3's mitochondrial localization, they proceed to characterize SIRT3 as a nuclear-localized decrotonylase (Bao et al., 2014). Intriguingly, they demonstrated that knockdown of SIRT3 increased global and local levels of histone crotonylation, while knockdown of SIRT1 and SIRT2 had no measurable effect.

Here, I present data demonstrating decrotonylase activities of SIRT1, 2, 6, and 7. Intriguingly, SIRT6 and SIRT7 only exhibit substrate-specific activities, in that they only have deacetylase or decrotonylase activity on nucleosomal substrates. I also demonstrate that HDAC1 has decrotonylase activity. Unlike the HATs, where most families tested could not catalyze crotonylation, making p300/CBP unique, the HDAC families appear to be generally promiscuous to decrotonylation. Further kinetic analysis is required to distinguish the rates of deacetylation and decrotonylation for these described activities.

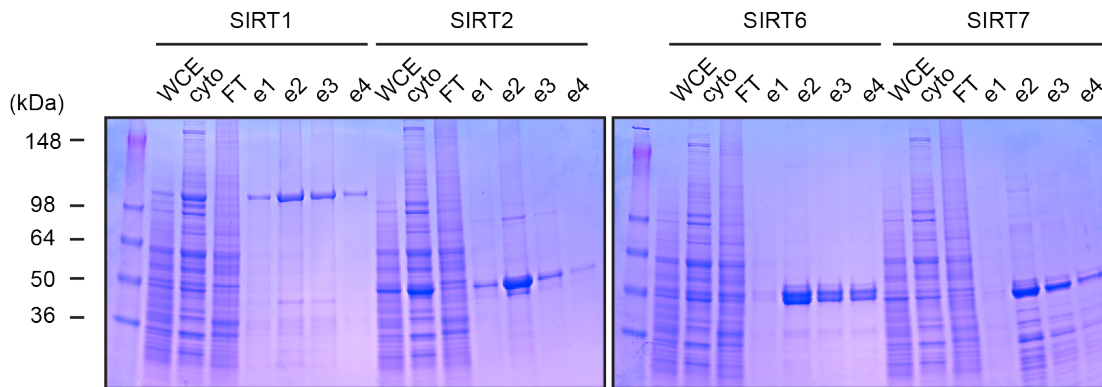


**Figure 6.1: Purification of Recombinant Sirtuins.**

cDNA for SIRT1, SIRT2, SIRT6, and SIRT7 were FLAG-tagged and cloned into pFastbac1. Baculovirus were generated through the bac-to-bac protocol and viral particles were added to sf9 cultures in exponential growth. FLAG-tagged protein was purified from nuclear extract by immuno-affinity chromatography with M2 resin (Invitrogen). Shown here are coomassie stained SDS-PAGE gels of the serial elutions (e1-e4), the column flow through (FT), the cytoplasm fraction from the nuclear preparation (cyto), and the whole cell extract (WCE).

## RESULTS

### Nuclear Localized Sirtuins Exhibit Substrate Dependent Decrotonylase Activities

The seven mammalian sirtuin proteins have specific cellular localizations. SIRT1 and SIRT2 localize to the nucleus and the cytosol, SIRT3, 4, and 5 localize to the mitochondria, and SIRT6 and SIRT7 localize to the nucleus and nucleolus (Michishita et al., 2005). In my efforts to identify a histone decrotonylase activity I focused my attention on the nuclear localized sirtuins, SIRT1, 2, 6, and 7. I first generated recombinant protein via the sf9/baculovirus expression system. Baculovirus were generated encoding FLAG-tagged cDNA for all four of these sirtuins and full-length protein was purified from nuclear extracts of infected sf9 cells (**Figure 6.1**).

To test the decrotonylase activity of the nuclear-localized sirtuins, I established a decrotonylase activity assay where the readout was reduction in immunoblot signal from crotonyl-specific antibodies. As an initial test of the decrotonylase activities, histones acid extracted from crotonate treated cells were used as generically hyper-crotonylated substrate. Under identical reaction conditions, with all reactions containing the necessary cofactor NAD<sup>+</sup>, SIRT1 and SIRT2 exhibited decrotonylase activity while SIRT6 and SIRT7 were inert (**Figure 6.2**). SIRT1 and SIRT2 reduced the amount of histone crotonylation to levels below detection on all four core histones. I next sought to test whether these sirtuins could specifically decrotonylate p300-catalyzed crotonylation or acetylation.

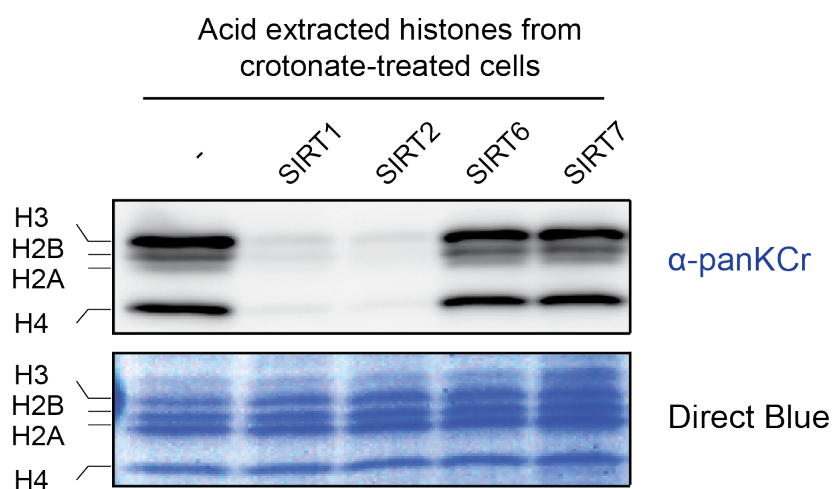


**Figure 6.2: Sirtuin Activity Assay with Acid Extracted Histones as Substrate.**

Histones were acid extracted from crotonate treated HeLa cells (as in Chapter 3) and used as substrate for the recombinant sirtuin enzymes. All reactions contain NAD<sup>+</sup>. Reaction products were immunoblotted with panKCr antibody.

I prepared both recombinant histone octamers and oligonucleosomes purified by sucrose gradient from MNase digested nuclei. The oligonucleosomes were previously used as substrate in the histone crotonyltransferase (HCT) purification (**Figure 2.1**) and the octamers were used as substrate in the validation of HCT activity (**Figures 2.3 and 2.4**). The oligonucleosomes contain a wide range of nucleosome lengths from mononucleosomes to >12mers (**Figure 6.3A**). Because the oligonucleosomes are purified by sedimentation from complex extract they do contain contaminating proteins (**Figure 6.3B**). The octamers were assembled *in vitro* from recombinant histones purified under stringent conditions from bacteria essentially as in (Dyer et al., 2004), with slight modifications taken from (Ruthenburg et al., 2011). As such, these octamer preparations did not contain unknown contaminating proteins. The only contaminant was trace amounts of the rhinovirus 3C protease used during the processing of recombinant histones, which co-elutes with histone octamers (**Figure 6.3C**). Under the salt concentrations used in all reaction conditions, these octamers were in fact tetramers of H3-H4 and dimers of H2A-H2B. Octamers were used because several HATs, specifically GCN5, cannot modify nucleosomal substrates unless they are within their respective multi-subunit complex (Brownell et al., 1996; Grant et al., 1997). p300 can modify either substrate.

Octamer or oligonucleosomes were acetylated or crotonylated by p300 and then diluted and added as substrate to sirtuin reactions containing NAD<sup>+</sup> and SIRT1, SIRT2, SIRT6, or SIRT7. Deacylase activity was measured by reduction in signal from immunoblot with antibodies against H3K18Cr and H3K18Ac, the dominant p300-catalyzed acylation. The reactions with acylated octamers looked very similar to the reactions with acid extracted histones, SIRT1

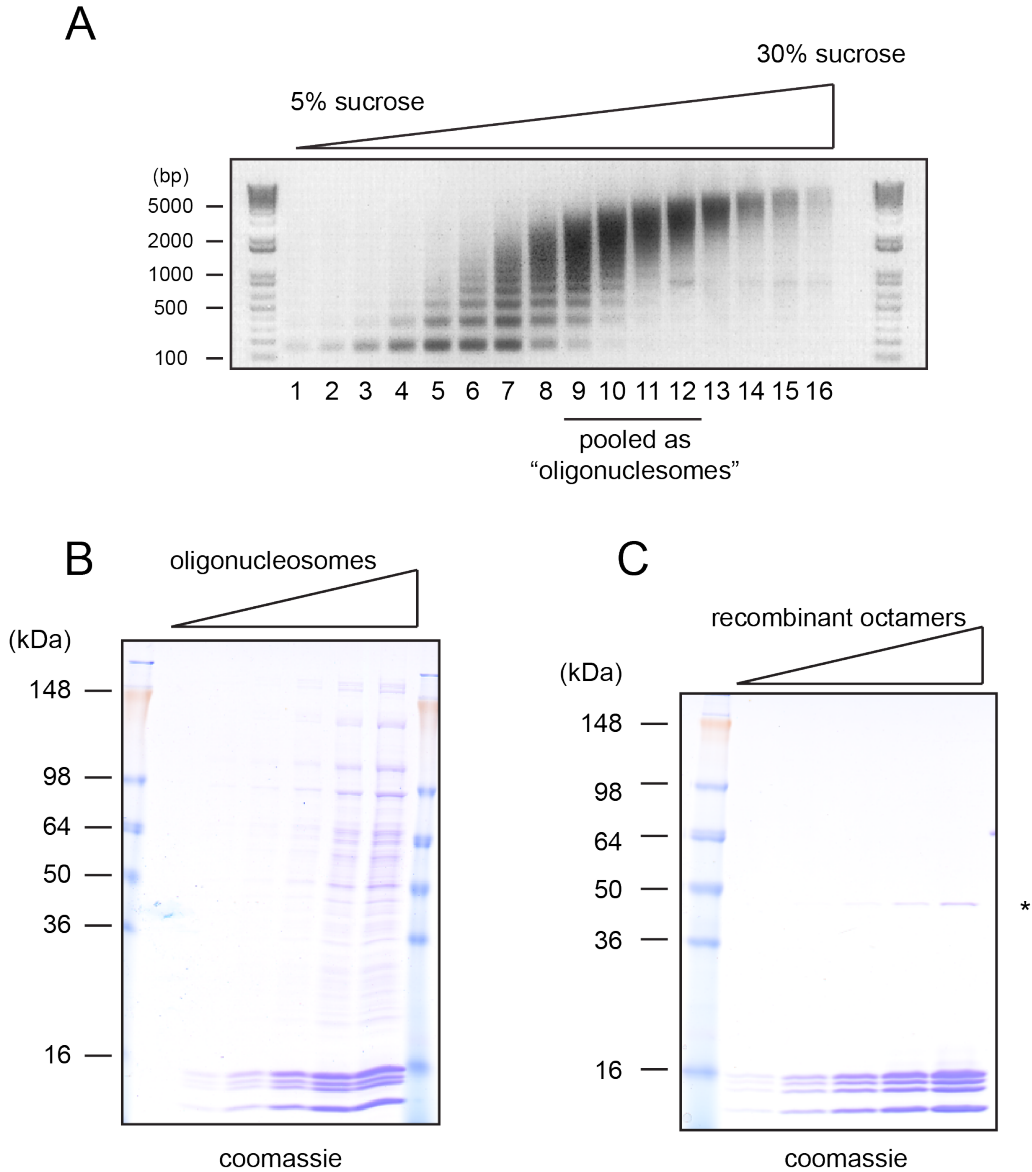


**Figure 6.3: Composition of Oligonucleosome and Octamer Substrates.**

(A) The DNA purified from sucrose gradient fractions resolved over a 2% agarose gel and stained with ethidium bromide. The fractions pooled as oligonucleosomes are indicated. (B) Increasing volume of purified oligonucleosomes resolved over SDS-PAGE and coomassie stained. High molecular weight contaminants can be observed. (C) Increasing volume of recombinant histone octamers assayed as in (B). The asterisk designates trace amounts of rhinovirus 3C protease used in HIS-tag cleavage that co-elutes with histone octamers.

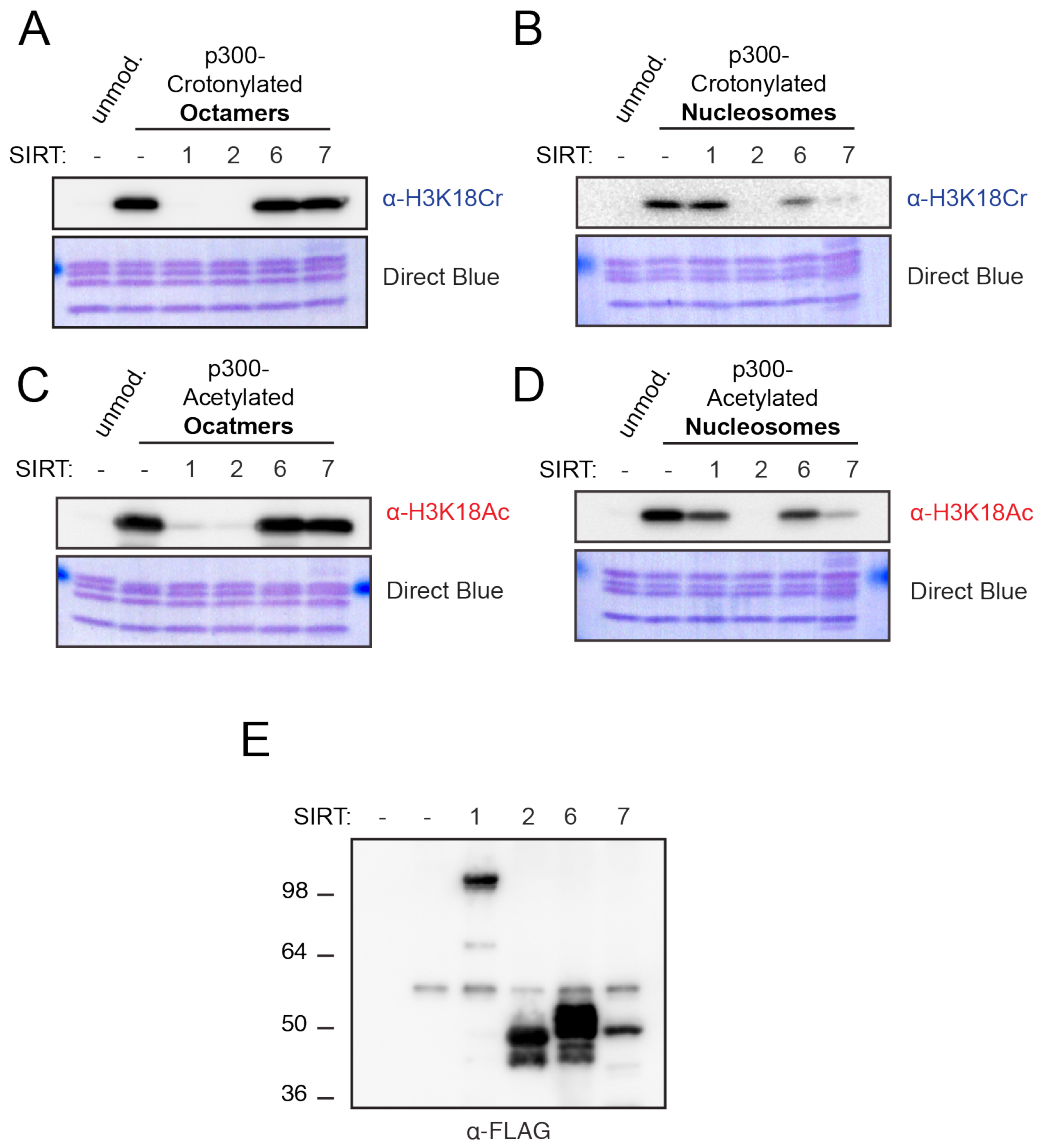


**Figure 6.4: Sirtuin Activity Assay with p300-catalyzed Octamers or Oligonucleosomes as Substrate.**

(A-B) Histone octamers (A) or oligonucleosomes (B) are crotonylated by p300 and then added as substrate to reactions with the designated sirtuin. Unmodified substrate and modified substrate in the absence of a sirtuin are included. Immunoblot of reaction products are shown here. (C-D) same as (A-B) except substrate are acetylated by p300. (E) anti-FLAG immunoblot of reactions with FLAG-tagged sirtuins.

and SIRT2 exhibited decrotonylase and deacetylase activity (**Figures 6.4A and 6.4C**). Surprisingly, the activities of the sirtuins changed when nucleosomal substrates were used. SIRT1 was substantially inhibited and SIRT6 and SIRT7 gained deacylase activity, all while SIRT2 remained the dominant deacylase (**Figures 6.4B and 6.4D**). These experiments did not detect a dramatic difference between the decrotonylase and deacetylase activities. More thorough investigation and development of quantitative activity assays will be required to compare the rates of the two activities. An immunoblot with FLAG antibody demonstrated the loading differences of the FLAG-tagged sirtuins (**Figure 6.4E**).

#### **Overexpression of SIRT2, SIRT6, or SIRT7 Reduces Global Levels of H3K18Cr**

To test whether these *in vitro* reactions were predictive of the sirtuins cellular activity, I overexpressed SIRT2, SIRT6, and SIRT7 in 293T cells by transient transfection. I also generated cDNA for catalytically dead SIRT2, SIRT6, and SIRT7 by mutating the conserved histidine within the catalytic pocket to a tyrosine (HY-mutants), and overexpressed these constructs in parallel along with an empty vector control. Immunoblots of extracted histones demonstrated that global levels of both H3K18Ac and H3K18Cr were reduced upon transfection of SIRT2, SIRT6, and SIRT7, but not upon transfection of the respective HY-mutants or empty vector (**Figure 6.5**). The reductions for SIRT2 and SIRT6 were more pronounced than the slight reduction observed with SIRT7 overexpression, but SIRT2 and SIRT6 were expressed at higher levels (**Figure 6.5**). SIRT1 overexpression did not lead to a marked reduction in global histone acylation, but the protein was not effectively expressed upon transient transfection (data not shown). The reductions in immunoblot signal from cells transfected with

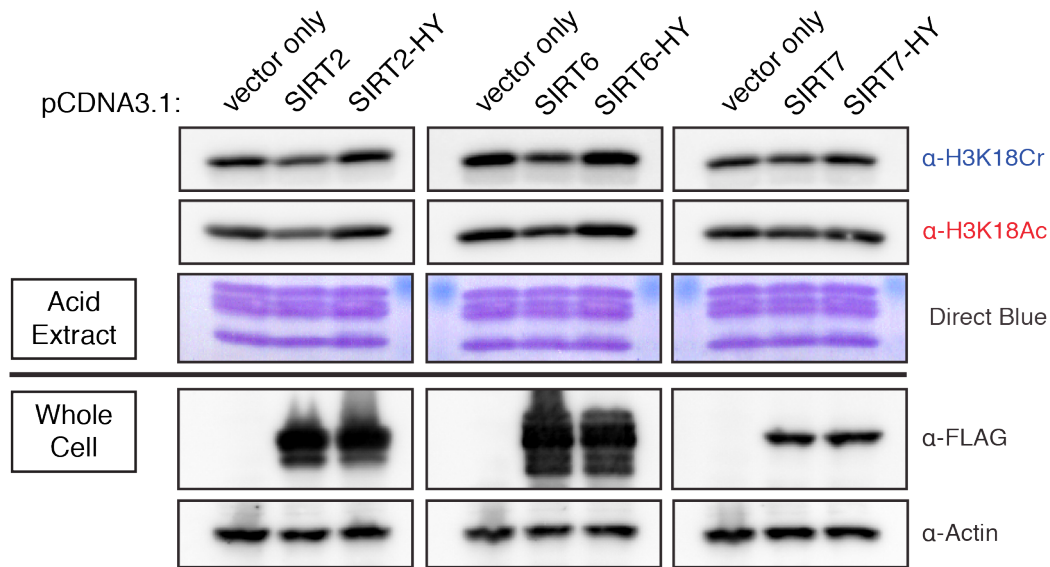


**Figure 6.5: Overexpression of SIRT2, SIRT6, and SIRT7 in 293T cells Reduces Global Levels of H3K18Cr and H3K18Ac.**

293T cells were transfected with pCDNA3.1 containing FLAG-tagged wildtype or HY-mutant SIRT2, SIRT6, or SIRT7, or an empty vector. Histones were acid extracted and whole cell extracts were prepared. Immunoblots with the indicated antibodies are shown here.

sirtuin cDNA mirrored the *in vitro* reactions with oligonucleosome substrates, demonstrating that the nucleosome is most likely the physiological substrate for these enzymes. The levels of both H3K18Ac and H3K18Cr showed the same trend in response to sirtuin overexpression.

### **HDAC1 Exhibits Decrotonylase Activity**

To test whether decrotonylase activity was unique to sirtuins, I purified recombinant HDAC1, the best-studied member of the Class I HDACs, from baculovirus infected sf9. I performed several *in vitro* reactions comparing HDAC1 to SIRT2. First, I used histones acid extracted from crotonate treated cells as a source of acetylated and hyper-crotonylated substrate and immunoblotted the products with either acetyl-specific antibodies to detect deacetylation or crotonyl-specific antibodies to detect decrotonylation. As expected, HDAC1 and SIRT2 deacetylated acid extracted histones as measured by immunoblot with panKAc and H3K18Ac antibodies (**Figure 6.6A**). HDAC1 also decrotonylated this substrate and reduced immunoblot signal for both panKCr and H3K18Cr antibodies to below detection levels, as did SIRT2 (**Figure 6.6A**). Next, p300-acetylated or -crotonylated octamers were used as substrate and both SIRT2 and HDAC1 were able to effectively decrotonylate and deacetylate these substrates, as measured by reduction in H3K18Cr and H3K18Ac immunoblot signal (**Figure 6.6B**). To test whether HDAC1 exhibited decrotonylation activity in cells, I overexpressed HDAC1 in 293T cells and, in parallel, transfected cells with SIRT2 and an empty vector control. Immunoblots of acid extracted histones

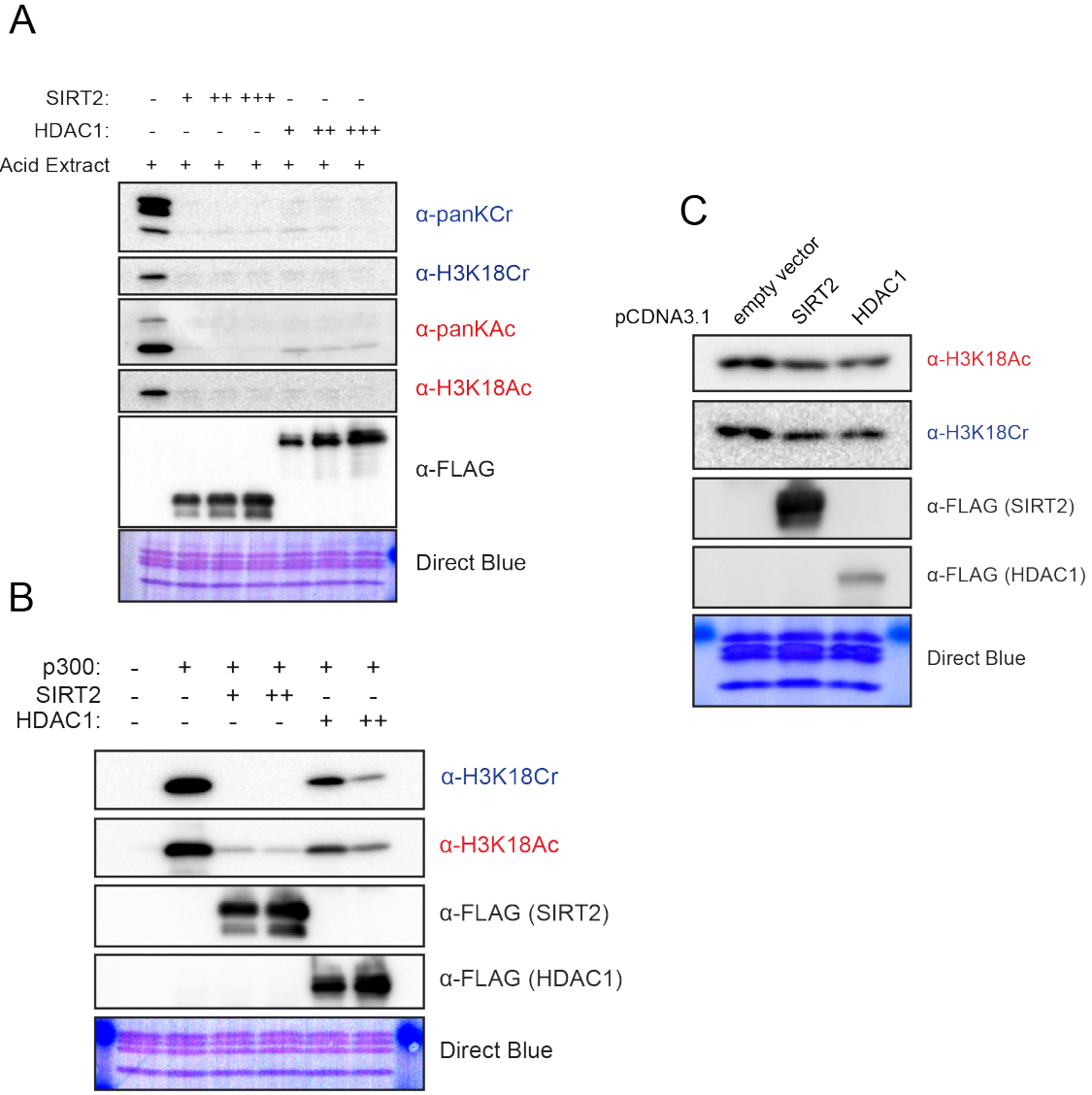


**Figure 6.6: HDAC1 has Decrotonylase Activity.**

(A) Acid extracted histones from crotonate treated cells were used as substrate in reactions with SIRT2 or HDAC1. Reaction products were immunoblotted with the indicated antibodies. Reactions with SIRT2 contained NAD<sup>+</sup>. (B) p300-acetylated or –crotonylated histone octamers were used as substrate in reactions with SIRT2 and HDAC1 as in (A). (C) 293T cells were transfected with FLAG-tagged cDNA for SIRT2, HDAC1 or an empty vector. Acid extracted histones or whole cell extract were immunoblotted with the indicated antibody.

showed that overexpression of both SIRT2 and HDAC1 led to global reduction of both H3K18Ac and H3K18Cr (**Figure 6.6C**). While quantitative kinetics of HDAC1 or SIRT2 decrotonylation or deacetylation cannot be derived from these qualitative immunoblot-based activity assays, these data clearly demonstrated that decrotonylation is not a unique property of the sirtuin enzymes.

## DISCUSSION

The physiological substrate for the sirtuin and HDAC enzymes is presumably the nucleosome. Histone peptides, free histones, and histone octamers are all used as convenient proxies for the nucleosome, yet the data presented in this chapter suggest that the form of the substrate is critical for enzymatic activity. This is not a new phenomenon for chromatin modifying enzymes, as enzymes such as PRC2 and NSD2 have been shown to require the nucleosome structure for activity (Cao et al., 2002; Li et al., 2009b). Yet for the sirtuin field, peptides have been the dominant substrate since the discovery of sir2 deacetylase activity (Imai et al., 2000). Peptides are very convenient substrates for HDAC activity assays as they can be synthesized to carry any modification at any site at high purity. A recent systematic survey of the sirtuin enzymes' capacity to remove various histone acylations missed the activity of SIRT6 and SIRT7 described here presumably because peptides were used as substrates (Feldman et al., 2013).

The nucleosome dependency of SIRT6 deacetylation has been described (Gil et al., 2013) and the nucleosome enhanced deacetylase activity of SIRT7 has been implied without direct statement (Barber et al., 2012), neither group tested whether the enzymes could decrotonylate. A recent publication demonstrated that a measurable enhancement of SIRT2 deacetylase activity was observed with

nucleosome over peptide substrates (Hsu et al., 2016). Although my assays were not sensitive enough to observe a substrate effect for SIRT2, this study corroborates my findings that the sirtuin enzymes have substrate-dependent activities.

The results presented here are preliminary and many experiments should be conducted to explore these observations further. For example, unknown proteins and possibly chemical matter contaminate the oligonucleosomes I use in my reactions. It is a formal possibility that the difference in SIRT6 and SIRT7 activity is due to an unknown contaminating activity. Of potential concern is the observation made by Denu and colleagues that long-chain fatty acids activate SIRT6 activity (Feldman et al., 2013). It is possible that long-chain fatty acids or trace lipids contaminate my oligonucleosome preparation. Experiments comparing recombinant octamers with recombinant nucleosomes could solve this problem. Furthermore, experiments with recombinant nucleosomes acetylated or crotonyl via amber suppression (as in Chapter 5) would facilitate more quantitative assessment of rates for SIRT6's and SIRT7's decrotonylation and deacetylation reactions. A major limitation with the experiments presented here is the source of modified substrate. Neither acid extracted histones nor p300-modified octamers or oligonucleosomes begin with equivalent acetylation and crotonylation; even more reason to use pre-acylated histones via amber suppression.

The paper describing the discovery of histone crotonylation compared the activities of HDACs 1-11 on acetylated or crotonylated peptide substrates by a quantitative fluorometric assay (Tan et al., 2011). They did observe decrotonylation activity for HDAC1, but it was just above background signal and

~10x weaker than its deacetylation activity. As I do not measure rates of activity, but only end-point analysis, it is possible that the HDAC1 activity I observe is negligible compared to its deacetylase activity. It remains unclear whether a particular enzyme or enzyme family is solely responsible for decrotonylation. The data presented here point to broad promiscuity for HDACs and sirtuins in relation to deacetylation and decrotonylation.

## CHAPTER 7: GENERAL DISCUSSION

The discovery of histone lysine crotonylation prompted interest in the regulation and function of this novel histone PTM. In my thesis work I have identified and characterized the writers, readers, and erasers of histone crotonylation. I have demonstrated that the modification is regulated metabolically by the relative concentration of crotonyl-CoA and acetyl-CoA and that shifts in acyl-CoA metabolism are read out on the differential acylation state of chromatin. Furthermore, this change in levels of histone crotonylation affects gene activation, in part through the recruitment of YEATS domain containing proteins, readers of crotonyl-lysine (**Figure 7.1**). These studies establish a previously unrecognized link between acyl-CoA metabolism and potency of the transcriptional response. Many questions still remain unresolved and new questions are introduced by the results of these studies. In the general discussion I will go through a few potential future directions and address open questions that have not been sufficiently addressed in individual chapter discussions.

### **Histone Crotonyltransferase(s)**

The initial purification of HCT activity from HeLa cells yielded p300 as a known HAT with HCT activity. Other HATs tested did not exhibit HCT activity. While I have been able to make fundamental observations about Kcr by studying p300's HCT activity *in vitro* and in cells, it is likely not the sole HCT activity in the cell for the reasons described below. From MS/MS analysis of p300 reaction products, there are specific lysine residues that p300 prefers to crotonylate, yet

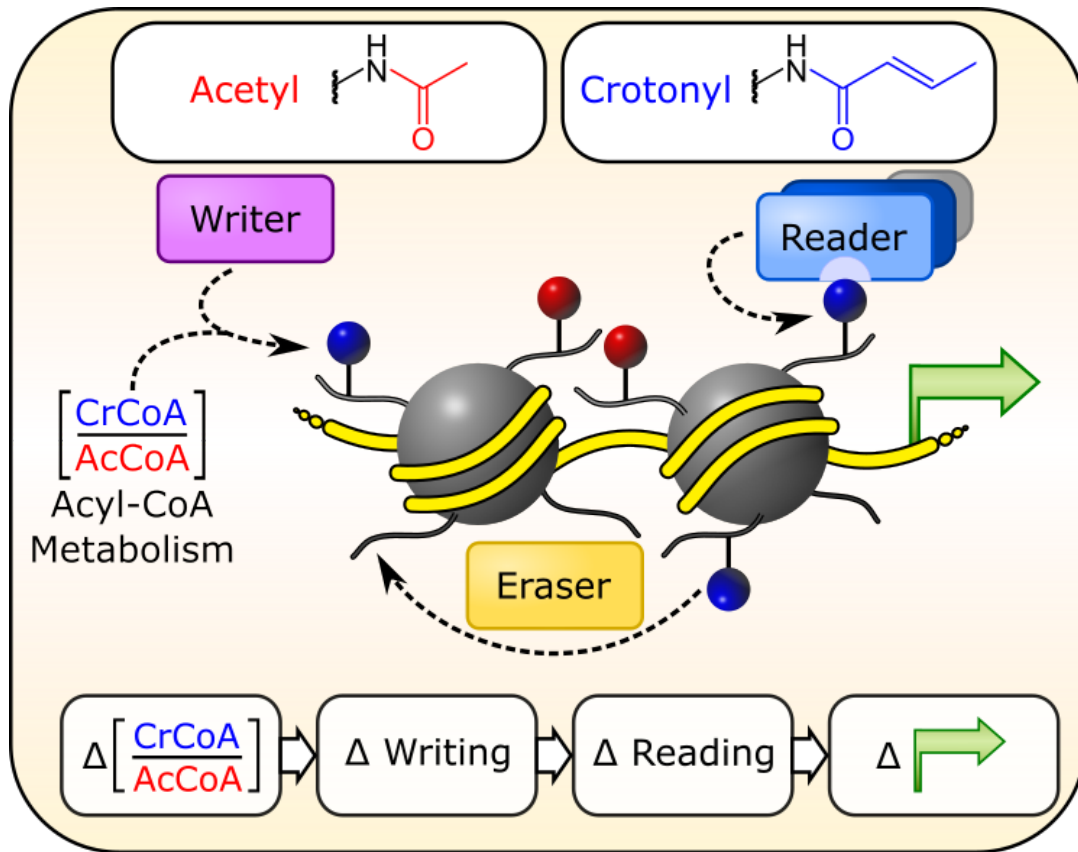


**Figure 7.1: The Regulation and Function of Histone Crotonylation.**

Schematic of the pathways involved in the regulation and function of histone crotonylation. The model presented here is a summary of the experiments described in the previous chapters of this thesis. p300/CBP (writer) catalyze histone crotonylation (Chapter 2), which is regulated by the relative concentration of acetyl-CoA and crotonyl-CoA (acyl-CoA metabolism) (Chapter 3). Enhanced levels of histone crotonylation lead to a boost in gene activation (Chapter 4), which is in part mediated through the increased localization of AF9 (reader) (Chapter 5). This process is reversible by the activity of decrotonylase activities (erasers) (Chapter 6). This illustration was designed by Dr. Tanya Panchenko.

this only explains a small percentage of the 37 known sites of crotonylation (Huang et al., 2014). Furthermore, while knockdown of p300 in cells ablates levels of the modifications identified as p300 targets (e.g. H3K18), it does not remove all histone crotonylation, as measured by immunoblot with a pan-Kcr antibody (**Figure 7.2A**). These observations suggest that there are other unidentified HCTs. Indeed, in unpublished data from the purification of HCT activity I have observed “side fractions” that contain unassigned crotonyltransferase activities (**Figure 7.2B**). Further purification and identification of these activities could yield other, as of yet unidentified, HCTs.

The field has not yet identified an enzyme that is solely a crotonyltransferase without any acetyltransferase activity. It is possible that these side fractions contain such an activity, but as HAT activity was also observed in these side fractions (data not shown) the HCT activity is most likely due to another HAT. It would be of interest to identify this HAT. If it were one of the HATs that tested negatively for HCT activity in its recombinant form, then it would be interesting to understand whether HCT activity was dependent upon complex formation or upon being covalently modified. If it were one of the HATs not tested, it would be interesting to compare the catalytic domain with that of p300 and CBP to better understand the mechanisms of crotonyltransferase activity.

During my thesis work, I explored the potential regulation of p300's HAT and HCT activities by PTM-induced conformational change, but with only inconclusive results. The hypothesis was that only a fraction of the recombinant p300 purified from sf9 cells was active as an HCT. If this were true it would most likely be due to a covalent modification that may allow for separation of the

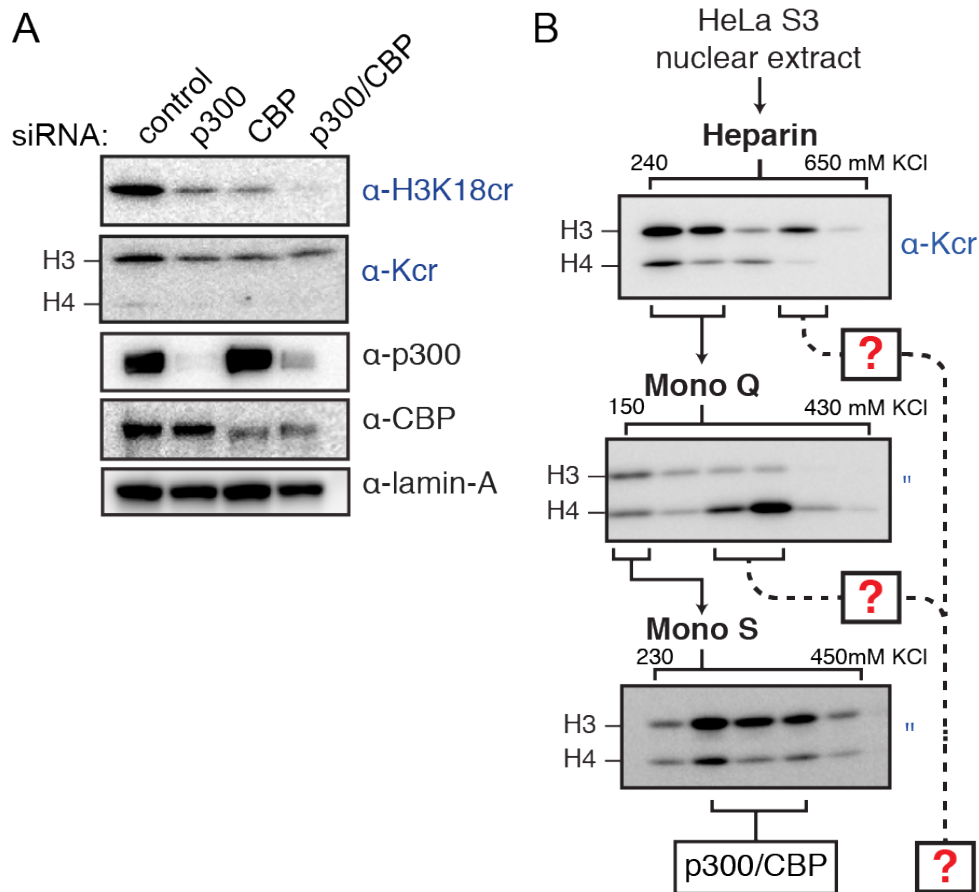


**Figure 7.2: Unidentified Histone Crotonyltransferase(s).**

(A) While knockdown of p300/CBP ablates H3K18cr signal, pan-Kcr signal persists. HeLa S3 cells were transfected with the indicated siRNA. 72 hours post transfection lysates were prepared and immunoblotted by the indicated antibodies. (B) At least two side fractions of HCT activity of unknown identity were observed through the partial purification of p300/CBP. HCT activity assays of fractions from the three column-chromatography stages are shown here. Arrowed line designates path of activities reported in Chapter 2, while the dashed line highlights the unexplored side fractions.

modified isoform by high-resolution ion-exchange chromatography. To this end, I loaded FLAG-purified p300 onto a Mono S column (cation-exchange) and eluted over a shallow KCl gradient collecting fractions along the broad peak of p300 elution. HAT and HCT assays were performed on every other fraction in order to detect whether any fraction contained more HAT or HCT activity than the rest. After several attempts at this line of experimentation, the separation of p300's HAT and HCT activities was not observed (**Figure 7.3**). Yet, these results do not conclusively show that there is no such isoform, but only that the potential isoform was not separable by ion-exchange chromatography. It is also a possibility that a modification occurring in the cell may not be recapitulated in baculovirus infected sf9 cells.

Another line of experimentation that could yield an HCT specific enzyme would be protein engineering of the p300 catalytic pocket, either by rationale design or by screening of random mutagenesis. Generation of a p300 or CBP with heightened preference or selectivity for acetylation or crotonylation would be an invaluable experimental tool for studying differential acylation in cells and potentially *in vivo*. It would also be interesting to explore how the cancer-associated mutations within the catalytic domain of p300/CBP affect the choice between acetyl-CoA and crotonyl-CoA.

*In vivo* experimentation as to the function of histone crotonylation has been hampered by the shared enzymology with histone acetylation. For example, it is unclear whether the effects of knockout or knockdown of p300/CBP are due in any part to the loss of histone crotonylation. ACSS2, while implicated in my cell culture models in the generation of crotonyl-CoA is also known to be critical

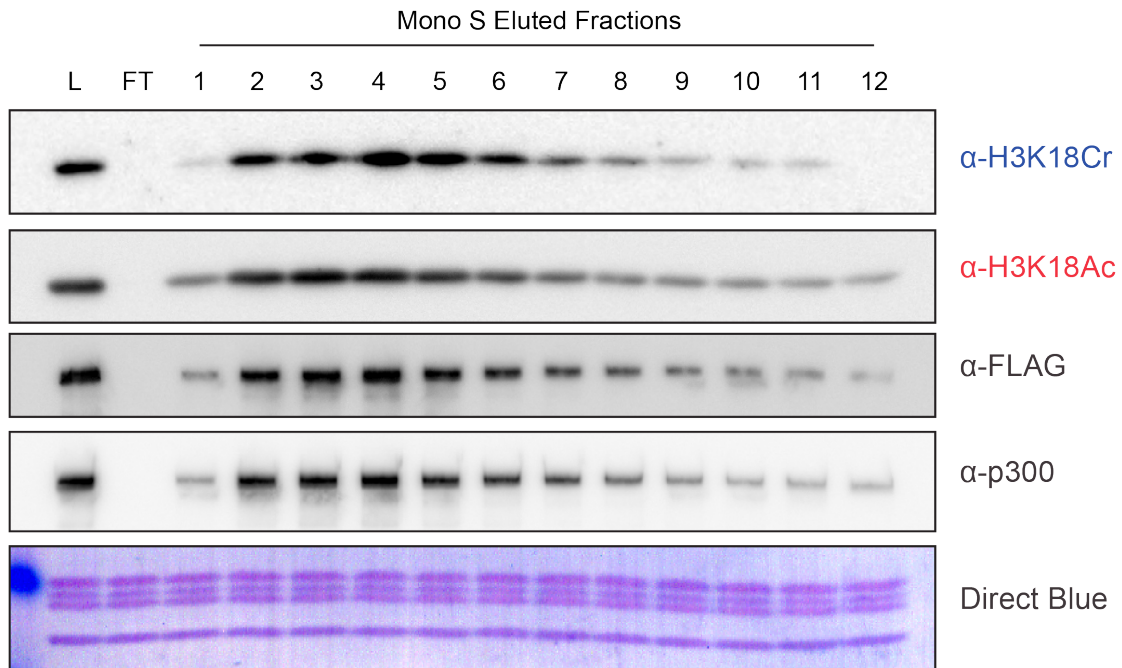


**Figure 7.3: Ion-Exchange Chromatography of p300 Does Not Separate its HCT and HAT Activities.**

HAT and HCT activity assays were conducted with the indicated source of enzyme and immunoblotted with the indicated antibodies. Reactions blotted with H3K18cr contained only crotonyl-CoA, while reactions blotted with H3K18ac contained only acetyl-CoA. L is the column input/load, FT is the column flow through, and 1-12 are the eluted fractions. Equal volumes of all fractions were assayed.

for acetate derived acetyl-CoA for histone acetylation and fatty acid synthesis. Therefore it will be difficult to determine whether effects of ACSS2 knockout or overexpression are mediated in any part by histone crotonylation. The identification of crotonyl-specific enzymes or the engineering of enzymes to prefer or reject crotonylation is needed for the field to expand. To make specific statement about histone crotonylation in the cell, my experiments have mainly relied on the selective regulation of histone crotonylation by crotonyl-CoA. This was mainly accomplished by the addition of supraphysiological concentrations of crotonate, a convenient method for cell culture, but one a bit trickier for mouse based models. Further development of tools for the selective perturbation of Kcr is required.

### **Intracellular Concentrations of Crotonyl-CoA and other Acyl-CoAs**

A major outstanding question remains whether the concentrations of crotonyl-CoA fluctuate in the cell or in tissues to a degree where differential acylation and its influence on gene expression could be expected to impact physiological processes. Quantitative measurements of acetyl-CoA, CoA-SH, and the various acyl-CoAs have been hampered by the lability of these molecules in complex extracts (Theodoulou et al., 2014). These molecules are heavily derivatized during standard methanol extraction used in a majority of metabolomic studies. Specific extraction protocols for the purification, isolation, and stabilization of acyl-CoA species have been developed and used in combination with LC-MS to measure whole cell concentrations of various acyl-CoAs (Tsuchiya et al., 2014) and have been successfully utilized to study the levels of acyl-CoAs in cell culture and their impact on histone modification (Lee et al., 2014; Sabari et al.,

2015). Whole cell measurements include mitochondrial pools of acyl-CoA, which are distinct from cyto/nuclear pools regulating the modification of histones, yet subcellular measurements of small molecules are hampered by diffusion between organelles upon cell lysis. Even so, whole cell measurements of the various acyl-CoAs across tissue types would provide valuable information as to the physiological dynamic range of the lesser-studied acyl-CoAs, including crotonyl-CoA.

Measuring the concentrations of acyl-CoA pools and in parallel characterizing histone acylation in tissues from mice following metabolic stress such as starvation or variation in diet composition will be a major first step in understanding the dynamic range possible for acyl-CoAs and their impact on histone acylation. Low calorie, low carbohydrate, or ketogenic diets are known to cause major rewiring on metabolic pathways in a number of organs. Verdin and colleagues showed that the short chain fatty acid (SCFA) and product of ketogenesis, 3-hydroxybutyric acid, has effects on chromatin leading to the activation of FOXO3A and protection from oxidative stress (Shimazu et al., 2013). 3-hydroxybutyric acid was elevated in the serum of mice fasted or under caloric restriction which correlated with increased histone acetylation in a number of organs including kidney, brain, liver, and large intestine. The authors concluded that the effects are due to 3-hydroxybutyrate's activity as an HDAC inhibitor. The results from my thesis work suggest that these effects could be due to changes in acyl-CoA metabolism. While histone lysine 3-hydroxybutyrylation has not yet been described in the literature, the effects observed by Verdin and colleagues could be due to enhanced levels of 3-hydroxybutyryl-CoA or butyryl-

CoA leading to increased levels of the respective acylation. The potential impact of SCFAs is discussed in the next section.

Various differentiation pathways as well as the process of maintaining pluripotency would be interesting conditions to profile. Histone crotonylation has been implicated in spermatogenesis (Chapter 1) (Tan et al., 2011). It is of interest to understand whether a unique metabolic state exists in the testis to facilitate histone crotonylation. Studies with mouse embryonic stem cells have observed that pluripotency is associated with a unique metabolic state (Wang et al., 2009) with intriguing consequences for the chromatin landscape and its regulation of transcriptional networks (Carey et al., 2014; Shyh-Chang et al., 2013).

While unbiased profiling of primary tissue or cells under the discussed conditions will likely yield useful associative data, a more rationale approach would be to study acyl-CoA metabolism in established cell lines under genetic depletion of various metabolic enzymes known to interact with either crotonyl-CoA or acetyl-CoA. For example, siRNA knockdown of enzymes known to be involved in the metabolism and catabolism of acetyl-CoA (ACCC1, ACAT, PDH, ACLY) and crotonyl-CoA (ACSS2, GCDH, HADHA, ECHS1) followed by immunoblot of cell lysates with acyl-specific antibodies and measurements of acyl-CoAs by LC-MS would extend the observation made in Chapter 3 for ACSS2. Acetyl-CoA metabolism was already discussed in Chapter 1 (**Figure 1.4**). Crotonyl-CoA can be synthesized as an intermediate in both beta-oxidation and lysine and tryptophan degradation (Lin et al., 2012). In beta-oxidation, acyl-CoA dehydrogenase (ACAD) generates crotonyl-CoA from butyryl-CoA, which is

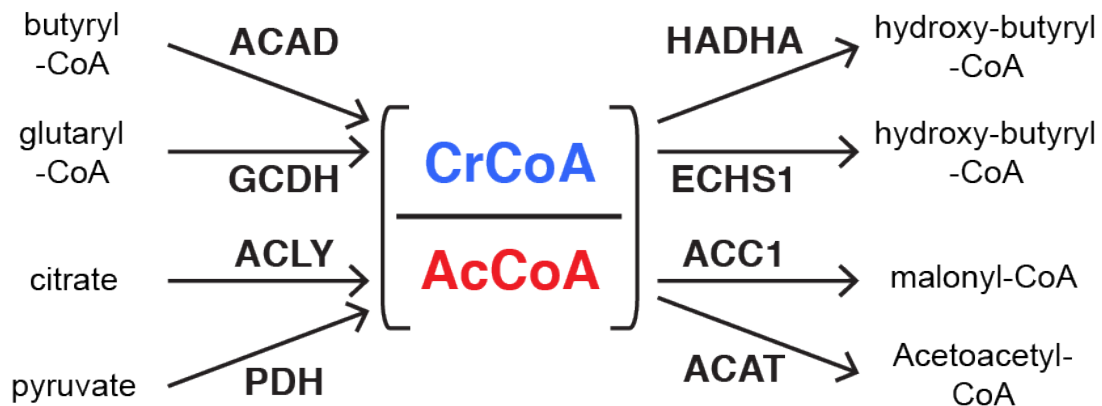


**Figure 7.4: Metabolic Enzymes Involved in Acetyl-CoA or Crotonyl-CoA metabolism.**

A simplified metabolic network of enzymes responsible for metabolism of acetyl-CoA (AcCoA) and crotonyl-CoA (CrCoA) is presented here. The enzymes listed followed by abbreviations in parentheses used are as follows: acyl-CoA dehydrogenase (ACAD), glutaryl-CoA dehydrogenase (GCDH), ATP-citrate lyase (ACLY), pyruvate dehydrogenase (PDH), hydroxylacyl-CoA dehydrogenase (HADHA), enoyl-CoA hydratase (ECHS1), acetyl-CoA carboxylase (ACC1), and acetyl-CoA acetyltransferase (ACAT).

followed by hydroxylation to form 3-hydroxy-butyryl-CoA catalyzed by either hydroxyacyl-CoA dehydrogenase (HADHA) or enoyl-CoA hydratase (ECHS1). Crotonyl-CoA can also be derived from glutaryl-CoA by glutaryl-CoA dehydrogenase (GCDH) in the degradation of lysine and tryptophan. See **Figure 7.4** for a simplified metabolic network, highlighting the roles of these candidate enzymes. These experiments could lead to the discovery of other metabolic enzymes critical to the production of crotonyl-CoA used for histone crotonylation.

### **The Influence of Environmental Short Chain Fatty Acids**

A major outstanding question from my thesis work is how crotonate is generated in the cell. If in fact ACSS2 knockdown decreases histone crotonylation then the assumed source of crotonyl-CoA will be from crotonate (Chapter 3). There are no obvious enzymatic reactions that would generate crotonate in mammalian metabolic pathways. Short chain fatty acids (SCFA) in general are thought of more as products of microbial metabolism than mammalian. The majority of my cellular studies rely on the addition of exogenous crotonate to cells, a potentially physiological situation for luminal cells of the mammalian large intestine, which are exposed to the diverse ecology of the microbiota and its secretions. The microbes that reside in the large intestine secrete a large variety of SCFA, the most abundant of which tend to be acetate (2-carbon), propionate (3-carbon), butyrate (4-carbon), and valerate (5-carbon). While the luminal cells of the large intestine are in direct contact with microbial-secreted SCFA, these compounds are also found in hepatic, portal, and peripheral blood, suggesting they could have influence outside of the gut (Besten et al., 2013; Cummings et al., 1987).

Differences in the concentrations and makeup of SCFAs from environmental sources have been implicated in a variety of physiological and disease states ranging from gut microbiota dysbiosis leading to obesity, colitis, and cancer predisposition to the regulation of immune cell development (Lee and Hase, 2014; Tan et al., 2014a). SCFAs have numerous roles outside of feeding acyl-CoA pools used for histone modifications. SCFAs can also be utilized in host metabolism, particularly in colonocytes where they are the cell's major energy source (Roediger, 1980). SCFAs can also influence host fatty acid, glucose, and cholesterol metabolism (Besten et al., 2013). SCFA are also implicated in signaling pathways as they have been described as ligand activators of the G-protein coupled receptors GPR41 and GPR43 (Brown et al., 2003). Yet, whether observed fluctuations in SCFA lead to an increase or decrease in their corresponding histone acylation, as we have shown here with crotonate and histone crotonylation remains largely untested.

One way to test this hypothesis would be to compare specific pathogen free (SPF) mice from different vendors to germ free (GF) mice by both SCFA composition in serum and feces as well as measurement of crotonylation and acetylation in histone extracted from various tissues. SPF mice from different vendors or breeding centers are known to exhibit variation in their gut microbiota (Hufeldt et al., 2010) presumably with consequences on the SCFA composition. GF mice will not have any microbial-derived SCFA and comparisons with SPF mice as to the levels of histone acylations will reveal the extent to which these modifications are derived from environmental SCFAs. Tissue from various sections of the gut, including colon, cecum, small intestine and stomach, as well as other tissues including thymus, liver, kidney, and

pancreas could be collected and lysates generated for immunoblot detection and/or mass spectrometry. If differences in histone crotonylation are observed between SPF and GF mice, further experimentation could be carried out to inoculate GF mice with specific bacteria in an effort to identify the strain responsible for the effect. These types of gnotobiotic mouse models have been successfully utilized to study the effects of butyrate secreting bacteria on the activation of T<sub>H</sub>17 immune cells (Arpaia et al., 2013) and in the protection against colorectal cancer under high-fiber diet (Donohoe et al., 2014), both studies implicate the compounds HDAC inhibitor activity as the mechanism of action.

## **Conclusion**

The regulation of histone crotonylation or the functional consequence of a histone being acetylated versus crotonylated (differential acylation) has remained unclear since the discovery of the modification was reported. During my thesis work I have had the privilege of working with exceptional colleagues and together we have shown that histone crotonylation is regulated both enzymatically, by p300/CBP, and metabolically, by the relative concentration of crotonyl-CoA and acetyl-CoA. We established a role for histone crotonylation in transcription in both cell-free and cell-based models of transcriptional activation. We demonstrated that part of this transcriptional response is mediated through AF9 YEATS as a reader of crotonyl-lysine and characterized several decrotonylase activities. In conclusion, we have demonstrated that the differential acylation state of histones is an integration of environmental and metabolic information, which serves a functional role in the regulation of gene expression.

## CHAPTER 8: METHODS

### HeLa S3 Nuclear Extract Preparation

For nuclear extract, HeLa S3 cells were grown in suspension culture in DMEM supplemented with 10% FBS. Eight liters of HeLa S3 suspension culture ( $\sim 1 \times 10^{10}$  cells) were harvested by centrifugation and then washed in cold PBS. The pellet was resuspended in hypotonic lysis buffer (20 mM HEPES pH 7.9, 10 mM KCl, 5 mM MgCl<sub>2</sub>, 0.5 mM EGTA, 0.1 mM EDTA, 5 mM  $\beta$ ME, 1 mM sodium metabisulfite, 1 mM benzamidine, 0.8 mM PMSF) and dounced ten times with pestle A and ten times with pestle B or until >90% of cells were determined lysed by trypan blue staining. Lysed cells were centrifuged at 3000 rpm to pellet intact nuclei. Nuclei were resuspended in a nuclear resuspension buffer (20 mM HEPES pH 7.9, 110 mM KCl, 2 mM MgCl<sub>2</sub>, 0.1 mM EDTA, 5 mM BME, 1x complete protease inhibitor (Roche), 0.4 mM PMSF) and dounced ten times with pestle A to homogenize the suspension. Solid ammonium sulfate was added to a final concentration of 400 mM, samples were immediately mixed by inversion, and left rotating at 4°C for 30 minutes. The samples were then clarified by centrifugation at 35,000 rpm for 1 hour. The supernatant is the soluble nuclear extract. The soluble nuclear extract was then subject to ammonium sulfate precipitation/salting out to 60% saturation. The precipitate was collected and gently resuspended in buffer D (20mM HEPES pH 7.9, 100 mM KCl, 1 mM EDTA, 10% glycerol, 1 mM DTT, 1 mM PMSF) and dialyzed twice against 2 L of Buffer D for 2 hours. The dialyzed extract is the crude nuclear extract that was subject to further fractionation.

### **Chromatographic Fractionation**

Column chromatography was performed using the AKTA Purifier system with the following columns: in-house packed POROS Heparin 50  $\mu$ M (Invitrogen), Mono Q 5/50 GL (GE Healthcare), and Mono S 5/50 GL (GE Healthcare). Fractions were collected over a linear potassium chloride gradient from 0.15 M to 1 M.

### **Immunoblot Analysis**

Histones were purified from cells using a standard acid extraction protocol (Shechter et al., 2007). Whole cell lysates were prepared by boiling cell pellets in 2x Laemmli sample buffer for 5 minutes followed by brief vortexing. The following antibodies were used in this study: Pan-KCr (PTM-Biolabs 501), H3K18Cr (PTM-Biolabs 517), pan-KAc (PTM-Biolabs 105), H3K18Ac (Abcam 1191), H3K27Ac (Active Motif 39685), H3K56Ac (Abcam 76307), H3 (Abcam 1791), p300 (Santa Cruz 584), CBP (Santa Cruz 7300), ACSS2 (Cell Signaling 3658), alpha-actin (Sigma A2066), beta-actin (Abcam 8224), and lamin-A (Abcam 26300). The ACL antibody was a gift from the Thompson Lab.

### **Cell Culture and Transfections**

HeLa S3, HEK 293T, and RAW 264.7 cells were cultured in DMEM, supplemented with 10% FBS, and 1% GlutaMAX (Gibco) at 37°C under 5% CO<sub>2</sub>. Sodium crotonate was prepared by dissolving solid crotonic acid (MP 207938) in water, followed by titration with sodium hydroxide to pH 7.4. Sodium acetate was prepared similarly with acetic acid. siRNA transfections were performed

using Dharmafect 1 (Dharmacon) as per manufacturer's instruction. The following siRNAs were used at the following concentrations: non-target control (Dharmacon D-001810-10, 25nM), p300 (Dharmacon L-003486, 25nM), CBP (Dharmacon L-003477, 25nM), ACSS2 #1 (Ambion s31745, 20nM), ACSS2 #2 (Ambion s31746, 20nM), ACSS2 #3 (Ambion s31747, 20nM), ACSS2 #4 (Dharmacon L-010396, 20nM), ACL #1 (Ambion s915, 10nM), ACL #2 (Ambion s916, 10nM), ACL #3 (Ambion s917, 10nM), PDHE1 $\alpha$  (Ambion s10245, 20nM), mouse ACSS2 (Dharmacon L-065412, 25nM). DNA transfections were performed using lipofectomine 2000 as per manufacturer's instruction. For LPS stimulation, RAW 264.7 cells were plated at ~25% density >24 hours prior to stimulation. LPS from *Salmonella typhosa* (Sigma L2387) was added at 100 ng/mL and samples were collected at indicated time points.

### **Recombinant Enzymes**

Recombinant p300, MOF, Sirtuins and HDAC1 were expressed in Sf9 cells by baculovirus infection and purified by FLAG immuno-precipitation (IP) of nuclear extracts, described in next section. Recombinant p300 and p53 used in transcription assays were purified by Dr. Zhanyun Tang as described previously (Tang et al., 2013). SIRT1 (addgene #1791), SIRT2 (addgene #13813), SIRT6 (addgene #13817), SIRT7 (Open Biosystems MHS6278-202832829) cDNA were cloned into pFastbac1 with C-terminal FLAG tags. MOF cDNA (MHS6278-202808687) was cloned into pFastbac1 with an N-terminal FLAG tag. Baculovirus was generated by the Bac-to-bac system per manufacturer's instructions (Life). Amplified baculovirus was used to transduce sf9 cells and protein was purified by FLAG-IP, as described in the following section. The catalytic domains of

GCN5 (residues 505-670) and TIP60 (residues 181-462) were cloned from HeLaS3 cDNA libraries into pGEX6p1 to generate GST-fusion proteins. Rosseta2(DE3)pLysS were transformed, induced by IPTG, and soluble protein was purified by standard glutathione-sepharose chromatography.

### **FLAG Purification from Baculovirus Infected Sf9 Cells**

Baculovirus were generated by the Bac-to-Bac recombination strategy (Life). Baculovirus were amplified by serial infection of sf9 cells. 20-30 mL of high-titer baculovirus was added to 1 L of sf9 suspension culture in exponential growth ( $\sim 0.6 \times 10^6$  cells/ml). Three days post-infection, cells were harvested by centrifugation and washed in cold PBS. The washed cell pellets were then resuspended ( $\sim 2 \times 10^7$  cells/ml) in hypotonic lysis buffer (20 mM HEPES, 10 mM KCl, 5 mM MgCl<sub>2</sub>, 0.1 mM EDTA, 1 mM DTT, 1x Complete Protease inhibitor (Roche)) and dounced 10 times with pestle A and 10 times with pestle B, or until >90% of cells were lysed as detected by trypan blue staining. Samples were centrifuged at 3000 rpm to pellet intact nuclei. Pellets were resuspended ( $\sim 4 \times 10^7$  cells/ml) in Buffer B (20 mM HEPES, 300 mM KCl, 1 mM EDTA, 0.1% TritonX-100, 1 mM DTT, 0.4 mM PMSF) and dounced with pestle A to homogenize. Samples were incubated rotating at 4°C for 30 minutes followed by centrifugation at 35,000 rpm for 1 hour. The supernatant is the soluble nuclear extract. Equilibrated Anti-FLAG M2 conjugated to agarose beads (Sigma A2220) were added to soluble nuclear extract and incubated rotating at 4°C for 4 hours. The FLAG M2 agarose beads were washed on column twice with ten times column volume (CV) Buffer W (Buffer B/0.01% TritonX-100, 10% glycerol).

Protein was eluted with four 0.5CV elutions of buffer E (Buffer W + 300  $\mu\text{g}/\text{mL}$  3X FLAG peptide). Peak fractions were pooled and dialyzed to buffer W.

### ***In Vitro Assays***

HAT/HCT assays were incubated at 30°C for 1 hour in Buffer A (50 mM Tris pH 8.0, 10% glycerol, 1 mM DTT, 0.2 mM PMSF). When extract was used as an enzyme source 10mM Sodium Butyrate was included in Buffer A. 2-100  $\mu\text{M}$  of either crotonyl-CoA or acetyl-CoA (Sigma 28007 and A2181) was used as the high-energy acyl donor. Unless otherwise noted, 100  $\mu\text{M}$  was used in initial purifications, 2  $\mu\text{M}$  in subsequent HAT and HCT *in vitro* assays, and 50  $\mu\text{M}$  in the transcription assays. The oligonucleosome substrate was sucrose-gradient purified from micrococcal nuclease-digested HeLaS3 nuclei, as previously described (Fang et al., 2003). Recombinant chromatin used in p300 reactions and transcription assays was prepared as described (Tang et al., 2013). Recombinant histone proteins were purified and assembled into octamers as previously described (Ruthenburg et al., 2011). Under reaction conditions the “octamers” are most likely present as H3-H4 tetramers and H2A-H2B dimers, while oligonucleosome and recombinant chromatin substrate will maintain their structure. Sirtuin reactions were incubated at 30°C for 2 hours in Buffer S (10 mM Tris-HCl, pH 8.0, 5 mM  $\text{NAD}^+$ , 150 mM NaCl, 0.2 mM DTT). Fluorescence-based HDAC assays were performed using an HDAC Assay Kit (Active Motif 56200) according to manufacturer’s instruction. p53-dependent *in vitro* transcription assays were performed as previously described (Tang et al., 2013). Densitometry of autoradiographs was performed with ImageJ.

### **H3K18Ac and H3K18Cr ChIP**

Cross-linking ChIP was performed with anti-H3K18Ac (Abcam 1191) and anti-H3K18Cr (PTM-biolabs 517). RAW 264.7 cells were grown in full media, pretreated with the indicated concentration of crotonate for six hours, and then stimulated with 100 ng/mL of LPS for two hours. Chromatin from  $\sim 5 \times 10^7$  cells was used per immuno-precipitation. Media was aspirated and cells washed with PBS followed by addition of 1% formaldehyde (in PBS). Cells were cross-linked directly on the plate for 10 minutes with gentle shaking. Glycine was added to a final concentration of 125 mM to quench the crosslinking and allowed to incubate for 5 minutes. Cells were scraped off the plates, pelleted, and washed in PBS plus 1x Complete protease inhibitors (Roche), 10 mM Butyrate, and 10 mM nicotinamide. Pellets were resuspended in 10mL LB1 (50 mM HEPES, 140 mM NaCl, 1 mM EDTA, 10% glycerol, 0.5% NP40, 1% TritonX-100, 1x Complete protease inhibitor (Roche), 10 mM Butyrate, 10 mM nicotinamide) and incubated rotating at 4°C for 20 minutes. Samples were centrifuged and pellets were resuspended in 10 mL LB2 (10 mM Tris pH 8.0, 200 mM NaCl, 1 mM EDTA, 0.5 mM EGTA, 1x Complete protease inhibitors (Roche), 10 mM butyrate, 10 mM nicotinamide). Samples were incubated rotating at 4°C for 10 minutes and then centrifuged. Pellets were resuspended in 1.2 mL LB3 (10 mM Tris pH 8.0, 100 mM NaCl, 1 mM EDTA, 0.5 mM EGTA, 0.1% sodium-deoxycholate, 0.5% sodium lauroyl sarcosinate, 1% TritonX-100, 1x Complete protease inhibitors (Roche), 10 mM butyrate, 10 mM nicotinamide) and passed through a 27-gauge needle until suspension was homogenized. The samples were then sonicated in a Bioruptor cooled water bath sonicator (Diagenode) for 60 cycles of 30' on 30' off on high intensity. Samples were clarified by centrifugation at 16,000 g for 15 minutes. The

supernatant is the soluble chromatin extract. 5% of input volume was set aside. 7.5 µg of H3K18Cr or H3K18Ac antibody were conjugated to 75 µL protein A Dynabeads (Novex) per immuno-precipitation. After unbound antibody was washed away, the beads were added to the clarified soluble chromatin extract and incubated rotating overnight at 4°C. A magnetic stand was used to separate beads from the extract and beads were washed under the following conditions: three times with 1 mL wash buffer 1 (50 mM HEPES, 100 mM LiCl, 1 mM EDTA, 1% NP-40, 0.7% sodium deoxycholate, 10 mM butyrate, 10 mM nicotinamide), three times with 1mL wash buffer 2 (20mM Tris-HCl pH 8.0, 350mM NaCl, 1% TritonX-100, 0.1% SDS, 2mM EDTA, 10 mM butyrate, 10 mM nicotinamide), and once with 1 mL buffer TE plus 50 mM NaCl. The washed beads were resuspended in 210 µL elution buffer (50 mM Tris pH 8.0, 10 mM EDTA, 1% sodium dodecyl sulfate) and incubated at 65°C for 30 minutes while shaking to prevent beads from settling. The eluate was transferred to a new tube, 5% inputs were brought up to equal volume with elution buffer, and both were incubated at 65°C overnight to reverse crosslinks. The samples were then treated with RNase and Proteinase K. DNA was recovered using the Qiagen PCR purification kit according to manufacturer's instruction. A 1/100 dilution of each sample was used for qPCR analysis as described in experimental procedures.

### **ChIP-qPCR**

ChIP products and inputs were diluted 1/100 and then analyzed by qPCR using Power SYBR Green (Life) and StepOnePlus Real-Time PCR system (Applied Biosystems).

The sequences of ChIP-qPCR primer pairs used for H3K18Ac and H3K18Cr ChIP are:

	Forward	Reverse
<b>Il6</b>	AATGTGGGATTTTCCCATGA	GCTCCAGAGCAGAATGAGCTA
<b>Gbp2</b>	GCCCAGGGCTAGGTGACA	TGTGAAGTCTTCTTTCCAGAGTTT
<b>Ifit1</b>	GCCATCCTAAGACCCCCTAGTG	TCTGCAGTTCCTCCTTGGAAGT
<b>Pim1</b>	CTGGCCTCGGTGTGCAA	GGCGAAGGCTGTGCAAGA
<b>Rsad2</b>	CAATCCCAACTCCTTTCCCAACA	TCTGACCTCCATAACCAAATGAACT
<b>Ccl3</b>	ATCTCCAGCTCGAGCAATGG	AGTCACTTTGCGGCTGATGA
<b>Ccl5</b>	TGAGCCTTTGAGGAGGTTGG	CACTGCAAGTCACGGCCATA

The sequences of ChIP-qPCR primer pairs used for FLAG-AF9 ChIP are:

	Forward	Reverse
<b>Rsad2</b>	GGTCCAGGAACTTACCAGCC	TCCACACAGCCAAGACATCC
<b>Il6</b>	CTGCTCACTTGCCGGTTTTTC	AGCATCAGTCCCAAGAAGGC
<b>Ifit1</b>	CCTGAGGGTCCAGGGAGTTT	TCCAGCACCAGGCACACA
<b>Cmpk2</b>	TGTTAGACACGGATGCTGCC	GGTAGGTGTTGGATGCACGA
<b>Gbp2</b>	GCCCAGGGCTAGGTGACA	TGTGAAGTCTTCTTTCCAGAGTTT

Melt-curve analysis along a dilution series was carried out to ensure unique product amplification for all primer pairs. All statistical analysis was performed using PRISM v6.0 (Graph Pad).

## RT-qPCR

RAW264.7 cells were plated at ~25% confluency >24 hours prior to harvest. Sodium crotonate was added 12-16 hours prior to harvest. LPS was added to a final concentration of 100ng/ml 2 hours prior to harvest. Total RNA was extracted using the RNeasy Kit (Qiagen) and Dnase treated on column according to manufacturer's instructions (Qiagen). cDNA was prepared using the High Capacity cDNA Reverse Transcription Kit (Applied Biosystems) according to manufacturer's instructions. cDNA fragments were analyzed by qPCR using Power SYBR Green (Life) and StepOnePlus Real-Time PCR system (Applied Biosystems). A standard curve for each primer pair was used to ensure linear dilution and to quantitate cDNA abundance. Relative expression values were derived by normalization to Gapdh quantity for each sample. The sequences of RT-qPCR primer pairs with forward followed by reverse are:

	Forward	Reverse
<b>Il6</b>	GTTCTCTGGGAAATCGTGGA	TTTCTGCAAGTGCATCATCG
<b>Gbp2</b>	CTCTACCGCACAGGCAAATC	GATGCCCTTGGTGTGAGACT
<b>Ifit1</b>	AGTGAGGTCAACCGGGAATCT	TCTAGGTGCTTTATGTAGGCCA
<b>Pim1</b>	TCAAGGACACAGTCTACACGG	AGCGATGGTAGCGAATCC
<b>Rsad2</b>	AACCCCGTGAGTGTCAACTA	AACCAGCCTGTTGAGCAGAA
<b>Ccl3</b>	TACAGCCGGAAGATTCCACG	TCAGGAAAATGACACCTGGCT
<b>Ccl5</b>	GTGCCACGTCAAGGAGTAT	CCCACTTCTTCTCTGGGTTG
<b>Cmpk2</b>	GACCTAGTTGACCAGTGCCC	AGTGTGGTCTTACCAGTGCC
<b>Cxcl10</b>	ATGACGGGCCAGTGAGAATG	TCGTGGCAATGATCTCAACAC
<b>Ifnb</b>	TGGGAGATGTCCTCAACTGC	CCAGGCGTAGCTGTTGTACT
<b>Gapdh</b>	TGGTGAAGGTCGGTGTGAAC	CCATGTAGTTGAGGTCAATGAAGG

**Gbp5**      CGGACCTCGTCTAGAAAGCC      CCGGGCCAAGGTTACTACTG  
**FLAG-**    TGGACTACAAAGACCATGACGG    GGCACGTCGTAGGGGTATC  
**AF9**

Melt-curve analysis along a dilution series was carried out to ensure unique product amplification for all primer pairs. All statistical analysis was performed using PRISM v6.0 (Graph Pad).

### **RNA-seq**

RNA-seq libraries were prepared using the TruSeq RNA Sample Prep Kit (Illumina) as per manufacturer's instruction. The procedure includes purification of poly-adenylated RNAs. Libraries were sequenced with 50bp single read sequencing on the HiSeq2500 (Illumina). Sequencing data was processed and analyzed as described in (Trapnell et al., 2012). RNA-seq data sets are available through GEO under the accession number GSE63889.

### **ChIP-seq for H3K18Ac and H3K18Cr**

ChIP-seq libraries were prepared using the TruSeq ChIP Sample Prep Kit (Illumina) as per manufacturer's instruction. Libraries were sequenced with 50bp single read sequencing on the HiSeq2500 (Illumina). 50bp reads were aligned using bowtie (v1.0.1) to the mouse mm9 reference assembly reporting only unique reads in the best stratum, with up to 2 mismatches (bowtie -p 8 -S -q -v 2 -m 1 -k 1 --best --strata). Samtools (v0.1.19) was then used to convert files to bam format, sort, and remove PCR duplicates (Li et al., 2009a). For genome browser representation, tdf files were generated by IGVtools (v2.3.7) and data were

visualized using IGV (v2.1.28) (Thorvaldsdottir et al., 2013). Ngs.plot (v2.08) was used to generate average profiles of ChIPseq reads (Shen et al., 2014). MACS (v1.4.2) was used to call peaks (Zhang et al., 2008). BEDOPs (v2.4.1), bedmap --basses function, was used for read counting within specified genomic regions (Neph et al., 2012). ChIP-Seq data sets (H3K18Ac, H3K18Cr, and inputs) are available through GEO under the accession number GSE63889. The p300 ChIP-seq data presented here were reanalyzed from publically available data available through GEO at accession number GSE19553 (Ghisletti et al., 2010).

### **Immuno-detection of Secreted Inflammatory Mediators**

Supernatants from RAW 264.7 cells under indicated conditions and for indicated length of LPS stimulation were assayed by two distinct immuno-assays. A standard immobilized ELISA for mouse Il6 (Life KMC0061) was used as per manufacturer's instruction. And a bead-based assay that uses the principles of sandwich ELISA to quantify soluble analytes using a flow cytometer (Biolegend: Legendplex assay) was used to quantify the concentration of a number of secreted chemokines and cytokines, as per manufacturer's instruction.

## Mass Spectrometry Analysis of p300 Reaction Products

[The methods described here were carried out by He Huang and members of the Zhao group]

Recombinant chromatin was acetylated or crotonylated by p300 in the presence of p53 and reaction products were resolved on an 8% Tris-Glycine SDS-PAGE gel. The gel bands of core histone proteins were excised and subjected to in-gel tryptic digestion. The tryptic digests were desalted with Ziptip C18 and loaded onto a homemade capillary column (10 cm length with 75  $\mu\text{m}$  inner diameter) packed with Jupiter C12 resin (4  $\mu\text{m}$  particle size, 90  $\text{\AA}$  pore size, Phenomenex Inc.) connected to a NanoLC-1D plus HPLC system (Eksigent Technologies LLC, Dublin, CA). Peptides were eluted with a gradient of 5% to 90% HPLC buffer B (0.1% formic acid in acetonitrile, v/v) in buffer A (0.1% formic acid in water, v/v) at a flow rate of 300 nL/min over 76 min. The eluted peptides were ionized and introduced into a LTQ-Orbitrap Velos mass spectrometer (Thermo Fisher Scientific Inc., Waltham, MA) using a nanospray source. Full MS scans were acquired in the Orbitrap mass analyzer over the range  $m/z$  300-1800 with a mass resolution of 60000 at  $m/z$  400. Twenty of the most intense ions were isolated for MS/MS analysis. Database searching was performed against the NCBI protein sequence database, using Mascot. The database searching parameters included: lysine acetylation, protein N-terminal acetylation, lysine crotonylation, lysine trimethylation, lysine/arginine di-methylation, lysine/arginine mono-methylation, and methionine oxidation as variable modifications. All the identified peptides were manually verified.

## Mass Spectrometry Analysis of Mono S Fractions

[The methods described here were carried out by Dr. Henrik Molina]

50  $\mu\text{L}$  of each fraction was precipitated overnight using 500  $\mu\text{L}$  ice cold acetone. Same process was followed for the 'input' sample with the exception that sample volume was 100  $\mu\text{L}$  and 1000  $\mu\text{L}$  ice cold acetone was used for precipitation. Acetone was carefully removed, first by suction, then by evaporation. Precipitates was dissolved in 30  $\mu\text{L}$  8M Urea/0.1M ammonium bicarbonate/10mM Dithiothreitol and vortexed at room temperature for 45 minutes. Reduced proteins was alkylated in the dark by adding 7  $\mu\text{L}$  100mM iodoacetamide to each vial. Samples was then diluted 2-fold with 0.1M ammonium bicarbonate and 1 $\mu\text{g}$  Endopeptidase Lys-C (Wako Chemicals USA, Inc, Richmond, VA) in 10  $\mu\text{L}$  in 0.1M ammonium bicarbonate was added to each vial. Digestion was allowed to proceed for 6h. Samples were further diluted by adding 80  $\mu\text{L}$  0.1M ammonium bicarbonate prior to the addition of 1 $\mu\text{g}$  trypsin (Promega, Madison, WI, USA) dissolved in 20  $\mu\text{L}$  0.1M ammonium bicarbonate. Trypsination of the samples was allowed to proceed overnight, and the digestion was halted by adding 2  $\mu\text{L}$  trifluoroacetic acid. Half of each sample was desalted using in-house SPE columns made with Empore  $\text{C}_{18}$  (Rappsilber et al., 2003). Generated peptides were measured by nano LC-MS/MS using a Q-Exactive mass spectrometer (Thermo, Bremen, Germany) coupled to a Dionex NCP3200RS HPLC setups (Thermo, Sunnyvale, CA, USA). Samples were desalted and concentrated on a trap column prior to separation on a packed-in-emitter  $\text{C}_{18}$  column (75  $\mu\text{m}$  by 12 cm, 3  $\mu\text{m}$  particles - Nikkyo Technos Co., Ltd. Japan). The analytical gradient was generated at 300 nL/min increasing from 10% Buffer B (0.1% formic acid in acetonitrile) / 90% Buffer A (0.1% formic acid) to 45% Buffer

B / 55% Buffer A in 137 minutes, followed by a wash step with 90% Buffer B / 10% Buffer A for 16 minutes and conditioning for 10 minutes with 1% Buffer B / 99% Buffer A Buffer B. Data Dependent Acquisition experiment: MS survey scans was scanned from m/z 300 to m/z 1400 at resolution of 70,000@200 Th (AGC: 5e5 and maximum IT: 100 ms). Up to the 20 most abundant ions were subjected to MS/MS and measured at a resolution of 17,500 (AGC: 5e5 and maximum IT: 60 ms) with m/z 100 as lowest mass. Precursor ions were isolated at 2.0 Th. Lock mass of m/z 371.10123 was used for all measurements. All samples were analyzed in technical duplicates. Data were searched and quantified using MaxQuant 1.5.30 (Cox et al., 2014). Technical replicates were merged for the analysis. The Uniprot Complete Proteome human protein database (July 2014) was queried. Match between runs was utilized. Combining all samples approximately 3,700 proteins were matched at 1% protein and peptide False Discovery Rate. For the comparison of the data set intensity Based Absolute Quantitation (iBAQ) (Schwanhäusser et al., 2011) was used. MaxQuant 'proteinGroups.txt' output is available in Table S1.

### **Mass Spectrometry Analysis of Acetyl-CoA and Crotonyl-CoA**

[The methods described here were carried out by Drs. Justin Cross and Vladimir Yong-Gonzalez]

HeLa S3 and RAW 264.7 cells were maintained in DMEM medium supplemented with 10% FBS, 2 mM of L-glutamine, 100 units/mL penicillin and 100 µg/mL streptomycin at 37°C under an atmosphere of 5% of CO<sub>2</sub>. The acyl-CoA extraction procedure was based upon the method previously described by (Basu and Blair, 2011), with minor modifications. Cultured cells were washed

once with cold deionized water and metabolites extracted by the addition of 1 mL of ice cold 10% trichloroacetic acid (TCA). Following 15 seconds incubation on ice, cells were collected by scrapping and transferred to a 1.5 mL Eppendorf tube. Cell extracts were sonicated for 3 x 30 seconds (Bioruptor, Diagenode) and then centrifuged at 14,000 rpm for 5 minutes at 4°C to remove protein. Acyl-CoAs were further purified using a HLB 96-well plate solid phase extraction plate (30 mg) and vacuum manifold (Waters Corporation). SPE wells were conditioned with 1 mL of methanol, and equilibrated with 1 mL of water. Supernatants were applied and then SPE wells were washed with 1 mL of water; acyl-CoAs were eluted using three successive applications of 0.5 mL of methanol containing 25 mM ammonium acetate. Eluted acyl-CoAs were dried for 5 hours in a bench top solvent evaporator (Genevac EZ-2 Elite). Dried samples were stored at -80°C and re-suspended in 100  $\mu$ L of 5% 5-sulfosalicylic acid (SSA) immediately prior to analysis by liquid chromatography/mass spectrometry (LC/MS).

Acyl-CoA were separated using a Phenomenex Luna C18 column (2.0 mm x 50 mm, 5  $\mu$ m) using 10 mM ammonium acetate in water, pH 8 as the aqueous mobile phase and 90% acetonitrile, 10% water with 10 mM ammonium acetate, pH 8 as the organic phase. The injection volume was 15  $\mu$ l (Accela Open Autosampler, Thermo Fisher Scientific) and a constant column temperature was maintained at 30°C using a thermostatically controlled column oven (MayLab). LC-20A pumps (Shimadzu) were used for the primary LC gradient: 0 min, 3% B; 1 min, 3% B; 6 min, 40% B; 7 min, 40% B; with an additional 6 min allowed for column re-equilibration between injections. A constant flow rate of 0.2 mL/min was maintained, with an additional 0.1 mL/min of 90% acetone, 10% dimethyl

sulfoxide added post-column by means of an Accela 1250 pump (Thermo Fisher Scientific) and PEEK tee, to increase the sensitivity of acyl-CoAs detection.

Acyl-CoAs were detected using a TSQ Vantage triple quadrupole mass spectrometer (Thermo Fisher Scientific) equipped with H-ESI II probe, operating in positive ionization mode. MS parameters were: spray voltage, 3000 V; sheath gas pressure, 35 psi; auxiliary gas pressure, 30 psi; capillary temperature, 270°C; and vaporizer temperature, 250°C. Data acquisition was performed in single reaction monitoring (SRM) mode using S-lens of 200 V, collision energy of 26 eV, 50 millisecond scan time and compound specific parameters: Acetyl-CoA 810.1 → 303.1 m/z, Crotonyl-CoA 836.1 → 329.1 m/z. Data was acquired and analyzed using TraceFinder 3.1 software (Thermo Fisher Scientific).

### **Crystallization, Data Collection, and Structure Determination**

[The methods described here were carried out by members of The Li group]

Crystallization was performed via the sitting or hanging drop vapor diffusion method under 18°C or 4°C by mixing equal volumes (0.2-1.0 µl) of AF9 YEATS-H3K9cr/18cr (1:2 molar ratio, 6–8 mg/ml) or BRD3<sub>BRD2</sub>-H3K18ac (1:10 molar ratio, 6–8 mg/ml) and reservoir solutions: 20% (w/v) polyethylene glycol 4000, 0.2 M ammonium sulfate, and 0.1 M sodium citrate tribasic dihydrate, pH 5.6, supplemented with 3% MPD (AF9-H3K9cr) or with 0.1 M copper chloride dihydrate (AF9-H3K18cr); 30% (w/v) polyethylene glycol methyl ether 5000, 0.2 M ammonium sulfate, 0.1 M MES, pH 6.5, plus 0.1 M guanidine hydrochloride (BRD3-H3K18ac). The complex crystals were briefly soaked in cryoprotectant containing the reservoir solution supplemented with 20% glycerol and then flash frozen in liquid nitrogen for data collection. The

diffraction data set was collected at the beamline BL17U or BL19U of the Shanghai Synchrotron Radiation Facility at 0.9791 Å. All diffraction images were indexed, integrated, and merged using HKL2000 (Otwinowski and Minor, 1997). The structure was determined by molecular replacement using MOLREP (Vagin and Teplyakov, 2010) with the AF9-H3K9ac structure (PDB ID: 4TMP) as the search model. Structural refinement was carried out using PHENIX (Adams et al., 2010), and iterative model building was performed with COOT (Emsley and Cowtan, 2004). Detailed data collection and refinement statistics are summarized in Table S1. Structural figures were created using the PYMOL (<http://www.pymol.org/>) program.

### **FLAG-ChIP**

RAW264.7 cells were plated at ~25% confluence >24 hours prior to harvest. Sodium crotonate was added 12-16 hours prior to harvest. LPS was added to a final concentration of 100ng/ml 2 hours prior to harvest. Cells were fixed on plate with 1% PFA in PBS for 10 minutes. Glycine was added to a final concentration of 125mM. Cells were scraped off the plates, pelleted, and washed in PBS plus 1x Complete protease inhibitors (Roche), 10 mM Butyrate, and 10 mM nicotinamide. Pellets were resuspended to  $1 \times 10^7$  cells/mL LB1 (50 mM HEPES, 140 mM NaCl, 1 mM EDTA, 10% glycerol, 0.5% NP40, 1% TritonX-100, 1x Complete protease inhibitor (Roche), 10 mM Butyrate, 10 mM nicotinamide) and incubated rotating at 4°C for 20 minutes. Samples were centrifuged and pellets were resuspended to  $1 \times 10^7$  cells/mL LB2 (10 mM Tris pH 8.0, 200 mM NaCl, 1 mM EDTA, 0.5 mM EGTA, 1x Complete protease inhibitors (Roche), 10 mM butyrate, 10 mM nicotinamide). Samples were incubated rotating at 4°C for

10 minutes and then centrifuged. Pellets were resuspended to  $6 \times 10^7$  cells/mL LB3 (10 mM Tris pH 8.0, 100 mM NaCl, 1 mM EDTA, 0.5 mM EGTA, 0.1% sodium-deoxycholate, 0.5% sodium lauroyl sarcosinate, 1% TritonX-100, 1x Complete protease inhibitors (Roche), 10 mM butyrate, 10 mM nicotinamide) and passed through a 27-gauge needle until suspension was homogenized. Samples were then sonicated using Covaris ultrasonicator model S220 for 20 minutes with the following settings: 140W peak power, 5% duty, 200 cycles per burst. Samples were clarified by centrifugation at 16,000 g for 15 minutes. The supernatant is the soluble chromatin extract. 400ug of soluble chromatin was used per CHIP. For FLAG CHIP, soluble chromatin extract was mixed 1:1 with LB4 (10mM Tris pH 8.0, 100mM NaCl, 1mM EDTA, 0.5mM EGTA, 0.1% NP40, 1% TritonX-100, 1x Complete protease inhibitors (Roche), 10mM butyrate, and 10mM nicotinamide) to dilute FLAG-incompatible buffer components. FLAG-M2 (SIGMA F1804) was conjugated to Protein G Dynabeads (Novex) at 7.5ug antibody to 75ul bead slurry per IP. M2-beads were added to diluted extract and incubated rotating overnight at 4°C. A magnetic stand was used to separate beads from the extract and beads were washed six times with FLAG-ChIP wash buffer (50mM Hepes, 500mM NaCl, 1% TritonX-100, 0.1% NP40, 1x Complete protease inhibitor cocktail, 10mM butyrate, and 10mM nicotinamide) and then once with 1 mL buffer TE plus 50 mM NaCl. The washed beads were resuspended in 210  $\mu$ L elution buffer (50 mM Tris pH 8.0, 10 mM EDTA, 1% sodium dodecyl sulfate) and incubated at 65°C for 30 minutes while shaking to prevent beads from settling. The eluate was transferred to a new tube, inputs were brought up to equal volume with elution buffer, and both were incubated at 65°C overnight to reverse crosslinks. The samples were then treated with RNase and Proteinase K.

DNA was recovered using the Qiagen PCR purification kit according to manufacturer's instruction.

### **ChIP-Seq Analysis for FLAG-AF9**

ChIP-seq libraries were prepared using the TruSeq ChIP Sample Prep Kit (Illumina) as per manufacturer's instruction. Libraries were sequenced with 75bp single read sequencing on the NextSeq 500 (Illumina) for FLAG-AF9 or 50bp single read sequencing on the TruSeq 2500 for endogenous AF9. Reads were aligned using bowtie (v1.0.1) to the mouse mm9 reference assembly reporting only unique reads in the best stratum, with up to 2 mismatches (bowtie -p 8 -S -q -v 2 -m 1 -k 1 --best --strata). Samtools (v0.1.19) was then used to convert files to bam format and sort (Li et al., 2009). For genome browser representation, tdf files were generated by IGVtools (v2.3.7) and data were visualized using IGV (v2.1.28) (Thorvaldsdottir et al., 2013). Ngs.plot (v2.08) was used to generate average profiles of ChIPseq reads (Shen et al., 2014). BEDOPs (v2.4.1), bedmap --bases function, was used for read base counting within specified genomic regions (Neph et al., 2012). RPKM values were derived as follows:  $[(\text{read-bases})/(\text{region-length in kb})]/(\text{total mapped reads in Mb})$ . FLAG-AF9 marked genes were defined by RPKM value +/- 1kb TSS >70. H3K18cr and H3K18ac marked genes were defined by RPKM value +/- 1kb TSS >50. Different cutoffs were used due to the different levels of background noise between FLAG-AF9 and H3K18ac/cr ChIP-Seq. Publically available H3K18cr ChIP-Seq, H3K18ac ChIP-Seq, and RNA-seq data used in this study can be accessed through GEO accession number GSE63889.

## Protein Production Related to Chapter 5

[The methods described here were carried out by members of The Li group]

Recombinant wild type and mutant AF9 YEATS (residues 1-138) was produced as previously described (Li et al., 2014). Briefly, AF9 YEATS was expressed in *E. coli* strain BL21 (DE3) (Novagen) with 0.4 mM IPTG induction at 16°C. After cell lysis by an Emulsiflex C3 (Avestin) high-pressure homogenizer thrombin and centrifugation, the supernatant was kept and applied to a HisTrap (GE Healthcare) nickel column and the protein was eluted with a linear imidazole gradient from 20 mM to 500 mM. After thrombin (Sigma) digestion overnight for His-tag removal, AF9 YEATS was further purified by a HiTrap SP (GE Healthcare) cation-exchange column and a HiLoad 16/60 Superdex 75 (GE Healthcare) gel filtration column using AKTA Purifier 10 systems (GE Healthcare). AF9 YEATS proteins were stored in 500 mM NaCl, 25 mM Tris, pH 7.5, and 2 mM β-ME at ~ 10 mg/ml in an -80°C freezer. All chromatographic steps were performed using AKTA Purifier 10 systems (GE Healthcare).

Recombinant YEATS domains of human ENL (1-138), and yeast Yaf9 (1-171), Taf14 (1-136) were constructed based on the pET28b vector. All above proteins were expressed and purified essentially the same as WT AF9 YEATS.

Recombinant bromodomains were constructed into pET28b vector, expressed with N-terminal 6xHis tag, and purified as previously described (Filippakopoulos et al., 2012; Li et al., 2014). After removal of the N-terminal His tag, purified Bromodomains were stored in buffer containing 150 mM NaCl, 25 mM HEPES, pH 7.5 for future use, except that the second bromodomain of TAF1 was stored in buffer containing 150 mM NaCl, 25 mM HEPES, pH 7.0).

### **Isothermal Titration Calorimetry (ITC)**

[The methods described here were carried out by members of The Li group]

ITC measurement was performed as previously described (Li et al., 2014). Briefly, synthetic pre-modified histone H3 peptides (SciLight Biotechnology, LLC) and the recombinant YEATS and Bromodomain proteins were extensively dialyzed against ITC buffer: 500 mM NaCl, 25 mM Tris, pH 7.5, and 2 mM  $\beta$ -ME for YEATS proteins; 150 mM NaCl and 25 mM HEPES, pH 7.5 for Bromodomain proteins (except that 150mM NaCl and 25 mM HEPES, pH 7.0 used for TAF1<sub>Brd2</sub>). The concentrations of peptides and proteins were measured using A205nm and A280nm, respectively. The titration was performed using MicroCal iTC200 system (GE Healthcare) at 15°C for YEATS proteins and 25°C for Bromodomain proteins. Each ITC titration consisted of 17 successive injections with 0.4  $\mu$ l for the first and 2.41  $\mu$ l for the rest. Usually, H3 peptides at 1.0-1.2 mM were titrated into YEATS or Bromodomain proteins at 0.07-0.1 mM. The resultant ITC curves were processed using the Origin 7.0 software (OriginLab) according to the “One Set of Sites” fitting model.

### **MNase Digestion and FLAG AF9 IP**

[The methods described here were carried out by Dr. Tanya Panchenko]

The micrococcal nuclease (MNase) IP was performed essentially as described (Bailey et al., 2013). Briefly, approximately  $5 \times 10^7$  HeLa cells stably expressing FLAG tagged AF9 (Li et al., 2014) were harvested and resuspended in hypotonic lysis buffer (3.75 mM Tris at pH 7.5, 20 mM KCl, 0.5 mM EDTA, 0.5 mM DTT, 0.05 mM spermidine, 0.125 mM spermine, 1 mM PMSF, and 0.1% digitonin). All buffers contained 20 mM nicotinamine, 10 mM sodium butyrate, cOmplete,

EDTA-free protease inhibitor and phosSTOP phosphatase inhibitor cocktails (Roche). Cells were homogenized to release the nuclei and then pelleted at 300 g. The pellets containing the nuclei were resuspended in Wash Buffer A (20 mM HEPES at pH 7.5, 20 mM KCl, 0.5 mM EDTA, 0.5 mM DTT and 1 mM PMSF , pelleted and resuspended in Wash Buffer B (Wash Buffer A supplemented with 300 mM NaCl). Nuclei were resuspended in Wash Buffer B supplemented with 3 mM CaCl<sub>2</sub>. Chromatin was digested for 5 minutes at 37°C using 2000 units of MNase (Worthington). The MNase digestion was stopped by adding 5 mM EGTA and 0.05% TritonX and pelleted at 10,000 g for 15 min at 4°C. The supernatant contained predominantly mono-nucleosomes as confirmed by agarose gel electrophoresis was used for FLAG IP. FLAG M2 agarose (Sigma) was used to bind the mononucleosome containing nuclear extract overnight at 4°C. Beads were washed 3 times using Wash Buffer B and boiled in SDS loading buffer for western blot analysis. The following antibodies were used for analysis of the IP: anti- H3K9cr and H3K18cr (PTM Biolabs PTM-516 and PTM-517), anti-ELL2 (Bethyl A302-505A), anti-AFF4 (ab103586), anti-FLAG (Sigma A8592).

### **Generation of Pre-modified Histones by Amber Suppression**

[The methods described here were carried out by Dr. Tanya Panchenko]

All histones not containing site specifically modified lysines were expressed and purified as previously described by A. J. Ruthenburg (Ruthenburg et al., 2011). For site specific incorporation of crotonylated lysine, amber suppression system developed by Peter Schultz's lab was used (Kim et al., 2012). Briefly, an orthogonal *Methanosarcina barkeri* tRNA/pyrrolyl-tRNA synthetase (Mb-PylRS) pair was used where Mb-PylRS was mutated to accept crotonylated

lysine (Kim et al., 2012). The crotonylated lysine was synthesized as described by Gattner M. J. (Gattner et al., 2013) as was used to supplement bacterial culture at 5 mM in the presence of 20mM nicotnamide expressing H3 from a plasmid containing an amber stop codon “TAG” at either lysine 9 or lysine 18. Similarly, an amber suppression system developed by the Chason Chin lab was used in order to generate site specifically acetylated histones. Here an Mb-PyIRS was mutated to accept acetylated lysine (Neumann et al., 2009). N-e-Acetylated lysine was purchased from Sigma and was used to supplement bacterial culture at 5 mM in the presence of 20 mM nicotnamide expressing H3 from a plasmid containing an amber stop codon “TAG” at either lysine 9 or lysine 18.

### **Nucleosome Assembly**

Octamers were reconstituted as described (Ruthenburg et al., 2011). The 601 nucleosome positioning sequence was used for nucleosome reconstitution (Lowary and Widom, 1998). The DNA was amplified by PCR using primers containing a biotin tag on the 5' end to produce 189 bp linear DNA and purified using QIAEXII kit (Qiagen). Nucleosomes were assembled using the standard step-wise dialysis method (Dyer et al., 2004).

### **Generation of AF9 Transgenic and Mutant Cell Lines**

[The methods described here were carried out by Dr. Tanya Panchenko]

For overexpression and rescue studies, PCDH plasmids containing 3xFLAG tagged AF9 or AF9 F59A were used (Li et al., 2014). All lentivirus construct plasmids were packaged into virus using HEK293-T cells as packaging cell lines together with helper plasmids VSV-G (envelope) and psPAX2 (packaging, gag-

pol) following standard protocols. Primary cells were spin infected with concentrated virus-containing media supplemented with 8 µg/mL Polybrene for 1.5 hours at 2500 rpm at 37°C and then selected with 5 µg /ml blasticidin. For knockout of AF9 in RAW264.7 mouse macrophage cells, several CRISPR guides were designed using the CRISPR design tool (<http://crispr.mit.edu/>) and cloned into the pSpCas9(BB)-2A-GFP (PX458) plasmid (Ran et al., 2013). Plasmids were transfected into RAW264.7 cells using LipofectamineLTX (ThermoFisher) and FACS sorted 24 hours after transfection. Single clones were selected and tested for AF9 expression using anti-AF9 specific antibody (Bethyl A300-595A) and genotyped for the deletion (Figure S7D). The guide RNA sequence used in this study targeted the 3<sup>rd</sup> exon of AF9 which corresponds to the YEATS domain. The guide RNA sequence is GTAGAAGAGTCCGGGTACGC. The sequencing primers to test the AF9 deletion were: TGAGCTACACTCCACTCAGA (forward) and TTCAGAATGGCAATCACTCTTCA (reverse).

## CHAPTER 9: REFERENCES

Agalioti, T., Lomvardas, S., Parekh, B., Yie, J., Maniatis, T., and Thanos, D. (2000). Ordered recruitment of chromatin modifying and general transcription factors to the IFN-beta promoter. *Cell* 103, 667–678.

Allfrey, V.G., Faulkner, R., and Mirsky, A.E. (1964). Acetylation and methylation of histones and their possible role in the regulation of RNA synthesis. *Proceedings of the National Academy of Sciences* 51, 786–794.

An, W., Kim, J., and Roeder, R.G. (2004). Ordered cooperative functions of PRMT1, p300, and CARM1 in transcriptional activation by p53. *Cell* 117, 735–748.

An, W., Palhan, V.B., Karymov, M.A., Leuba, S.H., and Roeder, R.G. (2002). Selective requirements for histone H3 and H4 N termini in p300-dependent transcriptional activation from chromatin. *Molecular Cell* 9, 811–821.

Annunziato, A.T., Frado, L.L., Seale, R.L., and Woodcock, C.L. (1988). Treatment with sodium butyrate inhibits the complete condensation of interphase chromatin. *Chromosoma* 96, 132–138.

Arany, Z., Sellers, W.R., Livingston, D.M., and Eckner, R. (1994). E1A-associated p300 and CREB-associated CBP belong to a conserved family of coactivators. *Cell* 77, 799–800.

Arpaia, N., Campbell, C., Fan, X., Dikiy, S., van der Veecken, J., Deroos, P., Liu, H., Cross, J.R., Pfeiffer, K., Coffey, P.J., et al. (2013). Metabolites produced by commensal bacteria promote peripheral regulatory T-cell generation. *Nature* 504, 451–455.

Bannister, A.J., and Kouzarides, T. (1996). The CBP co-activator is a histone acetyltransferase. *Nature* 384, 641–643.

Bao, X., Wang, Y., Li, X., Li, X.-M., Liu, Z., Yang, T., Wong, C.F., Zhang, J., Hao, Q., and Li, X.D. (2014). Identification of “erasers” for lysine crotonylated histone marks using a chemical proteomics approach. *Elife* 3.

Barber, M.F., Michishita-Kioi, E., Xi, Y., Tasselli, L., Kioi, M., Moqtaderi, Z., Tennen, R.I., Paredes, S., Young, N.L., Chen, K., et al. (2012). SIRT7 links H3K18 deacetylation to maintenance of oncogenic transformation. *Nature* 487, 114–118.

Basu, S.S., and Blair, I.A. (2011). SILEC: a protocol for generating and using isotopically labeled coenzyme A mass spectrometry standards. *Nat Protoc* 7, 1–12.

Besten, den, G., van Eunen, K., Groen, A.K., Venema, K., Reijngoud, D.J., and Bakker, B.M. (2013). The role of short-chain fatty acids in the interplay between diet, gut microbiota, and host energy metabolism. *The Journal of Lipid Research* 54, 2325–2340.

Bhatt, D.M., Pandya-Jones, A., Tong, A.-J., Barozzi, I., Lissner, M.M., Natoli, G., Black, D.L., and Smale, S.T. (2012). Transcript Dynamics of Proinflammatory Genes Revealed by Sequence Analysis of Subcellular RNA Fractions. *Cell* 150, 279–290.

Biswas, D., Milne, T.A., Basrur, V., Kim, J., Elenitoba-Johnson, K.S.J., Allis, C.D., and Roeder, R.G. (2011). Function of leukemogenic mixed lineage leukemia 1 (MLL) fusion proteins through distinct partner protein complexes. *Proceedings of the National Academy of Sciences* 108, 15751–15756.

Boffa, L.C., Vidali, G., Mann, R.S., and Allfrey, V.G. (1978). Suppression of histone deacetylation in vivo and in vitro by sodium butyrate. *J. Biol. Chem.* 253, 3364–3366.

Braunstein, M., Rose, A.B., Holmes, S.G., Allis, C.D., and Broach, J.R. (1993). Transcriptional silencing in yeast is associated with reduced nucleosome acetylation. *Genes & Development* 7, 592–604.

Brown, A.J., Goldsworthy, S.M., Barnes, A.A., Eilert, M.M., Tcheang, L., Daniels, D., Muir, A.I., Wigglesworth, M.J., Kinghorn, I., Fraser, N.J., et al. (2003). The Orphan G Protein-coupled Receptors GPR41 and GPR43 Are Activated by Propionate and Other Short Chain Carboxylic Acids. *Journal of Biological Chemistry* 278, 11312–11319.

Brownell, J.E., and Allis, C.D. (1995). An activity gel assay detects a single, catalytically active histone acetyltransferase subunit in *Tetrahymena* macronuclei. *Proc. Natl. Acad. Sci. U.S.A.* 92, 6364–6368.

Brownell, J.E., Zhou, J., Ranalli, T., Kobayashi, R., Edmondson, D.G., Roth, S.Y., and Allis, C.D. (1996). *Tetrahymena* histone acetyltransferase A: a homolog to yeast Gcn5p linking histone acetylation to gene activation. *Cell* 84, 843–851.

Cai, L., Sutter, B.M., Li, B., and Tu, B.P. (2011). Acetyl-CoA Induces Cell Growth and Proliferation by Promoting the Acetylation of Histones at Growth Genes. *Molecular Cell* 42, 426–437.

Cai, S.F., Chen, C.-W., and Armstrong, S.A. (2015). Drugging Chromatin in Cancer: Recent Advances and Novel Approaches. *Molecular Cell* 60, 561–570.

Candido, E.P., Reeves, R., and Davie, J.R. (1978). Sodium butyrate inhibits histone deacetylation in cultured cells. *Cell* 14, 105–113.

Cao, R., Wang, L., Wang, H., Xia, L., Erdjument-Bromage, H., Tempst, P., Jones, R.S., and Zhang, Y. (2002). Role of histone H3 lysine 27 methylation in Polycomb-group silencing. *Science* 298, 1039–1043.

Carey, B.W., Finley, L.W.S., Cross, J.R., Allis, C.D., and Thompson, C.B. (2014). Intracellular  $\alpha$ -ketoglutarate maintains the pluripotency of embryonic stem cells. *Nature* 518, 413–416.

Carvalho, P.C., Hewel, J., Barbosa, V.C., and Yates, J.R. (2008). Identifying differences in protein expression levels by spectral counting and feature selection. *Genet. Mol. Res.* 7, 342–356.

Chakravarti, D., LaMorte, V.J., Nelson, M.C., Nakajima, T., Schulman, I.G., Juguilon, H., Montminy, M., and Evans, R.M. (1996). Role of CBP/P300 in nuclear receptor signalling. *Nature* 383, 99–103.

Chen, Y., Sprung, R., Tang, Y., Ball, H., Sangras, B., Kim, S.C., Falck, J.R., Peng, J., Gu, W., and Zhao, Y. (2007). Lysine propionylation and butyrylation are novel post-translational modifications in histones. *Mol. Cell Proteomics* 6, 812–819.

Choudhary, C., Kumar, C., Gnad, F., Nielsen, M.L., Rehman, M., Walther, T.C., Olsen, J.V., and Mann, M. (2009). Lysine Acetylation Targets Protein Complexes and Co-Regulates Major Cellular Functions. *Science* 325, 834–840.

Choudhary, C., Weinert, B.T., Nishida, Y., Verdin, E., and Mann, M. (2014). The growing landscape of lysine acetylation links metabolism and cell signalling. *Nat Rev Mol Cell Biol* 15, 536–550.

Chrivia, J.C., Kwok, R.P., Lamb, N., Hagiwara, M., Montminy, M.R., and Goodman, R.H. (1993). Phosphorylated CREB binds specifically to the nuclear protein CBP. *Nature* 365, 855–859.

Comerford, S.A., Huang, Z., Du, X., Wang, Y., Cai, L., Witkiewicz, A.K., Walters, H., Tantawy, M.N., Fu, A., Manning, H.C., et al. (2014). Acetate Dependence of Tumors. *Cell* 159, 1591–1602.

Cox, J., Hein, M.Y., Lubner, C.A., Paron, I., Nagaraj, N., and Mann, M. (2014). Accurate proteome-wide label-free quantification by delayed normalization and maximal peptide ratio extraction, termed MaxLFQ. *Molecular & Cellular Proteomics* 13, 2513–2526.

Creyghton, M.P., Cheng, A.W., Welstead, G.G., Kooistra, T., Carey, B.W., Steine, E.J., Hanna, J., Lodato, M.A., Frampton, G.M., Sharp, P.A., et al. (2010). Histone H3K27ac separates active from poised enhancers and predicts developmental state. *Proceedings of the National Academy of Sciences* 107, 21931–21936.

Cummings, J.H., Pomare, E.W., Branch, W.J., Naylor, C.P., and Macfarlane, G.T. (1987). Short chain fatty acids in human large intestine, portal, hepatic and venous blood. *Gut* 28, 1221–1227.

Dai, L., Peng, C., Montellier, E., Lu, Z., Chen, Y., Ishii, H., Debernardi, A., Buchou, T., Rousseaux, S., Jin, F., et al. (2014). Lysine 2-hydroxyisobutyrylation is a widely distributed active histone mark. *Nature Chemical Biology* 10, 365–370.

Dawson, M.A., and Kouzarides, T. (2012). Cancer Epigenetics: From Mechanism to Therapy. *Cell* 150, 12–27.

Delmore, J.E., Issa, G.C., Lemieux, M.E., Rahl, P.B., Shi, J., Jacobs, H.M., Kastiris, E., Gilpatrick, T., Paranal, R.M., Qi, J., et al. (2011). BET Bromodomain Inhibition as a Therapeutic Strategy to Target c-Myc. *Cell* 146, 904–917.

Dhalluin, C., Carlson, J.E., Zeng, L., He, C., Aggarwal, A.K., and Zhou, M.M. (1999). Structure and ligand of a histone acetyltransferase bromodomain. *Nature* 399, 491–496.

Doenecke, D., and Karlson, P. (1984). 100 years ago Albrecht Kossel and the discovery. *Trends in Biochemical Sciences* 9, 404–405.

Donohoe, D.R., Holley, D., Collins, L.B., Montgomery, S.A., Whitmore, A.C., Hillhouse, A., Curry, K.P., Renner, S.W., Greenwalt, A., Ryan, E.P., et al. (2014). A Gnotobiotic Mouse Model Demonstrates That Dietary Fiber Protects against Colorectal Tumorigenesis in a Microbiota- and Butyrate-Dependent Manner. *Cancer Discovery* 4, 1387–1397.

Donohoe, D.R., and Bultman, S.J. (2012). Metaboloepigenetics: interrelationships between energy metabolism and epigenetic control of gene expression. *J. Cell. Physiol.* 227, 3169–3177.

Doyon, Y., Selleck, W., Lane, W.S., Tan, S., and Cote, J. (2004). Structural and Functional Conservation of the NuA4 Histone Acetyltransferase Complex from Yeast to Humans. *Molecular and Cellular Biology* 24, 1884–1896.

Du, J., Zhou, Y., Su, X., Yu, J.J., Khan, S., Jiang, H., Kim, J., Woo, J., Kim, J.H., Choi, B.H., et al. (2011). Sirt5 Is a NAD-Dependent Protein Lysine Demalonylase and Desuccinylase. *Science* 334, 806–809.

Dyer, P.N., Edayathumangalam, R.S., White, C.L., Bao, Y., Chakravarthy, S., Muthurajan, U.M., and Luger, K. (2004). Reconstitution of nucleosome core particles from recombinant histones and DNA. *Meth. Enzymol.* 375, 23–44.

Eckner, R., Ewen, M.E., Newsome, D., Gerdes, M., DeCaprio, J.A., Lawrence, J.B., and Livingston, D.M. (1994). Molecular cloning and functional analysis of the adenovirus E1A-associated 300-kD protein (p300) reveals a protein with properties of a transcriptional adaptor. *Genes & Development* 8, 869–884.

Ernst, J., Kheradpour, P., Mikkelsen, T.S., Shoresh, N., Ward, L.D., Epstein, C.B., Zhang, X., Wang, L., Issner, R., Coyne, M., et al. (2011). Mapping and analysis of chromatin state dynamics in nine human cell types. *Nature* 473, 43–49.

Evertts, A.G., Zee, B.M., DiMaggio, P.A., Gonzales-Cope, M., Coller, H.A., and Garcia, B.A. (2013). Quantitative Dynamics of the Link between Cellular Metabolism and Histone Acetylation. *Journal of Biological Chemistry* 288, 12142–12151.

- Falkenberg, K.J., and Johnstone, R.W. (2014). Histone deacetylases and their inhibitors in cancer, neurological diseases and immune disorders. *Nat Rev Drug Discov* 13, 673–691.
- Fan, J., Krautkramer, K.A., Feldman, J.L., and Denu, J.M. (2015). Metabolic Regulation of Histone Post-Translational Modifications. *ACS Chem. Biol.* 10, 95–108.
- Fang, J., Wang, H., and Zhang, Y. (2003). Purification of histone methyltransferases from HeLa cells. *Meth. Enzymol.* 377, 213–226.
- Feldman, J.L., Baeza, J., and Denu, J.M. (2013). Activation of the protein deacetylase SIRT6 by long-chain fatty acids and widespread deacylation by mammalian sirtuins. *Journal of Biological Chemistry* 288, 31350–31356.
- Felsenfeld, G., and Groudine, M. (2003). Controlling the double helix. *Nature* 421, 448–453.
- Filippakopoulos, P., and Knapp, S. (2014). Targeting bromodomains: epigenetic readers of lysine acetylation. *Nat Rev Drug Discov* 13, 337–356.
- Filippakopoulos, P., Picaud, S., Mangos, M., Keates, T., Lambert, J.-P., Barsyte-Lovejoy, D., Felletar, I., Volkmer, R., Müller, S., Pawson, T., et al. (2012). Histone Recognition and Large-Scale Structural Analysis of the Human Bromodomain Family. *Cell* 149, 214–231.
- Filippakopoulos, P., Qi, J., Picaud, S., Shen, Y., Smith, W.B., Fedorov, O., Morse, E.M., Keates, T., Hickman, T.T., Felletar, I., et al. (2011). Selective inhibition of BET bromodomains. *Nature* 468, 1067–1073.
- Fischer, U., Heckel, D., Michel, A., Janka, M., Hulsebos, T., and Meese, E. (1997). Cloning of a novel transcription factor-like gene amplified in human glioma including astrocytoma grade I. *Hum. Mol. Genet.* 6, 1817–1822.
- Fischer, U., Meltzer, P., and Meese, E. (1996). Twelve amplified and expressed genes localized in a single domain in glioma. *Human Genetics* 98, 625–628.
- Flynn, E.M., Huang, O.W., Poy, F., Oppikofer, M., Bellon, S.F., Tang, Y., and Cochran, A.G. (2015). A Subset of Human Bromodomains Recognizes Butyryllysine and Crotonyllysine Histone Peptide Modifications. *Structure* 23, 1801–1814.
- Frenkel, E.P., and Kitchens, R.L. (1977). Purification and properties of acetyl coenzyme A synthetase from bakers' yeast. *J. Biol. Chem.* 252, 504–507.
- Gattner, M.J., Vrabel, M., and Carell, T. (2013). Synthesis of  $\epsilon$ -N-propionyl-,  $\epsilon$ -N-butyryl-, and  $\epsilon$ -N-crotonyl-lysine containing histone H3 using the pyrrolysine system. *Chem. Commun. (Camb.)* 49, 379–381.

Gayther, S.A., Batley, S.J., Linger, L., Bannister, A., Thorpe, K., Chin, S.F., Daigo, Y., Russell, P., Wilson, A., Sowter, H.M., et al. (2000). Mutations truncating the EP300 acetylase in human cancers. *Nat Genet* 24, 300–303.

Ghisletti, S., Barozzi, I., Mietton, F., Polletti, S., De Santa, F., Venturini, E., Gregory, L., Lonie, L., Chew, A., Wei, C.-L., et al. (2010). Identification and Characterization of Enhancers Controlling the Inflammatory Gene Expression Program in Macrophages. *Immunity* 32, 317–328.

Gil, R., Barth, S., Kanfi, Y., and Cohen, H.Y. (2013). SIRT6 exhibits nucleosome-dependent deacetylase activity. *Nucleic Acids Research* 41, 8537–8545.

Grant, P.A., Duggan, L., Cote, J., Roberts, S.M., Brownell, J.E., Candau, R., Ohba, R., Owen-Hughes, T., Allis, C.D., Winston, F., et al. (1997). Yeast Gcn5 functions in two multisubunit complexes to acetylate nucleosomal histones: characterization of an Ada complex and the SAGA (Spt/Ada) complex. *Genes & Development* 11, 1640–1650.

Gu, W., and Roeder, R.G. (1997). Activation of p53 sequence-specific DNA binding by acetylation of the p53 C-terminal domain. *Cell* 90, 595–606.

Guarente, L. (2007). Sirtuins in aging and disease. *Cold Spring Harbor Symposia on Quantitative Biology* 72, 483–488.

Guarente, L. (2012). Sirtuins, Aging, and Metabolism. *Cold Spring Harbor Symposia on Quantitative Biology* 76, 81–90.

Guermah, M., Palhan, V.B., Tackett, A.J., Chait, B.T., and Roeder, R.G. (2006). Synergistic Functions of SII and p300 in Productive Activator-Dependent Transcription of Chromatin Templates. *Cell* 125, 275–286.

Gut, P., and Verdin, E. (2013). The nexus of chromatin regulation and intermediary metabolism. *Nature* 502, 489–498.

Haynes, S.R., Dollard, C., Winston, F., Beck, S., Trowsdale, J., and Dawid, I.B. (1992). The bromodomain: a conserved sequence found in human, Drosophila and yeast proteins. *Nucleic Acids Research* 20, 2603.

He, N., Chan, C.K., Sobhian, B., Chou, S., Xue, Y., Liu, M., Alber, T., Benkirane, M., and Zhou, Q. (2011). Human Polymerase-Associated Factor complex (PAFc) connects the Super Elongation Complex (SEC) to RNA polymerase II on chromatin. *Proceedings of the National Academy of Sciences* 108, E636–E645.

He, N., Liu, M., Hsu, J., Xue, Y., Chou, S., Burlingame, A., Krogan, N.J., Alber, T., and Zhou, Q. (2010). HIV-1 Tat and Host AFF4 Recruit Two Transcription Elongation Factors into a Bifunctional Complex for Coordinated Activation of HIV-1 Transcription. *Molecular Cell* 38, 428–438.

Hebbes, T.R., Clayton, A.L., Thorne, A.W., and Crane-Robinson, C. (1994). Core histone hyperacetylation co-maps with generalized DNase I sensitivity in the chicken beta-globin chromosomal domain. *Embo J.* *13*, 1823–1830.

Hebbes, T.R., Thorne, A.W., and Crane-Robinson, C. (1988). A direct link between core histone acetylation and transcriptionally active chromatin. *Embo J.* *7*, 1395–1402.

Heintzman, N.D., Hon, G.C., Hawkins, R.D., Kheradpour, P., Stark, A., Harp, L.F., Ye, Z., Lee, L.K., Stuart, R.K., Ching, C.W., et al. (2009). Histone modifications at human enhancers reflect global cell-type-specific gene expression. *Nature* *459*, 108–112.

Hilton, I.B., D'Ippolito, A.M., Vockley, C.M., Thakore, P.I., Crawford, G.E., Reddy, T.E., and Gersbach, C.A. (2015). Epigenome editing by a CRISPR-Cas9-based acetyltransferase activates genes from promoters and enhancers. *Nature Biotechnology* *33*, 510–517.

Horwitz, G.A., Zhang, K., McBrian, M.A., Grunstein, M., Kurdistani, S.K., and Berk, A.J. (2008). Adenovirus Small e1a Alters Global Patterns of Histone Modification. *Science* *321*, 1084–1085.

Hsu, W.W., Wu, B., and Liu, W.R. (2016). Sirtuins 1 and 2 Are Universal Histone Deacetylases. *ACS Chem. Biol.*

Huang, H., Lin, S., Garcia, B.A., and Zhao, Y. (2015). Quantitative Proteomic Analysis of Histone Modifications. *Chem. Rev.* *115*, 2376–2418.

Huang, H., Sabari, B.R., Garcia, B.A., Allis, C.D., and Zhao, Y. (2014). SnapShot: Histone Modifications. *Cell* *159*, 458–458.e1.

Huang, R.C., and Bonner, J. (1962). Histone, a suppressor of chromosomal RNA synthesis. *Proc. Natl. Acad. Sci. U.S.A.* *48*, 1216–1222.

Hufeldt, M.R., Nielsen, D.S., Vogensen, F.K., Midtvedt, T., and Hansen, A.K. (2010). Variation in the gut microbiota of laboratory mice is related to both genetic and environmental factors. *Comp. Med.* *60*, 336–347.

Imai, S., Armstrong, C.M., Kaeberlein, M., and Guarente, L. (2000). Transcriptional silencing and longevity protein Sir2 is an NAD-dependent histone deacetylase. *Nature* *403*, 795–800.

Janeway, C.A., and Medzhitov, R. (2002). Innate immune recognition. *Annu. Rev. Immunol.* *20*, 197–216.

Jeanmougin, F., Wurtz, J.M., Le Douarin, B., Chambon, P., and Losson, R. (1997). The bromodomain revisited. *Trends in Biochemical Sciences* *22*, 151–153.

Jenuwein, T., and Allis, C.D. (2001). Translating the histone code. *Science* *293*, 1074–1080.

Jeppesen, P., and Turner, B.M. (1993). The inactive X chromosome in female mammals is distinguished by a lack of histone H4 acetylation, a cytogenetic marker for gene expression. *Cell* 74, 281–289.

Jiang, H., Khan, S., Wang, Y., Charron, G., He, B., Sebastian, C., Du, J., Kim, R., Ge, E., Mostoslavsky, R., et al. (2013). SIRT6 regulates TNF- $\alpha$  secretion through hydrolysis of long-chain fatty acyl lysine. *Nature* 496, 110–113.

Johnson, L.M., Kayne, P.S., Kahn, E.S., and Grunstein, M. (1990). Genetic evidence for an interaction between SIR3 and histone H4 in the repression of the silent mating loci in *Saccharomyces cerevisiae*. *Proc. Natl. Acad. Sci. U.S.A.* 87, 6286–6290.

Kaelin, W.G., Jr., and McKnight, S.L. (2013). Influence of Metabolism on Epigenetics and Disease. *Cell* 153, 56–69.

Kamei, Y., Xu, L., Heinzl, T., Torchia, J., Kurokawa, R., Gloss, B., Lin, S.C., Heyman, R.A., Rose, D.W., Glass, C.K., et al. (1996). A CBP integrator complex mediates transcriptional activation and AP-1 inhibition by nuclear receptors. *Cell* 85, 403–414.

Karanam, B., Jiang, L., Wang, L., Kelleher, N.L., and Cole, P.A. (2006). Kinetic and mass spectrometric analysis of p300 histone acetyltransferase domain autoacetylation. *J. Biol. Chem.* 281, 40292–40301.

Katada, S., Imhof, A., and Sassone-Corsi, P. (2012). Connecting Threads: Epigenetics and Metabolism. *Cell* 148, 24–28.

Kharchenko, P.V., Alekseyenko, A.A., Schwartz, Y.B., Minoda, A., Riddle, N.C., Ernst, J., Sabo, P.J., Larschan, E., Gorchakov, A.A., Gu, T., et al. (2011). Comprehensive analysis of the chromatin landscape in *Drosophila melanogaster*. *Nature* 471, 480–485.

Kim, C.H., Kang, M., Kim, H.J., Chatterjee, A., and Schultz, P.G. (2012). Site-Specific Incorporation of  $\epsilon$ -N-Crotonyllysine into Histones. *Angew. Chem. Int. Ed.* 51, 7246–7249.

Kim, S.C., Sprung, R., Chen, Y., Xu, Y., Ball, H., Pei, J., Cheng, T., Kho, Y., Xiao, H., Xiao, L., et al. (2006). Substrate and Functional Diversity of Lysine Acetylation Revealed by a Proteomics Survey. *Molecular Cell* 23, 607–618.

King, M.T., and Reiss, P.D. (1985). Separation and measurement of short-chain coenzyme-A compounds in rat liver by reversed-phase high-performance liquid chromatography. *Analytical Biochemistry* 146, 173–179.

Kornberg, R.D. (1977). Structure of chromatin. *Annu. Rev. Biochem.* 46, 931–954.

Kossel, A. (1884). Über einen peptonartigen bestandteil des zellkerns. *Z. Physiol. Chem* 8, 511–515.

- Krivtsov, A.V., and Armstrong, S.A. (2007). MLL translocations, histone modifications and leukaemia stem-cell development. *Nat Rev Cancer* 7, 823–833.
- Kundu, T.K., Palhan, V.B., Wang, Z., An, W., Cole, P.A., and Roeder, R.G. (2000). Activator-dependent transcription from chromatin in vitro involving targeted histone acetylation by p300. *Molecular Cell* 6, 551–561.
- Kurdistani, S.K., Tavazoie, S., and Grunstein, M. (2004). Mapping global histone acetylation patterns to gene expression. *Cell* 117, 721–733.
- Lai, F., Gardini, A., Zhang, A., and Shiekhattar, R. (2015). Integrator mediates the biogenesis of enhancer RNAs. *Nature* 525, 399–403.
- Le Gallo, M., O'Hara, A.J., Rudd, M.L., Urick, M.E., Hansen, N.F., O'Neil, N.J., Price, J.C., Zhang, S., England, B.M., Godwin, A.K., et al. (2012). Exome sequencing of serous endometrial tumors identifies recurrent somatic mutations in chromatin-remodeling and ubiquitin ligase complex genes. *Nat Genet* 44, 1310–1315.
- Le Masson, I., Yu, D.Y., Jensen, K., Chevalier, A., Courbeyrette, R., Boulard, Y., Smith, M.M., and Mann, C. (2003). Yaf9, a Novel NuA4 Histone Acetyltransferase Subunit, Is Required for the Cellular Response to Spindle Stress in Yeast. *Molecular and Cellular Biology* 23, 6086–6102.
- Leder, A., and Leder, P. (1975). Butyric acid, a potent inducer of erythroid differentiation in cultured erythroleukemic cells. *Cell* 5, 319–322.
- Lee, D.Y., Hayes, J.J., Pruss, D., and Wolffe, A.P. (1993). A positive role for histone acetylation in transcription factor access to nucleosomal DNA. *Cell* 72, 73–84.
- Lee, J.V., Carrer, A., Shah, S., Snyder, N.W., Wei, S., Venneti, S., Worth, A.J., Yuan, Z.-F., Lim, H.-W., Liu, S., et al. (2014). Akt-dependent metabolic reprogramming regulates tumor cell histone acetylation. *Cell Metabolism* 20, 306–319.
- Lee, K.K., and Workman, J.L. (2007). Histone acetyltransferase complexes: one size doesn't fit all. *Nat Rev Mol Cell Biol* 8, 284–295.
- Lee, W.-J., and Hase, K. (2014). Gut microbiota-generated metabolites in animal health and disease. *Nature Chemical Biology* 10, 416–424.
- Lee, Y.-H., Coonrod, S.A., Kraus, W.L., Jelinek, M.A., and Stallcup, M.R. (2005). Regulation of coactivator complex assembly and function by protein arginine methylation and demethylation. *Proc. Natl. Acad. Sci. U.S.A.* 102, 3611–3616.
- Li, H., Handsaker, B., Wysoker, A., Fennell, T., Ruan, J., Homer, N., Marth, G., Abecasis, G., Durbin, R., 1000 Genome Project Data Processing Subgroup (2009a). The Sequence Alignment/Map format and SAMtools. *Bioinformatics* 25, 2078–2079.

Li, Y., Trojer, P., Xu, C.-F., Cheung, P., Kuo, A., Drury, W.J., Qiao, Q., Neubert, T.A., Xu, R.-M., Gozani, O., et al. (2009b). The target of the NSD family of histone lysine methyltransferases depends on the nature of the substrate. *Journal of Biological Chemistry* 284, 34283–34295.

Li, Y., Wen, H., Xi, Y., Tanaka, K., Wang, H., Peng, D., Ren, Y., Jin, Q., Dent, S.Y.R., Li, W., et al. (2014). AF9 YEATS Domain Links Histone Acetylation to DOT1L-Mediated H3K79 Methylation. *Cell* 159, 558–571.

Lin, C., Smith, E.R., Takahashi, H., Lai, K.C., Martin-Brown, S., Florens, L., Washburn, M.P., Conaway, J.W., Conaway, R.C., and Shilatifard, A. (2010). AFF4, a Component of the ELL/P-TEFb Elongation Complex and a Shared Subunit of MLL Chimeras, Can Link Transcription Elongation to Leukemia. *Molecular Cell* 37, 429–437.

Lin, H., Su, X., and He, B. (2012). Protein Lysine Acylation and Cysteine Succination by Intermediates of Energy Metabolism. *ACS Chem. Biol.* 7, 947–960.

Lin, R., Leone, J.W., Cook, R.G., and Allis, C.D. (1989). Antibodies specific to acetylated histones document the existence of deposition- and transcription-related histone acetylation in *Tetrahymena*. *The Journal of Cell Biology* 108, 1577–1588.

Liu, X., Wang, L., Zhao, K., Thompson, P.R., Hwang, Y., Marmorstein, R., and Cole, P.A. (2008). The structural basis of protein acetylation by the p300/CBP transcriptional coactivator. *Nature* 451, 846–850.

Lovén, J., Hoke, H.A., Lin, C.Y., Lau, A., Orlando, D.A., Vakoc, C.R., Bradner, J.E., Lee, T.I., and Young, R.A. (2013). Selective Inhibition of Tumor Oncogenes by Disruption of Super-Enhancers. *Cell* 153, 320–334.

Lu, C., and Thompson, C.B. (2012). Metabolic Regulation of Epigenetics. *Cell Metabolism* 16, 9–17.

Luger, K., Mäder, A.W., Richmond, R.K., Sargent, D.F., and Richmond, T.J. (1997). Crystal structure of the nucleosome core particle at 2.8 Å resolution. *Nature* 389, 251–260.

Mansour, M.R., Abraham, B.J., Anders, L., Berezovskaya, A., Gutierrez, A., Durbin, A.D., Etchin, J., Lawton, L., Sallan, S.E., Silverman, L.B., et al. (2014). Oncogene regulation. An oncogenic super-enhancer formed through somatic mutation of a noncoding intergenic element. *Science* 346, 1373–1377.

Mashimo, T., Pichumani, K., Vemireddy, V., Hatanpaa, K.J., Singh, D.K., Sirasanagandla, S., Nannepaga, S., Piccirillo, S.G., Kovacs, Z., Foong, C., et al. (2014). Acetate Is a Bioenergetic Substrate for Human Glioblastoma and Brain Metastases. *Cell* 159, 1603–1614.

Medzhitov, R., and Horng, T. (2009). Transcriptional control of the inflammatory response. *Nat Rev Immunol* 9, 692–703.

- Megee, P.C., Morgan, B.A., Mittman, B.A., and Smith, M.M. (1990). Genetic analysis of histone H4: essential role of lysines subject to reversible acetylation. *Science* 247, 841–845.
- Meier, J.L. (2013). Metabolic Mechanisms of Epigenetic Regulation. *ACS Chem. Biol.* 8, 2607–2621.
- Merika, M., Williams, A.J., Chen, G., Collins, T., and Thanos, D. (1998). Recruitment of CBP/p300 by the IFN beta enhanceosome is required for synergistic activation of transcription. *Molecular Cell* 1, 277–287.
- Michishita, E., Park, J.Y., Burneskis, J.M., Barrett, J.C., and Horikawa, I. (2005). Evolutionarily conserved and nonconserved cellular localizations and functions of human SIRT proteins. *Mol. Biol. Cell* 16, 4623–4635.
- Mizzen, C.A., Brownell, J.E., Cook, R.G., and Allis, C.D. (1999). Histone acetyltransferases: preparation of substrates and assay procedures. *Meth. Enzymol.* 304, 675–696.
- Montellier, E., Boussouar, F., Rousseaux, S., Zhang, K., Buchou, T., Fenaille, F., Shiota, H., Debernardi, A., Hery, P., Curtet, S., et al. (2013). Chromatin-to-nucleoprotamine transition is controlled by the histone H2B variant TH2B. *Genes & Development* 27, 1680–1692.
- Montellier, E., Rousseaux, S., Zhao, Y., and Khochbin, S. (2011). Histone crotonylation specifically marks the haploid male germ cell gene expression program. *Bioessays* 34, 187–193.
- Murray, K. (1964). The Occurrence of Epsilon-N-Methyl Lysine in Histones. *Biochemistry* 3, 10–15.
- Musselman, C.A., Lalonde, M.-E., Côté, J., and Kutateladze, T.G. (2012). Perceiving the epigenetic landscape through histone readers. *Nat Struct Mol Biol* 19, 1218–1227.
- Neph, S., Kuehn, M.S., Reynolds, A.P., Haugen, E., Thurman, R.E., Johnson, A.K., Rynes, E., Maurano, M.T., Vierstra, J., Thomas, S., et al. (2012). BEDOPS: high-performance genomic feature operations. *Bioinformatics* 28, 1919–1920.
- Ogryzko, V.V., Schiltz, R.L., Russanova, V., Howard, B.H., and Nakatani, Y. (1996). The transcriptional coactivators p300 and CBP are histone acetyltransferases. *Cell* 87, 953–959.
- Park, E.C., and Szostak, J.W. (1990). Point mutations in the yeast histone H4 gene prevent silencing of the silent mating type locus HML. *Molecular and Cellular Biology* 10, 4932–4934.
- Parker, S.C.J., Stitzel, M.L., Taylor, D.L., Orozco, J.M., Erdos, M.R., Akiyama, J.A., van Bueren, K.L., Chines, P.S., Narisu, N., NISC Comparative Sequencing Program, et al. (2013). Chromatin stretch enhancer states drive cell-specific gene

regulation and harbor human disease risk variants. *Proceedings of the National Academy of Sciences* 110, 17921–17926.

Pasqualucci, L., Dominguez-Sola, D., Chiarenza, A., Fabbri, G., Grunn, A., Trifonov, V., Kasper, L.H., Lerach, S., Tang, H., Ma, J., et al. (2011). Inactivating mutations of acetyltransferase genes in B-cell lymphoma. *Nature* 471, 189–195.

Patel, D.J., and Wang, Z. (2013). Readout of Epigenetic Modifications. *Annu. Rev. Biochem.* 82, 81–118.

Pavlova, N.N., and Thompson, C.B. (2016). The Emerging Hallmarks of Cancer Metabolism. *Cell Metabolism* 23, 27–47.

Phillips, D.M. (1963). The presence of acetyl groups of histones. *Biochem. J.* 87, 258–263.

Plass, C., Pfister, S.M., Lindroth, A.M., Bogatyrova, O., Claus, R., and Lichter, P. (2013). Mutations in regulators of the epigenome and their connections to global chromatin patterns in cancer. *Nature Reviews Genetics* 14, 765–780.

Pokholok, D.K., Harbison, C.T., Levine, S., Cole, M., Hannett, N.M., Lee, T.I., Bell, G.W., Walker, K., Rolfe, P.A., Herbolsheimer, E., et al. (2005). Genome-wide Map of Nucleosome Acetylation and Methylation in Yeast. *Cell* 122, 517–527.

Rada-Iglesias, A., Bajpai, R., Swigut, T., Brugmann, S.A., Flynn, R.A., and Wysocka, J. (2011). A unique chromatin signature uncovers early developmental enhancers in humans. *Nature* 470, 279–283.

Ramirez-Carrozzi, V.R., Braas, D., Bhatt, D.M., Cheng, C.S., Hong, C., Doty, K.R., Black, J.C., Hoffmann, A., Carey, M., and Smale, S.T. (2009). A Unifying Model for the Selective Regulation of Inducible Transcription by CpG Islands and Nucleosome Remodeling. *Cell* 138, 114–128.

Rappsilber, J., Ishihama, Y., and Mann, M. (2003). Stop and Go Extraction Tips for Matrix-Assisted Laser Desorption/Ionization, Nanoelectrospray, and LC/MS Sample Pretreatment in Proteomics. *Anal. Chem.* 75, 663–670.

Riggs, M.G., Whittaker, R.G., Neumann, J.R., and Ingram, V.M. (1977). n-Butyrate causes histone modification in HeLa and Friend erythroleukaemia cells. *Nature* 268, 462–464.

Riggs, M.G., Whittaker, R.G., Neumann, J.R., and Ingram, V.M. (1978). Modified Histones in HeLa and Friend Erythroleukemia Cells Treated with n-Butyrate. *Cold Spring Harbor Symposia on Quantitative Biology* 42, 815–818.

Robinson, P.J.J., An, W., Routh, A., Martino, F., Chapman, L., Roeder, R.G., and Rhodes, D. (2008). 30 nm Chromatin Fibre Decompaction Requires both H4-K16 Acetylation and Linker Histone Eviction. *Journal of Molecular Biology* 381, 816–825.

Roediger, W.E. (1980). Role of anaerobic bacteria in the metabolic welfare of the colonic mucosa in man. *Gut* 21, 793–798.

Roelfsema, J.H., White, S.J., Ariyürek, Y., Bartholdi, D., Niedrist, D., Papadia, F., Bacino, C.A., Dunnen, den, J.T., van Ommen, G.-J.B., Breuning, M.H., et al. (2005). Genetic heterogeneity in Rubinstein-Taybi syndrome: mutations in both the CBP and EP300 genes cause disease. *Am. J. Hum. Genet.* 76, 572–580.

Roh, T.-Y., Cuddapah, S., and Zhao, K. (2005). Active chromatin domains are defined by acetylation islands revealed by genome-wide mapping. *Genes & Development* 19, 542–552.

Roth, S.Y., Denu, J.M., and Allis, C.D. (2001). Histone acetyltransferases. *Annu. Rev. Biochem.* 70, 81–120.

Ruthenburg, A.J., Li, H., Milne, T.A., Dewell, S., McGinty, R.K., Yuen, M., Ueberheide, B., Dou, Y., Muir, T.W., Patel, D.J., et al. (2011). Recognition of a Mononucleosomal Histone Modification Pattern by BPTF via Multivalent Interactions. *Cell* 145, 692–706.

Sabari, B.R., Tang, Z., Huang, H., Yong-Gonzalez, V., Molina, H., Kong, H.E., Dai, L., Shimada, M., Cross, J.R., Zhao, Y., et al. (2015). Intracellular Crotonyl-CoA Stimulates Transcription through p300-Catalyzed Histone Crotonylation. *Molecular Cell* 58, 203–215.

Sanchez, R., and Zhou, M.-M. (2009). The role of human bromodomains in chromatin biology and gene transcription. *Curr Opin Drug Discov Devel* 12, 659–665.

Schulze, J.M., Wang, A.Y., and Kobor, M.S. (2009). YEATS domain proteins: a diverse family with many links to chromatin modification and transcription. *Biochem. Cell Biol.* 87, 65–75.

Schübeler, D., MacAlpine, D.M., Scalzo, D., Wirbelauer, C., Kooperberg, C., van Leeuwen, F., Gottschling, D.E., O'Neill, L.P., Turner, B.M., Delrow, J., et al. (2004). The histone modification pattern of active genes revealed through genome-wide chromatin analysis of a higher eukaryote. *Genes & Development* 18, 1263–1271.

Schwanhäusser, B., Busse, D., Li, N., Dittmar, G., Schuchhardt, J., Wolf, J., Chen, W., and Selbach, M. (2011). Global quantification of mammalian gene expression control. *Nature* 473, 337–342.

Seligson, D.B., Horvath, S., McBrien, M.A., Mah, V., Yu, H., Tze, S., Wang, Q., Chia, D., Goodglick, L., and Kurdستاني, S.K. (2009). Global Levels of Histone Modifications Predict Prognosis in Different Cancers. *The American Journal of Pathology* 174, 1619–1628.

- Seligson, D.B., Horvath, S., Shi, T., Yu, H., Tze, S., Grunstein, M., and Kurdistani, S.K. (2005). Global histone modification patterns predict risk of prostate cancer recurrence. *Nature* 435, 1262–1266.
- Shechter, D., Dormann, H.L., Allis, C.D., and Hake, S.B. (2007). Extraction, purification and analysis of histones. *Nat Protoc* 2, 1445–1457.
- Shen, L., Shao, N., Liu, X., and Nestler, E. (2014). ngs.plot: Quick mining and visualization of next-generation sequencing data by integrating genomic databases. *BMC Genomics* 15, 284.
- Shikama, N., Lyon, J., and La Thangue, N.B. (1997). The p300/CBP family: integrating signals with transcription factors and chromatin. *Trends in Cell Biology* 7, 230–236.
- Shimazu, T., Hirschey, M.D., Newman, J., He, W., Shirakawa, K., Le Moan, N., Grueter, C.A., Lim, H., Saunders, L.R., Stevens, R.D., et al. (2013). Suppression of oxidative stress by  $\beta$ -hydroxybutyrate, an endogenous histone deacetylase inhibitor. *Science* 339, 211–214.
- Shogren-Knaak, M., Ishii, H., Sun, J.-M., Pazin, M.J., Davie, J.R., and Peterson, C.L. (2006). Histone H4-K16 acetylation controls chromatin structure and protein interactions. *Science* 311, 844–847.
- Shyh-Chang, N., Locasale, J.W., Lyssiotis, C.A., Zheng, Y., Teo, R.Y., Ratanasirintra-woot, S., Zhang, J., Onder, T., Unternaehrer, J.J., Zhu, H., et al. (2013). Influence of Threonine Metabolism on S-Adenosylmethionine and Histone Methylation. *Science* 339, 222–226.
- Sinclair, D.A., and Guarente, L. (2014). Small-Molecule Allosteric Activators of Sirtuins. *Annu. Rev. Pharmacol. Toxicol.* 54, 363–380.
- Smale, S.T. (2012). Transcriptional regulation in the innate immune system. *Current Opinion in Immunology* 24, 51–57.
- Smale, S.T., Tarakhovskiy, A., and Natoli, G. (2014). Chromatin Contributions to the Regulation of Innate Immunity. *Annu. Rev. Immunol.* 32, 489–511.
- Smith, B.C., and Denu, J.M. (2007). Acetyl-lysine Analog Peptides as Mechanistic Probes of Protein Deacetylases. *Journal of Biological Chemistry* 282, 37256–37265.
- Stedman, E. (1950). Cell specificity of histones. *Nature* 166, 780–781.
- Stedman, E., and Stedman, E. (1951). The basic proteins of cell nuclei. *Philosophical Transactions of the Royal Society of London. Series B, Biological Sciences* 565–595.
- Strahl, B.D., and Allis, C.D. (2000). The language of covalent histone modifications. *Nature* 403, 41–45.

- Su, X., Wellen, K.E., and Rabinowitz, J.D. (2016). Metabolic control of methylation and acetylation. *Current Opinion in Chemical Biology* 30, 52–60.
- Suganuma, T., Gutiérrez, J.L., Li, B., Florens, L., Swanson, S.K., Washburn, M.P., Abmayr, S.M., and Workman, J.L. (2008). ATAC is a double histone acetyltransferase complex that stimulates nucleosome sliding. *Nat Struct Mol Biol* 15, 364–372.
- Sutendra, G., Kinnaird, A., Dromparis, P., Paulin, R., Stenson, T.H., Haromy, A., Hashimoto, K., Zhang, N., Flaim, E., and Michelakis, E.D. (2014). A Nuclear Pyruvate Dehydrogenase Complex Is Important for the Generation of Acetyl-CoA and Histone Acetylation. *Cell* 158, 84–97.
- Suzuki, Y., Horikoshi, N., Kato, D., and Kurumizaka, H. (2015). Crystal structure of the nucleosome containing histone H3 with crotonylated lysine 122. *Biochemical and Biophysical Research Communications*.
- Takahashi, H., McCaffery, J.M., Irizarry, R.A., and Boeke, J.D. (2006). Nucleocytosolic acetyl-coenzyme a synthetase is required for histone acetylation and global transcription. *Molecular Cell* 23, 207–217.
- Takeuchi, O., and Akira, S. (2010). Pattern Recognition Receptors and Inflammation. *Cell* 140, 805–820.
- Tan, J., McKenzie, C., Potamitis, M., Thorburn, A.N., Mackay, C.R., and Macia, L. (2014a). The Role of Short-Chain Fatty Acids in Health and Disease. In *Advances in Immunology*, (Elsevier), pp. 91–119.
- Tan, M., Luo, H., Lee, S., Jin, F., Yang, J.S., Montellier, E., Buchou, T., Cheng, Z., Rousseaux, S., Rajagopal, N., et al. (2011). Identification of 67 Histone Marks and Histone Lysine Cronylation as a New Type of Histone Modification. *Cell* 146, 1016–1028.
- Tan, M., Peng, C., Anderson, K.A., Chhoy, P., Xie, Z., Dai, L., Park, J., Chen, Y., Huang, H., Zhang, Y., et al. (2014b). Lysine Glutarylation Is a Protein Posttranslational Modification Regulated by SIRT5. *Cell Metabolism* 19, 605–617.
- Tang, Z., Chen, W.-Y., Shimada, M., Nguyen, U.T.T., Kim, J., Sun, X.-J., Sengoku, T., McGinty, R.K., Fernandez, J.P., Muir, T.W., et al. (2013). SET1 and p300 Act Synergistically, through Coupled Histone Modifications, in Transcriptional Activation by p53. *Cell* 154, 297–310.
- Taunton, J., Hassig, C.A., and Schreiber, S.L. (1996). A mammalian histone deacetylase related to the yeast transcriptional regulator Rpd3p. *Science* 272, 408–411.
- Taverna, S.D., Li, H., Ruthenburg, A.J., Allis, C.D., and Patel, D.J. (2007). How chromatin-binding modules interpret histone modifications: lessons from professional pocket pickers. *Nat Struct Mol Biol* 14, 1025–1040.

Theodoulou, F.L., Sibon, O.C.M., Jackowski, S., and Gout, I. (2014). Coenzyme A and its derivatives: renaissance of a textbook classic. *Biochim. Soc. Trans.* *42*, 1025–1032.

Thorvaldsdottir, H., Robinson, J.T., and Mesirov, J.P. (2013). Integrative Genomics Viewer (IGV): high-performance genomics data visualization and exploration. *Briefings in Bioinformatics* *14*, 178–192.

Trapnell, C., Roberts, A., Goff, L., Pertea, G., Kim, D., Kelley, D.R., Pimentel, H., Salzberg, S.L., Rinn, J.L., and Pachter, L. (2012). Differential gene and transcript expression analysis of RNA-seq experiments with TopHat and Cufflinks. *Nat Protoc* *7*, 562–578.

Tropberger, P., Pott, S., Keller, C., Kamieniarz-Gdula, K., Caron, M., Richter, F., Li, G., Mittler, G., Liu, E.T., Bühler, M., et al. (2013). Regulation of Transcription through Acetylation of H3K122 on the Lateral Surface of the Histone Octamer. *Cell* *152*, 859–872.

Tsuchiya, Y., Pham, U., and Gout, I. (2014). Methods for measuring CoA and CoA derivatives in biological samples: Table 1. *Biochim. Soc. Trans.* *42*, 1107–1111.

Tu, B.P., Kudlicki, A., Rowicka, M., and McKnight, S.L. (2005). Logic of the yeast metabolic cycle: temporal compartmentalization of cellular processes. *Science* *310*, 1152–1158.

Turner, B.M., Birley, A.J., and Lavender, J. (1992). Histone H4 isoforms acetylated at specific lysine residues define individual chromosomes and chromatin domains in *Drosophila* polytene nuclei. *Cell* *69*, 375–384.

van Holde, K.E. (1989). *Chromatin* (Springer).

Vavra, K.J., Allis, C.D., and Gorovsky, M.A. (1982). Regulation of histone acetylation in *Tetrahymena* macro- and micronuclei. *J. Biol. Chem.* *257*, 2591–2598.

Verdin, E., and Ott, M. (2014). 50 years of protein acetylation: from gene regulation to epigenetics, metabolism and beyond. *Nat Rev Mol Cell Biol.*

Vollmuth, F., and Geyer, M. (2010). Interaction of Propionylated and Butyrylated Histone H3 Lysine Marks with Brd4 Bromodomains. *Angew. Chem. Int. Ed.* *49*, 6768–6772.

Wang, J., Alexander, P., Wu, L., Hammer, R., Cleaver, O., and McKnight, S.L. (2009). Dependence of mouse embryonic stem cells on threonine catabolism. *Science* *325*, 435–439.

Warburg, O., Wind, F., and Negelein, E. (1927). The Metabolism of Tumors in the Body. *J. Gen. Physiol.* *8*, 519–530.

Weintraub, H., and Groudine, M. (1976). Chromosomal subunits in active genes have an altered conformation. *Science* 193, 848–856.

Wellen, K.E., Hatzivassiliou, G., Sachdeva, U.M., Bui, T.V., Cross, J.R., and Thompson, C.B. (2009). ATP-Citrate Lyase Links Cellular Metabolism to Histone Acetylation. *Science* 324, 1076–1080.

Whyte, W.A., Orlando, D.A., Hnisz, D., Abraham, B.J., Lin, C.Y., Kagey, M.H., Rahl, P.B., Lee, T.I., and Young, R.A. (2013). Master Transcription Factors and Mediator Establish Super-Enhancers at Key Cell Identity Genes. *Cell* 153, 307–319.

Xie, Z., Dai, J., Dai, L., Tan, M., Cheng, Z., Wu, Y., Boeke, J.D., and Zhao, Y. (2012). Lysine succinylation and lysine malonylation in histones. *Molecular & Cellular Proteomics* 11, 100–107.

Yang, W., Hong, Y.H., Shen, X.Q., Frankowski, C., Camp, H.S., and Leff, T. (2001). Regulation of transcription by AMP-activated protein kinase: phosphorylation of p300 blocks its interaction with nuclear receptors. *J. Biol. Chem.* 276, 38341–38344.

Yao, T.P., Oh, S.P., Fuchs, M., Zhou, N.D., Ch'ng, L.E., Newsome, D., Bronson, R.T., Li, E., Livingston, D.M., and Eckner, R. (1998). Gene dosage-dependent embryonic development and proliferation defects in mice lacking the transcriptional integrator p300. *Cell* 93, 361–372.

Yokoyama, A., Lin, M., Naresh, A., Kitabayashi, I., and Cleary, M.L. (2010). A Higher-Order Complex Containing AF4 and ENL Family Proteins with P-TEFb Facilitates Oncogenic and Physiologic MLL-Dependent Transcription. *Cancer Cell* 17, 198–212.

Zhang, Y., Liu, T., Meyer, C.A., Eeckhoute, J., Johnson, D.S., Bernstein, B.E., Nussbaum, C., Myers, R.M., Brown, M., Li, W., et al. (2008). Model-based Analysis of ChIP-Seq (MACS). *Genome Biol* 9, R137.

Zhou, V.W., Goren, A., and Bernstein, B.E. (2010). Charting histone modifications and the functional organization of mammalian genomes. *Nature Reviews Genetics* 12, 7–18.